

UNIVERSITAT DE GIRONA  
ESCOLA POLITÈCNICA SUPERIOR  
Departament d'Arquitectura i Tecnologia de Computadors (ATC)



Màster en Informàtica Industrial,  
Automàtica, Computació i Sistemes  
(MIACS)

# Automatic source detection in astronomical images

Submitted by  
Marc Masias Moyset

Supervisors:  
Dr. Jordi Freixenet  
Dr. Xavier Lladó  
Dr. Marta Peracaula  
*Universitat de Girona*

## Agraïments

Després d'uns quants mesos de durs esforços miro aquest document i estic satisfet amb la feina feta. Entre d'altres coses, m'ha permès conèixer un xic millor certs aspectes relacionats amb l'astronomia, una ciència que era força desconeguda per mi, i que ara conec una mica més gràcies a l'estudi d'imatges astronòmiques. Però aquest treball de final de màster no hagués estat possible sense l'ajuda del grup VICOROB i d'algunes de les persones que en formen part. Especialment, m'agradaria donar les gràcies als meus directors Jordi, Marta i Xavi, ja que la seva inestimable ajuda m'ha servit per tirar endavant aquesta tesi de màster.

També voldria donar les gràcies als meus companys de laboratori, alguns d'ells tan enfeïnats com jo per culpa d'articles, projectes o altres assumptes. També als meus amics d'Olot i Girona (tot i que algun d'ells l'he tingut a l'estranger) i a la meva família, especialment a la meva iaia Mercè, a qui li dedico aquest treball. Tots ells m'han fet passar uns molt bons moments que m'han permès treballar amb encara més ganes.

A tots ells: moltíssimes gràcies!

# Contents

<b>1</b>	<b>Introduction</b>	<b>1</b>
1.1	Overview . . . . .	1
1.2	Research framework . . . . .	2
1.3	Objectives . . . . .	2
1.4	Planning . . . . .	3
1.5	Document structure . . . . .	3
<b>2</b>	<b>Problem definition</b>	<b>5</b>
2.1	Astronomical images . . . . .	5
2.1.1	Types of astronomical image . . . . .	5
2.1.2	The acquisition process . . . . .	11
2.1.3	The FITS format . . . . .	16
2.2	The detection problem . . . . .	17
2.2.1	Astronomical sources . . . . .	18
2.2.2	Background and noise . . . . .	22
2.2.3	How sources appear in images? . . . . .	23
<b>3</b>	<b>State-of-the-art</b>	<b>26</b>
3.1	Introduction . . . . .	26
3.2	Classification of object detection approaches . . . . .	27
3.2.1	Pre-processing . . . . .	31
3.2.2	Detection criteria . . . . .	41

3.3	Astronomical detection packages . . . . .	49
3.4	Reported results . . . . .	51
3.4.1	Evaluation measures . . . . .	51
3.4.2	Analysis of the results . . . . .	53
3.5	Discussion . . . . .	56
<b>4</b>	<b>Experimental work</b>	<b>59</b>
4.1	Data used . . . . .	59
4.2	State-of-the-art implemented approaches . . . . .	61
4.2.1	Methods implemented . . . . .	62
4.2.2	Experiments . . . . .	69
4.2.3	Analysis of the results . . . . .	71
4.3	Proposal of source detection . . . . .	77
<b>5</b>	<b>Conclusions and future work</b>	<b>82</b>
5.1	Conclusions . . . . .	82
5.2	Future work . . . . .	83
5.2.1	Thesis planning . . . . .	84

# List of Figures

1.1	The master thesis planning. . . . .	3
2.1	Electromagnetic spectrum. . . . .	6
2.2	An optical image (left), and the superimposition of the same optical image and a radio image at 1420 MHz of the same region of the sky (right). . . . .	7
2.3	An example of radio astronomical survey at corresponding to the Canadian Galactic Plane Survey . . . . .	8
2.4	An example of an infrared image with sources, gas, and dust. . . . .	9
2.5	Examples of high frequency images: ultraviolet (left), X-ray (middle), and $\gamma$ -ray (right) images . . . . .	10
2.6	Example of an image colouring . . . . .	10
2.7	Newtonian telescope diagram. . . . .	12
2.8	Two examples of the location of telescopes . . . . .	12
2.9	An example of an interferometer . . . . .	13
2.10	The CCD array of the camera incorporated in the XMM-Newton observatory (in orbit). . . . .	14
2.11	An artistic representation of the Solar System. . . . .	19
2.12	Distribution of the stars . . . . .	20
2.13	Diagram of the stellar evolution. . . . .	21
2.14	Examples of spiral, elliptical and irregular galaxies, respectively . . . . .	22
2.15	Interactions between galaxies . . . . .	22
2.16	An infrared mosaic with background variations . . . . .	24

2.17	Diagram of the representation of a point source in an image as the convolution of the object and the PSF. . . . .	25
2.18	The same image with different contrast stretching . . . . .	25
3.1	A 6-scale wavelet decomposition. . . . .	39
3.2	The appearance of the MHWT. . . . .	40
3.3	An example of the connectivity in the wavelet scales . . . . .	46
3.4	A simple example to explain TP, FP, FN, and TN measures . . . . .	52
4.1	The 19 circular images forming the resulting mosaic . . . . .	60
4.2	The resulting mosaic after excluding regions with high level of noise and interferences that may cause unreliable detections . . . . .	62
4.3	The 632 true sources manually detected in the GMRT image. . . . .	63
4.4	Application of a 5-scale WT to the central field of the GMRT mosaic. . . . .	65
4.5	Typical histogram of an astronomical image. . . . .	66
4.6	An scheme that shows how the $C_r F$ and its associated fitted polynomial are computed . . . . .	67
4.7	Graphical scheme of Torrent approach. . . . .	68
4.8	Sources detected in the central field of the GMRT mosaic by Slezak and Starck approaches . . . . .	73
4.9	Sources detected in the central field of the GMRT mosaic by Peracaula <sub>alg1</sub> and Peracaula <sub>alg2</sub> approaches . . . . .	74
4.10	Sources detected in the central field of the GMRT mosaic by SExtractor and SAD packages . . . . .	75
4.11	Sources detected in the central field of the GMRT mosaic by Torrent and some overlapped approaches . . . . .	76
4.12	Feature extraction through filtered images and wavelet scales. . . . .	78
4.13	Sources detected in the central field of the GMRT mosaic . . . . .	80
4.14	The 474 sources detected in the GMRT image. . . . .	81
5.1	PhD planning scheme. . . . .	85

# List of Tables

2.1	List of the most commonly used filters according to the band where they belong and their approximated central wavelength. . . . .	15
3.1	Summary of the analysed pre-processing methods . . . . .	29
3.2	Summary of the analysed detection methods . . . . .	30
3.3	Summary of the results presented in the analysed articles . . . . .	53
3.4	Overview of the different techniques reviewed with their advantages and drawbacks. . . . .	58
4.1	Results obtained with the experiments performed . . . . .	72
4.2	Comparison our proposal and Torrent approach . . . . .	79
4.3	Results obtained with the experiments performed in comparison with our proposal . . . . .	79

# Chapter 1

## Introduction

### 1.1 Overview

Astronomical images provide information about the great variety of celestial objects (sources) existing in the Universe, the physical processes taking place on it, and the formation and evolution of the Cosmos. In the last years high-resolution mappings and catalogues of objects have been obtained from many observatories that use vanguard technology. Many of these observatories, located both in the terrestrial surface and in orbit, use the classical optical telescopes, but it is also a common practice to acquire images with instruments that capture photons of frequencies not perceptible to the human eyes, as radio frequency or X-ray.

Observing a same region of the sky at different frequencies produces different types of images. Combined and comparative analysis of these images provide more comprehensive information of the objects of this region. These objects are of great richness and may mean spectacular discoveries for the astronomy. However, detecting objects in astronomical images is not a process as easy as it seems. Huge amounts of objects (sometimes up to thousands) without clear boundaries and with different sizes and intensity values within the same image, may difficult and slow down the detection of relevant objects. Furthermore, some other difficulties produced by the limitations of the instruments used may add some harmful effects to images and complicate even more the search of objects.

For this reason, the development of automated algorithms for detecting astronomical objects has become a research topic of interest for the astronomers. Moreover, astronomical object detection algorithm usually are accompanied by other algorithms for automatic

classification of objects and for obtaining of measures from them (however, these type of methods are out of the scope of this master thesis). The first automated methods for astronomical object detection were already developed in the seventies, and have evolved until today, although at relatively low pace due to the fact that simple image processing techniques are already useful to easily achieve better results than if the detection was performed manually. Nevertheless, more accurate and reliable detection are increasingly required by astronomers, and because of this, more complex strategies are implemented.

## 1.2 Research framework

This master thesis is located within the framework of two research projects which the Computer Vision and Robotics (VICOROB) group of the Universitat de Girona is part of: “Observational and theoretical studies of high energy galactic sources from the radio to the VHE gamma-rays” (reference AYA2007-68034-C03-03) awarded by the EMED - Ministerio de Educación y Ciencia (MEC), of which Dr. Marta Peracaula was responsible; and “High-energy phenomena in stellar objects. Theory and multi-wavelength observations” (reference AYA2010-21782-C03-02) awarded by EMCI - Ministerio de Ciencia e Innovación, of which Dr. Jordi Freixenet is the responsible.

Both projects are coordinated by the team of the Universitat de Barcelona [85], led by Dr. Josep Maria Paredes (IP). The third member involved in the projects is the team of the Universidad de Jaén [84], led by Dr. Josep Martí.

## 1.3 Objectives

The main objective of this master thesis is to investigate automatic methods of object detection and segmentation in astronomical images with the aim of help the astronomical community when making catalogues of huge amounts of stellar bodies. This is the general goal, but it can be subdivided in the following points:

- To exhaustively review the state-of-the-art of astronomical source detection techniques in order to point out their strengths and weaknesses.
- To implement the techniques with the best reported results and test them with the purpose of verify their results in the same sets of images.



2. **Problem definition.** After the initial chapter, we introduce the readers with some background of the problem to solve according to our research. We go deep into the different types of astronomical images, their main features and the way how they are acquired. We also explain the key points involved in the automatic detection of objects in astronomical images, especially the different elements that we can find in these images: sources, background and noise.
3. **State-of-the-art.** This chapter performs a review of the most remarkable works in the literature that deal, to a greater or lesser degree, with astronomical source detection. We distinguish the different techniques between pre-processing and detection steps, pointing out their advantages and disadvantages. Finally, the reported results are analysed and a discussion of the conclusions extracted is presented.
4. **Experimental work.** In this chapter we comment the experiments performed both with the outstanding approaches in the literature and with the new techniques that have arose from the analysis of the state-of-the-art. Finally, we present and discuss the results obtained with the different implemented methods.
5. **Conclusions and future work.** In this final chapter, we present the conclusions extracted from the work developed in the whole master thesis. From them, we arise some ideas to be develop as future works in the framework of the PhD thesis.

## Chapter 2

# Problem definition

*In astronomy, images play a fundamental role. Their study and interpretation can make the Universe more comprehensible. In this sense, the detection of cosmic objects is one of the most challenging tasks. However, due to the large amount of data that appear in astronomical images and the fact that many astronomical sources are at the detection level of the instrument, it is necessary the use of computer aided systems to perform such a detection. In this chapter, we go into the astronomical detection problem with more depth, taking into account the main points involved in it.*

### 2.1 Astronomical images

There are different types of astronomical images, each of them used with different purposes. We also describe the main elements involved in their acquisition process and the standard format used to store the data.

#### 2.1.1 Types of astronomical image

The different objects present in the universe emit large amounts of energy. People are able to perceive the visible light through their eyes, which is the region of the electromagnetic spectrum where the Sun emits most of its radiated energy. In fact, visible light is only a small portion of the whole electromagnetic radiation that travels through space. Initially the study of the universe was mainly focused on the visible band, with the building of observatories that included optical telescopes with associated devices as spectrometers or photometers. However, due to the fact that large amounts of relevant information of the

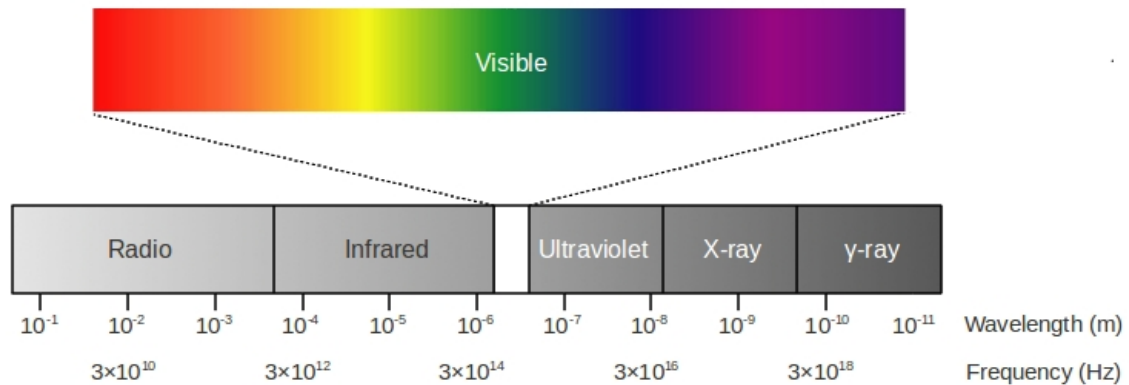


Figure 2.1: Electromagnetic spectrum.

invisible bands were necessary for the physical knowledge of the Universe, astronomers also made efforts to develop an astronomy able to capture this non-visible radiation. This radiation is emitted in different frequencies (and therefore, different wavelengths) as we can see in the electromagnetic spectrum in Figure 2.1. On one hand we have the radiation emitted in frequencies lower than the visible range (which has wavelengths between 400 and 700 nm), as radio and infrared. On the other hand we have the radiation emitted in frequencies higher than the visible range, as ultraviolet, X-ray, and  $\gamma$ -ray. Hence, there are different types of astronomical images depending on at which frequency the radiation is captured.

Different celestial bodies, gas, dust, and other elements may be visible at specific frequencies, and therefore, different types of images are used depending on the elements to visualise. Moreover, a common practice in astronomy is to superimpose images of different frequencies in order to combine the information provided by each frequency. An example can be seen in Figure 2.2, that shows the superimposition of an optical image which contains a galaxy and a radio image at 1420 MHz, which is the frequency that hydrogen atoms emit, so the new information provided by the radio image is basically the hydrogen present in this region of the sky.

In other words, what the analysis of the sky at different frequencies of the electromagnetic spectrum allows, is to study the phenomena of the universe from the least energetic to the most, from cooler to hotter radiation. For example, stars, depending on their masses and temperatures, have their emission peak at different bands of the frequency spectrum as optical, infrared or ultraviolet band. In our case, we happened to receive the solar light that peaks at yellow, and maybe for this reason our eyes are able to detect visible light.

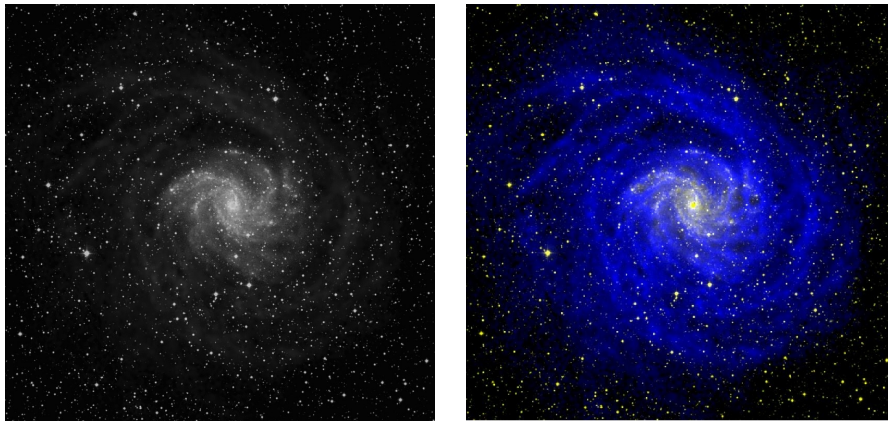


Figure 2.2: An optical image (left), and the superimposition of the same optical image and a radio image at 1420 MHz of the same region of the sky (right).

As we already mentioned, at the beginnings, astronomy was focused on the optical band, on the one hand, because of the lack of theoretical predictions by the astronomical community, and on the other hand, because there was not enough technical development. Most of the non visible bands except radio and the zones of infrared and ultraviolet near the visible light are blocked by the atmosphere, and for this reason, astronomy in these bands could not be developed until the space age in the sixties and seventies. Until this decades, optical astronomy allowed astronomers to observe stars and other phenomena which emit at medium temperatures as the sun.

Nevertheless, astronomy at radio frequencies was developed at the decade of the thirties, before than at other frequencies, since it was directly linked to the development of the radio receiver, that occurred at the beginnings of the 20th century. Unlike optical images that are characterised by have a high resolution, radio images have a poor resolution. The resolution is the ability to see in detail and it is given by the wavelength and the instrument diameter. The astronomers calculated that to have the same resolution in radio than in optical, they needed instruments 100000 times greater (a non-viable size, since it is technologically impossible to build antennas over 100 meters). To solve this problem, they decided to form the images by correlating (by pairs) the signal reached by multiple antennas located in fields, laid out in very large arrays (along kilometres). These antennas point to the same stellar object, but, as they are spaced out, the light reach them at different moments (these differences are tiny), simulating a huge antenna with kilometres of diameter. Afterwards the different signals are correlated and with some mathematical operations a high resolution image is formed. The whole set of antennas is

called radio interferometer. An example of interferometric radio survey is shown in Figure 2.3, which is the Canadian Galactic Plane Survey (CGPS) [81, 32]. Some of the most known interferometers are the Very Large Array (USA) [56] with 27 antennas of 25 meters laid out along three arms of a Y-shape (each of which measures 21 km), and the Very Long Baseline Array [57] with 10 antennas of 25 meters laid out in all North America (which implies distances between antennas up to thousands of kilometres). A new generation of interferometers is in development: the Atacama Large Millimeter/submillimeter Array (ALMA) [1] and the Square Kilometre Array (SKA) [70].

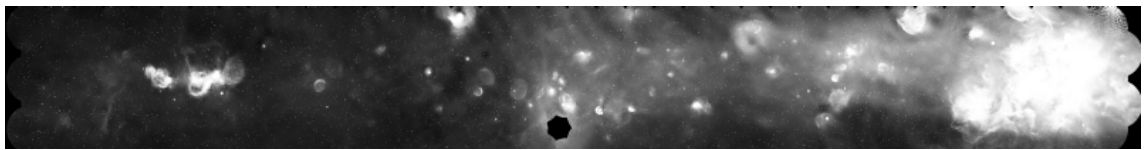


Figure 2.3: An example of radio astronomical survey at corresponding to the Canadian Galactic Plane Survey. It is a mosaic formed by 193 fields observed from years 1995 to 2000.

Years later astronomy in other invisible bands was also developed. Astronomers can observe the so-called near-infrared (infrared radiation close to the visible part of the spectrum) with the same devices that they use in optical, and the same happens with the near-ultraviolet radiation. As the infrared radiation moves away from the visible light, at more altitude the telescope must be placed, even above the atmosphere. Infrared observations are suitable to see emissions of cold clouds of gas and dust as shown in Figure 2.4 (an image of the WISE mission taken from [51]). Currently, there are some infrared telescopes in space, including the Herschel Space Observatory [18], the Spitzer Space Telescope [50], and the Wide-field Infrared Survey Explorer (WISE) [51] (also the Hubble Space Telescope [53] can observe at near-infrared frequencies); some other are placed in aeroplanes, including the Stratospheric Observatory for Infrared Astronomy (SOFIA) [52] and the Kuiper Airborne Observatory (KAO) [46]; or placed in the terrestrial surface as the James Clerk Maxwell Telescope at Mauna Kea Observatory (Hawaii) [36]. Even, to achieve better resolution, there are infrared interferometers as the one at Keck Observatory (Hawaii) [88].

Observations at high frequencies are usually performed from the upper atmosphere or from the space using rockets and satellites in orbit. In ultraviolet, it is possible to visualise young (massive) and very old stars, which are very hot, and therefore, emit at a zone of the spectrum closer to blue and ultraviolet. This band is also used to carry out measures as



Figure 2.4: An example of an infrared image with sources, gas, and dust.

density, composition, temperature of the interstellar medium, providing information about its evolution. Some examples of space telescopes that observe ultraviolet radiation are the Hubble Space Telescope (HST), the Far Ultraviolet Spectroscopic Explorer (FUSE) [35], and the Galaxy Evolution Explorer (GALEX) [49]. In X-ray the energies are very high and show violent phenomena or sources with extremely hot gas, while in  $\gamma$ -ray especially the very violent phenomena as black holes, supernova explosions, or destruction of atoms are detected. Some of the X-ray satellites in course today include the X-ray Multi-Mirror Mission-Newton (XMM-Newton) [20], Rossi X-ray Timing Explorer (RXTE) [45], and the Chandra X-ray Observatory [47], whereas some of the  $\gamma$ -ray satellites currently in orbit are the INTErnational Gamma-Ray Astrophysics Laboratory (INTEGRAL) [19], and the Fermi Gamma-ray Space Telescope [48]. Figure 2.5 shows examples of ultraviolet (extracted from the GALEX website [49]), X-ray (extracted from the XMM-Newton website [20]), and  $\gamma$ -ray images (extracted from the INTEGRAL website [19]).

### Multi-band images

In astronomy, some filters are used to focus the observation in specific frequency bands (we are going to see more details of these filters in the optical band in section 2.1.2). When an observation is performed by a unique filter, the image obtained is called mono-band image, whereas when several images of the same region of the sky are obtained using different filters they may form a multi-band image. The acquisition of multi-band images may be performed simultaneously in the same observation or through different observations. In the first case, the camera of the telescope includes a mosaic of capture

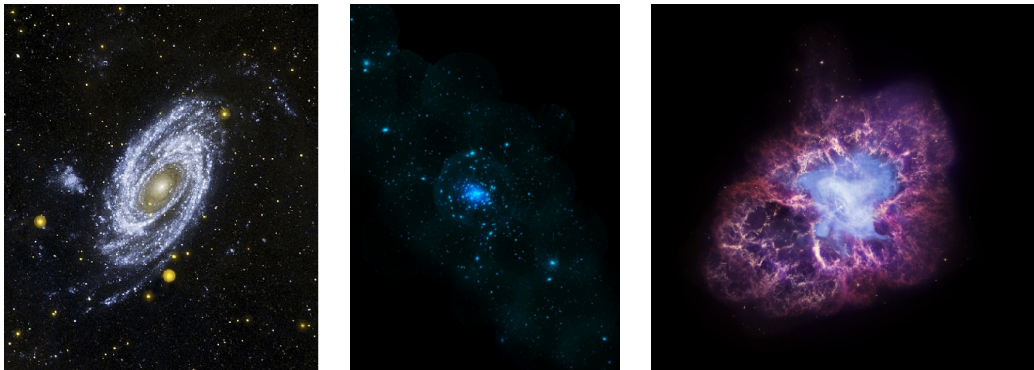


Figure 2.5: Examples of high frequency images: ultraviolet (left), X-ray (middle), and  $\gamma$ -ray (right) images. Some of them are compositions with other bands, although high frequency bands are the dominant ones.

sensors, each of them used for a specific wavelength. Using three bands of a multi-band image, it is possible to visualise an image with false colours. Depending on their position in the electromagnetic spectrum, a colour is assigned to a band, being red, green, and blue (RGB) the classical colour space used. For example, if a multi-band image has ultraviolet, visible, and infrared bands, the color blue will be usually assigned to the ultraviolet band, the green to the visible band, and the red to the infrared band. Thus, the resulting image can give additional information as the temperature of the different astronomical elements that contains. Figure 2.6 shows an example of an image colouring obtained from the Hubble Space Telescope website [53].

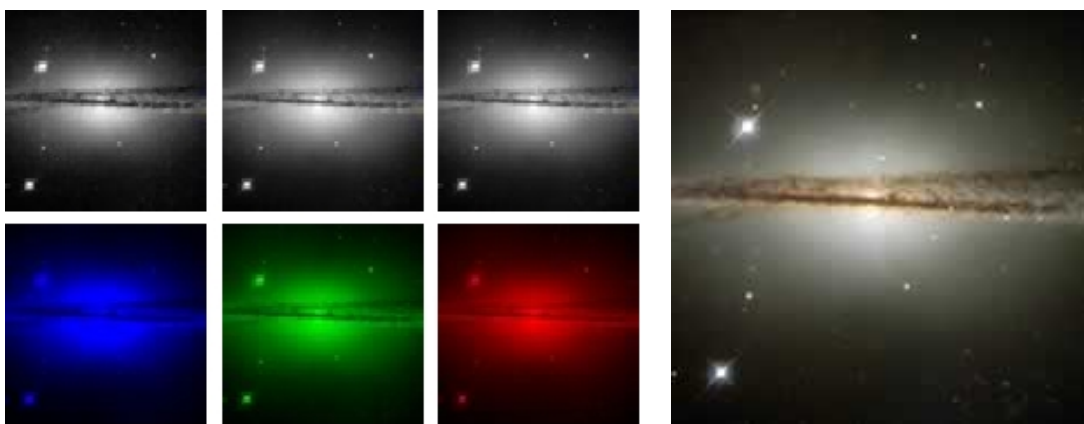


Figure 2.6: Example of an image colouring. On the left three visible bands of a multi-band image of a galaxy, and the colour assigned to each of them. On the right, resulting image in colour.

### 2.1.2 The acquisition process

Four main elements are involved in the acquisition process of astronomical images: the telescope (or antenna), the capture device, the filter system, and the atmosphere in ground-based observatories.

#### The telescope

Professional astronomical observations are made in observatories by means of large telescopes. Maybe the most popular telescopes are the optical ones, able to observe the visible light that emit the stellar bodies and some wavelengths of the ultraviolet and infrared bands. These telescopes are generally composed of two or three reflector mirrors: a primary and a secondary mirror and optionally other ones. The primary mirror has a concave shape, and it is used to gather and focus the light photons. Celestial objects (as stars, planets and galaxies) emit parallel light rays that reach the Earth, and because these rays are parallel to each other, the parabolic shape of the mirror focus the light rays to a single point on the secondary mirror. Afterwards, the secondary mirror, which is flat and diagonally oriented with respect to the primary one, redirects the light rays towards the focal point at the side of the top of the telescope tube. Telescopes designed in this way are so-called Newtonian telescopes (see the figure 2.7). There are other configurations of mirrors and other optical telescopes that, instead of use mirrors, redirect the light by lenses, and even combinations of mirrors and lenses.

Optical telescopes are usually placed in large observatories in high places as mountaintops to have optimal climatic conditions as clear skies or dry environments due to the thermal inversion (the dampness is below the location of the observatories). Figure 2.8 (left) shows an example of an observatory placed in a mountaintop in Canary Islands [25]. Due to the fact that atmosphere may perturb the observations, sometimes these telescopes and other kinds, are placed in higher altitudes using aeroplanes and satellites. Figure 2.8 (right) shows the Hubble Space Telescope orbiting around the Earth (image taken from the HST website [53]).

Following similar principles, there are other types of telescope according the wavelength to observe. Most of them are placed above the atmosphere, as infrared, ultraviolet, X-ray, and  $\gamma$ -ray telescopes. On the other hand, as we already mentioned, radio frequencies are captured by directional radio antennas. With a unique antenna it is only possible to perform cartographic analysis of single astronomical objects due to its low resolution.

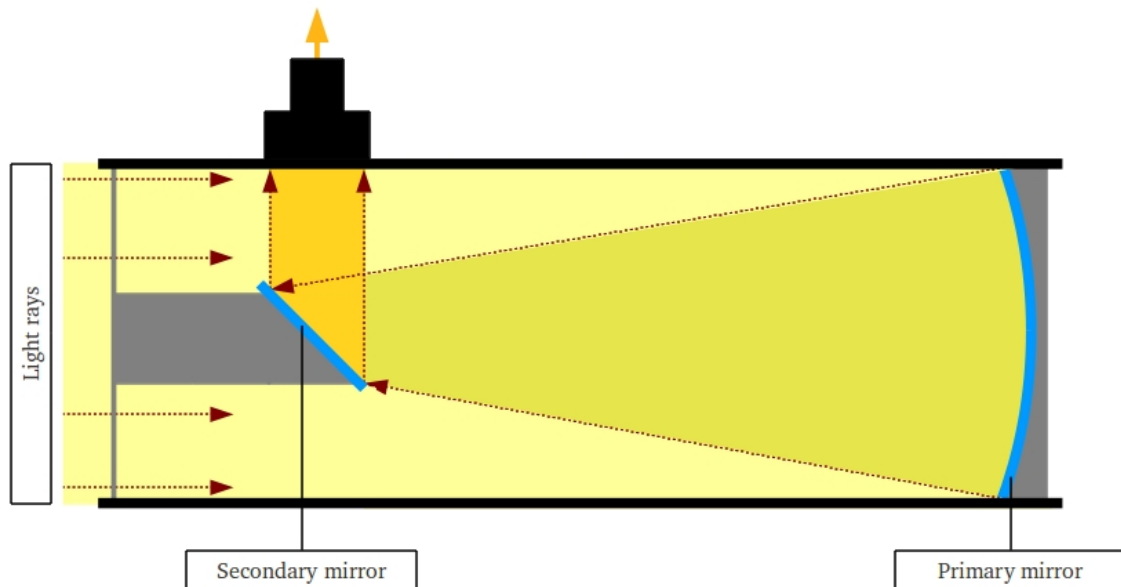


Figure 2.7: Newtonian telescope diagram.

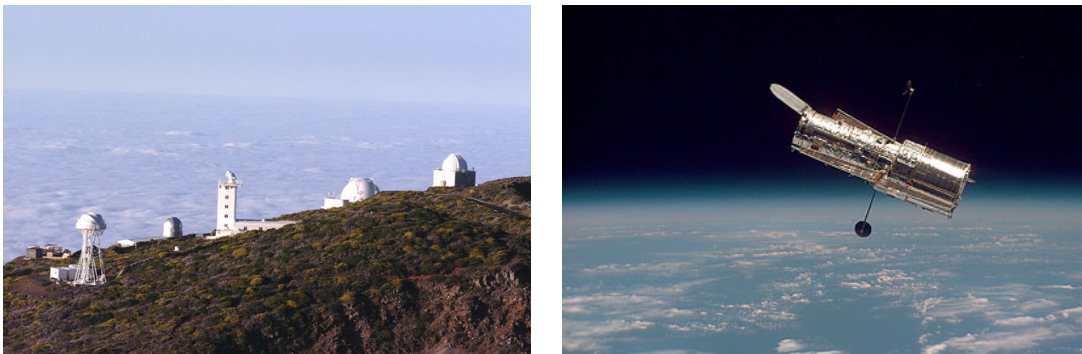


Figure 2.8: Two examples of the location of telescopes. On the left, the observatory in Roque de los Muchachos (La Palma), and on the right, the Hubble Space Telescope in orbit.

To have high resolution in radio, interferometry must be used, which consists in reaching the radio emissions with large arrays of antennas as can be seen in Figure 2.9 (left), which contains an image of the VLA (extracted from its website [56]). Moreover, the final resolution must preserve an angular resolution (antennas have a concave shape), so a technique called aperture synthesis is used. This technique simulate the distribution of the set of antennas by mathematical corrections, having into account the shape that the huge antenna to simulate should have (a parabola, a dish shape). Figure 2.9 (right) shows the parabolic shape simulated by the antenna set.



Figure 2.9: An example of an interferometer. On the left, the interferometer Very Large Array at USA. On the right, the diagram that shows the parabolic shape that aperture synthesis performs. Small triangles represent the set of radio antennas, while the big triangle represents the resulting big antenna that simulate the smaller ones.

### The capture device

In order to form the image by the radiation that reach the telescope many times a CCD (Charge-Coupled Device) camera is used. They are used mainly due to their high sensitivity in most of the electromagnetic spectrum and especially in visible range, their linear response to the light, their reduced size, and their low cost. CCD cameras consist on an array of CCD sensors, each one of them corresponding to an image pixel. Theses sensors are based on the photoelectric effect, which converts its received light into electric current, for afterwards, be translate to a pixel intensity on the digital image. Figure 2.10 shows the CCD-array of the XMM-Newton observatory, which is sensitive to X-rays (image taken from XMM-Newton website [20]). Thermal noise and cosmic rays<sup>1</sup> may alter the pixels in the CCD array. In order to counteract such effects, astronomers take several exposures varying the CCD shutter aperture, and fixing the image irregularities (as noise<sup>2</sup>) by performing averages and subtractions of different aperture images, and thus, achieve a useful image.

CCD cameras are able to capture visible, ultraviolet, infrared and even X-ray bands. In radio, the image is formed by the interpretation of the signal reached by the interferometer, while in  $\gamma$ -rays (and sometimes also in X-rays), the image is generally created by photon

<sup>1</sup>Energetic charged subatomic particles from the outer space that have a high energy due to their high speed.

<sup>2</sup>In images, the random variation of brightness produced by the capture instruments



Figure 2.10: The CCD array of the camera incorporated in the XMM-Newton observatory (in orbit).

counters.

### The filter system

Usually, in optical astronomy, some filters are used in the telescopes to select specific zones of the electromagnetic spectrum. They are used to isolate objects or phenomena visible at particular wavelengths. Thus, the astronomers have two choices: to perform a unique observation in the suitable frequency band (astronomy mono-band) or several observations of the same region of the sky using different filters (astronomy multi-band). When a set of these filters cover an important part of the spectrum, we are speaking about a photometric system. There are several famous photometric systems as Johnson system (U, B, V), Bessell photometric set (U, B, V, R, I), Sloan Digital Sky Survey filter set (U, G, R, L, Z), or J, H, K, L, M band set. Notice that each photometric system has specific associated filters known by letters according to the region of the spectrum that they deal with. These letters are not standards, but the astronomical community use them to refer to the different filters with specific names (for example B, G, and R are visible filters and refer to blue, green and red colours, respectively). As we can see in Table 2.1, the bands spanned by these filters are ultraviolet, visible and infrared (specifically near-infrared and mid-infrared). The filters are able to deal with a range of wavelengths, and it may vary among the different photometric systems.

The quality of a filter is given by their ability to be as transparent as possible for the desired frequency band, being as opaque as possible for the rest of bands.

Table 2.1: List of the most commonly used filters according to the band where they belong and their approximated central wavelength.

Filter	Wavelength
Ultraviolet	
U	360 nm
Visible	
B	440 nm
G	520 nm
V	550 nm
R	670 nm
Infrared	
I	790 nm
Z	910 nm
J	1220 nm
H	1600 nm
K	2220 nm
L	3450 nm
M	4750 nm

### The atmosphere

The atmosphere is a layer of gases that surrounds celestial bodies (that includes the Earth) and it is held in place by gravity. Although it has a weak density, the terrestrial atmosphere represents a significant obstacle when an astronomical observation is performed. It absorbs more or less the light according to their wavelength, the altitude of the observation point, and the meteorological conditions. This absorption may modify the true colour of the objects. Only radio and visible ranges and some wavelengths close to them pass through the atmosphere, while the other parts of the spectrum must be observed above the atmosphere. Moreover, atmosphere has refractory, dispersive, and diffusion effects. Most of these effects are relatively easy to correct (e.g. with normalisations and subtractions). However, the diffusion produces an effect so-called seeing, which due to atmospheric turbulences makes objects in images blurred and twinkled. The better way to avoid or at least decrease the seeing is, as we have already seen, locating the observatories as high as possible, preferably above the atmosphere. In most cases, this fact becomes non-viable due to its high cost, and for this reason, most of the current and further projects are focused on terrestrial observations. Therefore, some solutions to this problem are developed, for example the called adaptive optics, that reduce the effects of seeing by measuring the

distortions in a wavefront<sup>3</sup> and compensating for them with a device that correct these errors (as deformable mirrors).

### 2.1.3 The FITS format

FITS is the acronym of Flexible Image Transport System [63], and it is the standard computer data format widely used by astronomers to store, transmit and manipulate data files. Unlike many image formats, FITS is designed specifically for scientific data, and for this reason, offers the possibility of attach additional data as photometric and spatial calibration information. It is basically designed to store scientific data sets consisting of multidimensional arrays and 2-dimensional tables containing rows and columns of data. FITS is also often used to store non-image data, such as electromagnetic spectra, photon lists, data cubes, or even structured data. FITS files may contain extensions containing data objects. For instance, one file may store different exposures of the same zone of the sky (as x-ray and infrared exposures).

FITS was originally developed in the late seventies to provide a way to exchange astronomical data between computers of different type, with different word lengths, and different means to express numerical values. It was in 1981 when a first version of the FITS format becomes standardised, and after successive updates, the last version released was the 3.0, approved in July 2008.

The most commonly used type of FITS data is a data array of arbitrary dimension (for example the image) and one or more headers. So the file consists on several structures called HDU (Header and Data Units) consisting of a header and the data that the header describes. The first HDU is called the Primary HDU or the Primary Array. It contains a N-dimensional array of pixels, e.g. a 1-D spectrum, a 2-D image, or a 3-D data cube. The data types supported are: unsigned 8-bit bytes, 16 and 32-bit signed integers, and 32 and 64-bit single or double precision floating point reals (although 16 and 32-bit unsigned integers can also be stored). Additional HDUs may appear after Primary HDU, and they are called FITS extensions. Three types of extensions are available: image extensions, which are N-dimensional arrays of pixels, like in primary array; ASCII table extensions, which are rows and columns of data in the ASCII character format; and binary table extensions, which are rows and columns of data in binary representation.

An interesting point is that the information is stored in headers in a human readable way, so the users can examine the headers and understand the content of the file. These

---

<sup>3</sup>In a propagated wave, a surface of points having the same phase.

headers have a fixed length of 80 characters and have the general form:

```
KEYNAME = value / comment string
```

This keyword-value pair provide information such as size, date and time, origin, coordinates, binary data format, free-form comments, history of the data, and anything else. There are many rules governing the exact format of a keyword record, so for more detail, see the FITS standard [63].

The following lines show an example (inspired by another example in [63]) of 2-dimensional image primary array header. It begins with the following keywords:

#	Keyword
1	SIMPLE = T / file does conform to FITS standard
2	BITPIX = 16 / number of bits per data pixel
3	NAXIS = 2 / number of data axes
4	NAXIS1 = 440 / length of data axis 1
5	NAXIS2 = 300 / length of data axis 2
	⋮
	(other keywords)
	⋮
last	END

FITS format has support for several programming languages (e.g. C, Java, or FORTRAN). It has its support office at NASA/GSFC (a space research laboratory established in a NASA space flight center), available at [54].

## 2.2 The detection problem

The Universe contains billions and billions of astronomical objects in constant evolution. With the desire of understand a little better the cosmos, astronomers obtain thousands of images of these objects. They are at distances measured in light-years, so it is very likely that they appear as faint bright points or blended with other objects. It can also happen that some shapes in images may be considered as objects when actually they are not. For all these reasons astronomical images need exhaustive analyses in order to determine what is an object and what not. The optimal way to carry out these analyses would be with astronomical experts searching for the different objects in images. However, due to the

large amount of data and the fact that many objects can have intensities near the detection levels, a human search is inefficient, very slow, and inaccurate, if not almost impossible. Hence, it is necessary the development of highly robust, fast, efficient, and automated algorithms which detect the astronomical objects in images using image processing and computer vision techniques.

The detection of astronomical sources seems a quite straightforward task in comparison with other computer vision problems: the typical scenario is to deal with light-emitting sources on dark backgrounds. Nevertheless, there are some difficulties associated with the astronomical image processing that make this task not so easy. Astronomical objects do not have clear boundaries, and their sizes and intensities can vary considerably in the same image. This last issue is called dynamic range (the ratio between the largest and smallest possible values), and may cause problems in the image displaying due to the limited range of intensities perceptible by the human vision system. Moreover, astronomical images often have high component of noise.

Therefore, the main challenge in astronomical object detection is to separate those pixels that belong to astronomical bodies, from those others that belong to background or are noise. Because the goal is to find connected regions of pixels constituting the objects, this task is also referred as astronomical object segmentation (however, in this document we almost always speak about detection). Astronomical detection, usually is a first step in the process of making astronomical catalogues, which are lists of astronomical objects that share common features. For these reason, after astronomical detection two other processes are also performed: classification, which categorise the objects in different types (as stars, clusters, or galaxies), and photometry, which is an astronomical technique that measures the flux or intensity (the brightness) of the objects. This process of building a catalogue is also known as source extraction.

### 2.2.1 Astronomical sources

An astronomical source is the origin of something that suggests the presence of an astronomical object. Hereafter we are going to refer to sources and objects without distinction as those stellar bodies that can be detected in images.

Behind the sources detected we can find a variety of astronomical bodies. Beginning with those closest to us, we find different sources in the Solar System. Several planets are orbiting around the well-known star Sun (see the Figure 2.11): the four smaller inner planets called Mercury, Venus, Earth, and Mars, mainly composed of rock and metal;



Figure 2.11: An artistic representation of the Solar System.

the two largest planets called Jupiter and Saturn, mainly composed of gas (hydrogen and helium); and two outermost planets called Uranus and Neptune, mainly composed of water, ammonia and methane. Some other objects (resembling planets) massive enough to be spherical, orbit around the Sun but have not cleared the neighbourhood around its orbit, so they are called dwarf planets. Their names are Ceres, Pluto, Haumea, Makemake, and Eris. Some of the planets and dwarf planets are orbited by natural satellites, also called moons. Orbiting the sun there are millions of small rocky and metallic bodies called asteroids. Most of them are placed in a zone between Mars and Jupiter called main asteroid belt. Other icy bodies that display a visible thin, fuzzy, temporary atmosphere and sometimes also a tail are called comets.

Beyond the Solar System we find an incalculable number of stars, astronomical bodies that bright with own light. They are plasma spheres, that keep they shape due to the gravity force that pushes the matter to their center and the pressure that the plasma carries out outwards. This plasma pressure depends on the mass and the temperature of each star, producing different radiation (brightness) among stars.

Stars can be distributed in different ways:

- Individual (isolated) stars. An example is shown in Figure 2.12 (left).
- Binary stars: a system consisting of two stars orbiting around a common center of mass. An example is shown in Figure 2.12 (middle).
- Clusters: groups of stars. We can distinguish between globular clusters, which are roughly spherical groups of hundreds of thousands of old stars gravitationally bound,

and open clusters, which are more irregular groups of few thousands of young stars much less tightly gravitationally bound. An example is shown in Figure 2.12 (right).



Figure 2.12: Distribution of the stars. On the left, several isolated stars, in the middle, a binary system (the second star is very tiny, and it is located at the bottom left of the other star), and on the right, a cluster. All these images are extracted from the Hubble website [53].

Stars are formed in regions of higher density of the interstellar medium (described later) called molecular medium that basically are composed of hydrogen and helium. When due to a gravitational instability, a region achieve enough density of matter (gas and dust), a compact sphere with enough gravity in its center is formed. Afterwards, it starts to fuse hydrogen in its core in order to produce energy: a star has formed. Once the hydrogen of the core is exhausted (after up to billions of years), the evolution of the star depends on its mass, and can become a white dwarf (an stable cool star) or a red giant (an stable star that fuse hydrogen in a shell outside the core), or even exploit: massive and binary stars may exploit in a violent phenomenon called supernova, while white dwarfs may exploit as a less energetic phenomenon called nova. These two phenomena produces important remnants, structures resulting from the violent explosion of a star in a nova or a supernova. A supernova remnant, can form new astronomical bodies, as very hot neutron stars, or pulsars, which are neutron stars emitting radiation periodically detectable because they are rotating. Furthermore, the supernova explosion trigger turbulences and instabilities that may form new star formation regions. A schematic view of the stellar evolution process is shown in Figure 2.13.

Moreover, when groups of stars and stellar remnants, gas, and dust are gravitationally bound and evolve together in the Universe, we are speaking about galaxies. In fact, the Solar System where we live, belongs to a galaxy called Milky Way. Historically galaxies

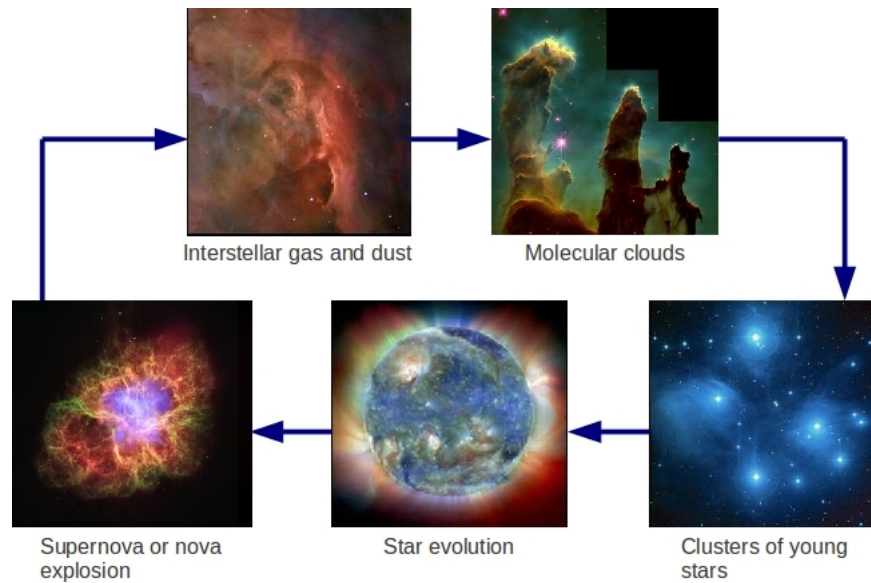


Figure 2.13: Diagram of the stellar evolution.

have been classified according to their apparent shape (morphology), often given by the point of view of the observer:

- **Elliptical:** galaxies with ellipsoidal shape light profile. An example is shown in Figure 2.14 (left).
- **Spiral:** disk-shaped galaxies that used to have two or more arms. An example is shown in Figure 2.14 (middle).
- **Irregular:** galaxies with rare forms usually due to the interaction of galaxies. An example is shown in Figure 2.14 (right).

Interactions between galaxies are relatively frequent (see the examples extracted from the HST website [53] in Figure 2.15). For example two galaxies may collide, which happens when one passes through the other without being merged. This collision may produce changes in the morphology of the galaxies. The interaction of gas and dust of the two galaxies produces disruptions and compressions, and favours the appearance of zones of star formation. Moreover, there are a portion of galaxies called active galactic nuclei (AGN), which are galaxies with a compact region at the center that emits a much higher energy than the entire rest of the galaxy, being the most persistent sources in the Universe. Current theory suggests that there is a supermassive black hole at the center of the AGN. A common type



Figure 2.14: Examples of spiral, elliptical and irregular galaxies, respectively. All these images are extracted from the Hubble website [53].

of AGN are the radio galaxies which are very bright at radio wavelengths, and within it we can find quasars (quasi-stellar radio sources) and blazars (blazing quasi-stellar objects).

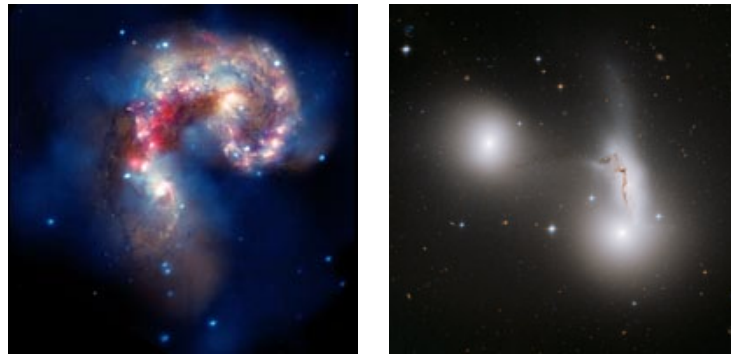


Figure 2.15: Interactions between galaxies. On the left, collision of two galaxies. On the right, trio of mixed galaxies.

The matter that exists between star systems in galaxies is called interstellar medium. It consists of gas, dust and cosmic rays, and it is favourable medium to have regions of star formation. In the interstellar medium we can also find clouds of ionised atomic hydrogen (called H II regions), clouds of neutral atomic hydrogen (H I regions), and nebulas, which are clouds of dust, hydrogen, helium, and other ionised gases.

### 2.2.2 Background and noise

Besides the sources, astronomical images have empty parts of the sky that are called background (sources sometimes are called foreground). Hereafter we are going to speak about background and sky without distinction. Even if there is not any object present

in that part of the sky, there is always a low luminosity mostly due to the light emitted by nearby sources. If the image is taken below the atmosphere, it is possible that some light from man-made sources as cities may be perceptible at the sky. Some regions of the background may be considered as such for human eyes. However, they may hide sources visible in other frequency bands, or so faint that are only detectable by computer tools.

Furthermore, background is diffuse, what means that it is difficult to be specific about the boundaries of the source. In other words, it is difficult to exactly define the exact line that shows where the sources end, and where the background begins. Moreover, background is normally non homogeneous due to the the fact that some astronomical images need a long exposure time to be acquired, and in many cases, they are combinations of images captured at different exposures (at different pointing center) forming a mosaic, as we can see in Figure 2.16.

Owing to the capture instruments, the background of astronomical images often have more or less noise. It can be measured with the called signal-to-noise ratio (SNR), which is a measure used in many fields to quantify how much a signal has been corrupted by noise. It is calculated by dividing the amount of signal from the amount of noise, so the higher the ratio, the less bother the background noise is. In the astronomical case, signal refers to all sources in the image, while noise usually have Gaussian and Poisson distributions (sometimes, it can be estimated through knowledge of the instrument properties). Noise is one of the main disadvantages in astronomical detection, since it makes difficult the detection process (see the zoom performed in Figure 2.16, where the high level of noise makes the background textured, and even may be confused with sources). For this reason, noise reduction has importance by astronomers, and they usually take some measures in pre-processing steps as filtering<sup>4</sup> and deconvolution<sup>5</sup> in order to increase the SNR.

### 2.2.3 How sources appear in images?

As we have seen, several types of astronomical objects may appear in images, and therefore, they may present different shapes. Often, the sources are point-shaped, and they are known as point sources (e.g. stars). These light sources usually have diffraction<sup>6</sup> rings and beam patterns produced mostly by the telescope. This is due to the fact that telescopes and their associated instruments are not perfect optical systems, and therefore do not

---

<sup>4</sup>In images, modify their pixels based on some functions of a local neighbourhood of the pixels.

<sup>5</sup>The process used to reverse the effects of perform a convolution with an instrument.

<sup>6</sup>Phenomena occurred when a wave encounter an obstacle or pass through a small opening.

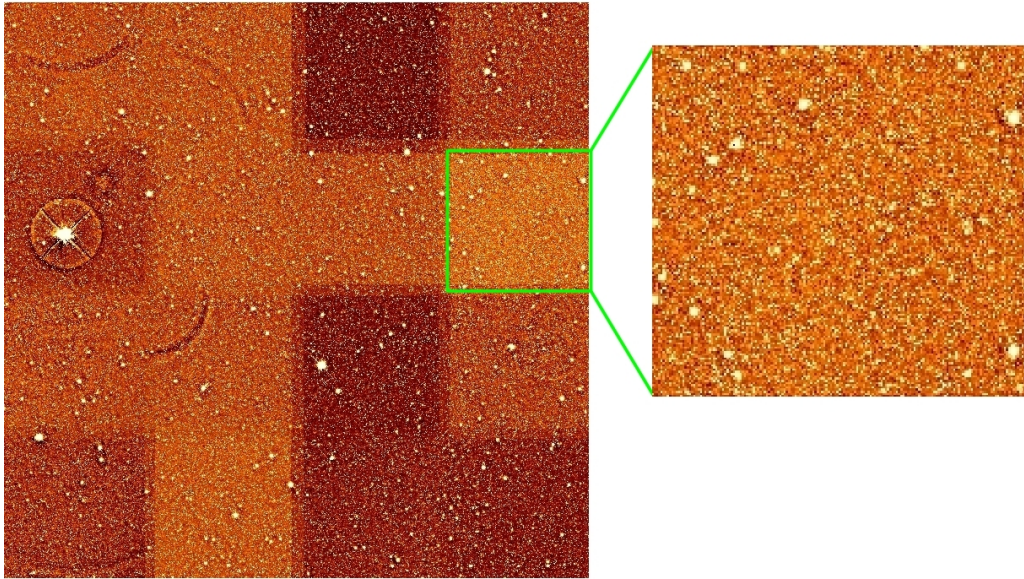


Figure 2.16: An infrared mosaic with background variations. This image, courtesy of J. Martí (private communication) [62], is quite noisy and even has some interferences (the darker curved regions on the top left of the image).

display the objects exactly how they are, being similar to smears with degraded boundaries. This response of our telescope to a point source is so-called point spread function (PSF). Therefore, the PSF describe the two-dimensional distribution of light in the telescope focal plane, being the representation of a point source in an image the convolution<sup>7</sup> of the object with the PSF (see Figure 2.17). Great efforts are taken in order to reduce the size of the PSF in great telescopes (each of them has its own known PSF).

Point sources use to have a few number of pixels, and because of that, sometimes are confused with image noise. A source can also appear in an image with other compact shapes (e.g. galaxies) or with extended structures (e.g. supernova remnants and H II regions). Moreover, they may have wide variety of scales and surface brightnesses. Figure 2.18 shows sources with different shapes and sizes in the same CGPS image [81] with different contrasts (contrast stretching is a common practice in astronomy that allows a better visualisation of the objects).

<sup>7</sup>The process of applying a filter to an image.

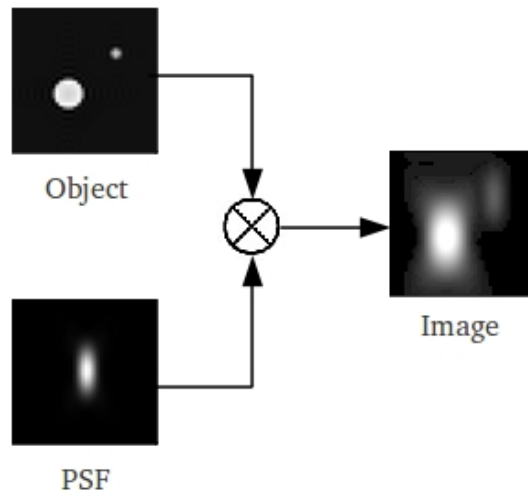


Figure 2.17: Diagram of the representation of a point source in an image as the convolution of the object and the PSF.

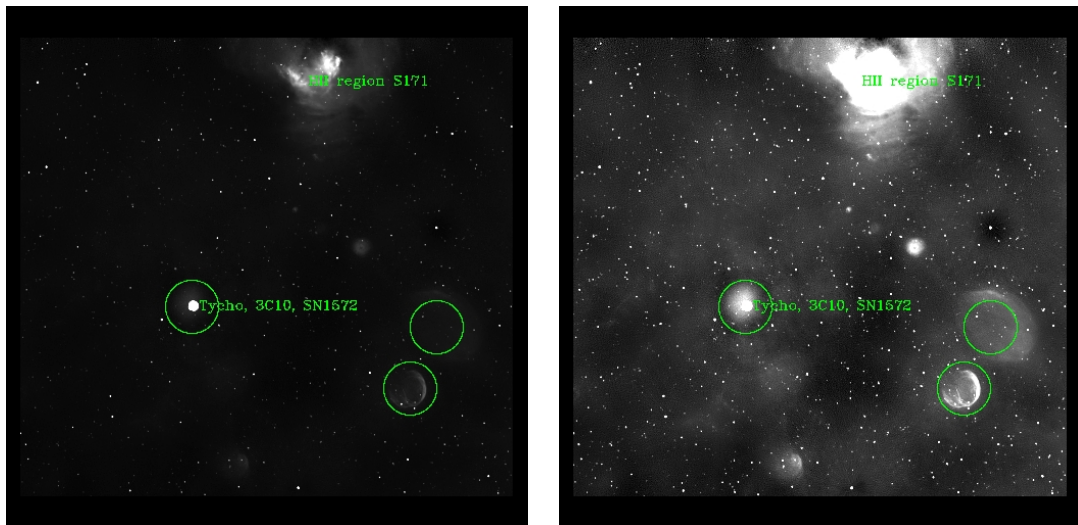


Figure 2.18: The same image with different contrast stretching (0.1% of outliers eliminated on the left, and 2% on the right). These images contain three extended sources encircled in green (supernova remnants), several irregular sources as the H II region on the top of the image, and multiple point sources. Notice that saturating image by changing the contrast, the structure of some extended sources is lost, but many point and faint sources appear.

## Chapter 3

# State-of-the-art

*In astronomical imaging, great efforts are made to perform automatic detections of stellar bodies in wide field images or large surveys. These images contain large volumes of data and often have a high component of noise, and for these reasons it is a difficult issue to locate stars, galaxies, planets, or other astronomical objects with a visual inspection. Because of that, automatic detection tools take much importance for this purpose. In this chapter, we review the main approaches to automated object detection in astronomical imaging published in the last years. Several approaches have been analysed in order to find out their advantages and disadvantages, and to specify the key points that make them remarkable for the astronomical community. Furthermore, this review must provide us new techniques to test and new methodologies to follow. We classify the most important techniques into different strategies according to the way they deal with the detection problem. We also show a comparison of the results of those approaches that present their results focused on the performance of the object detection problem. Finally, we summarise the main conclusions and present a discussion on astronomical object detection.*

### 3.1 Introduction

In this chapter, we analyse the state-of-the-art of strategies for automated astronomical object detection, pointing out their advantages and disadvantages, and specifying the key points that make them remarkable for the astronomical community that works developing software with this aim. Furthermore, this review must allow us to investigate new techniques to test and new methodologies and pipelines to follow in order to orientate and enrich our research. We analyse the most important approaches published in the last years

and classify them according to the strategy they used to perform this task. In particular, we first grouped the works depending on how they prepare the images (pre-processing), and what criteria use to establish which pixels belong to objects and which do not. We further divide the similar works of these two groups in more specific subgroups as we are going to see in the next section.

Although the detection of cosmic bodies in astronomical images is a thoroughly investigated topic, nowadays, there are no updated surveys covering the whole range of existing strategies. We have to go back several years to find any review on astronomical image detection. This fact may be due to that in many cases, the most important step in astronomical detection is not the detection as such (which can be performed for example with a simple thresholding), but the pre-processing steps as filtering or deconvolution. These processes are essential because all the types of astronomical images have a high SNR, which means that the whole image contains a high percentage of noise (basically owing to the acquisition sensors) with respect to the signal.

In 2001, Bertin [6] reviewed over 60 papers on astronomical source extraction and classification. Concerning detection, he divided the algorithms in two main categories: basic detection algorithms (such as local peak search, thresholding and segmentation, background estimation, filtering) and multi-scale approaches (mainly based on wavelet transforms).

Later, in 2003, Barreiro et al. [4] compared several filters (such as Mexican hat wavelet, matched filter, scale-adaptive filter) to optimise the detection of sources by a local peak strategy. More recently, in 2006, Starck and Murtagh [77] devoted some chapters of their book about astronomical image processing to review some strategies of filtering (mainly multi-scale methods as wavelet and curvelet transforms), deconvolution (e.g. linear regularised methods, Bayesian methodology, wavelet-based deconvolution, etc.), and detection (basically Multiscale Vision Model). In 2010, Starck and Bobin [74] also analysed and discussed multi-scale methods (based on wavelets, curvelets and ridgelets transforms) to astronomical data analysis.

## 3.2 Classification of object detection approaches

In this section, we give an overview of astronomical object detection methods according to the chosen classification proposal shown in Tables 3.1 and 3.2. Notice that these tables classify the different works with respect to the pre-processing, the detection as such, the type of images used, and the kind of objects dealt. The classification is carried out following

two main criteria: 1) the type of pre-processing used; and 2) the detection technique used.

The pre-processing is a basic step used to prepare the data in order to achieve the best performance in posterior steps. Within this pre-processing group we find techniques such as filtering, deconvolution, transforms, or morphological operations. A formal and more accurate classification can be performed dividing the pre-processing in multi-scale strategies, basic pre-processes, Bayesian approaches, and matched filter-based strategies. More information is described in the Table 3.1, which illustrates the pre-process followed by the different works reviewed.

The goal of the detection is to locate the astronomical objects and separate them from the background (the sky). Regarding to the detection step, two strategies stand out among the rest: thresholding and local peak search. Thresholding considers that connected pixel regions above a certain threshold belong to an object, whereas local peak search, find those pixels that are maximums in a pixel neighbourhood and, from this point, try to find all the object pixels. Even though these two methods are the most common, we also analyse other strategies that try to solve the detection problem in a different way (most of these strategies are relatively recent). More information is available in Table 3.2, which shows the detection strategy followed by the different works analysed.

Notice that some works only appear in one of the two tables. This is due to the fact that in some cases, the work is focused only on one of the two criteria, obviating the other one or giving the election of the other criteria to those who want to implement the approach. In other cases it may be due to that any pre-processing step is not needed. Another aspect to consider is that the type of image is not specified in all the works, due to the fact that the approach may be used with different types of images, or because they have used simulated images. In fact, almost all works have used both simulated and real images to experimentally validate their proposal.

Table 3.1: Summary of the analysed astronomical object detection methods according to the pre-processing methods, the type of the images and the detection aim. The methods are grouped by its pre-processing strategy. The acronyms for the detection aim stand for (in alphabetical order): extended source detection (ESD), faint source detection (FSD), point source detection (PSD), and source detection (SD).

	Article	Pre-processing	Images	Aim
Basic	Herzog (1977) [29]	Mean	Optical	SD
	Le fèvre (1986) [23]	Bijaoui	Multi-band	SD
	Stetson (1987) [78]	$\sigma$ -clipping + Gaussian	-	SD
	Slezak (1988) [71]	Gaussian + Bijaoui	Optical	SD
	Bertin (1996) [7]	$\sigma$ -clipping	-	SD
	Szalay (1999) [79]	Gaussian	Multi-band	FSD
	Mighell (1999) [44]	Mean	-	SD
	Hopkins (2002) [31]	Gaussian	Radio	SD
	Aptoula (2006) [3]	Morphological	Multi-band	SD
	Yang (2008) [89]	Median + Morphological	Optical	SD
	Perret (2008) [67]	$\sigma$ -clipping + Median + Morphological	Multi-band	SD
Haupt (2009) [27]	Distilled sensing	Radio	SD	
Bayesian	Hobson (2003) [30]	Markov-chain	-	SD
	Savage (2007) [69]	Markov-chain	Infrared	SD
	Feroz (2008) [21]	Nested sampling	-	SD
	Carvalho (2009) [15]	Multiple posterior maximisation	Optical	SD
	Guglielmetti (2009) [26]	Mixture model	X-ray	SD
Matched filter	Irwin (1985) [33]	Bijaoui + Matched filter	Optical	SD
	Vikhlinin (1995) [87]	$\sigma$ -clipping + Matched filter	X-ray	SD
	Makovoz (2005) [42]	Median + Matched filter	Multi-band	PSD
	Melin (2006) [43]	Matched multi-filters	Radio and multi-band	PSD
	Herranz (2009) [28]	Matched matrix filters	Radio	PSD
Multi-scale	Bijaoui (1995) [10]	Wavelet	Optical	SD
	Kaiser (1995) [37]	Mexican Hat	Multi-band	SD
	Damiani (1997) [16]	Gaussian + Median + Mexican Hat	X-ray	SD
	Starck (1999) [73]	Wavelet	Mid-infrared	FSD
	Freeman (2002) [22]	Mean + Mexican Hat	X-ray	SD
	Starck (2002) [72]	Wavelet + Ridgelet	Infrared	SD
	Starck (2003) [75]	Wavelet + Curvelet	Infrared	SD
	Vielva (2003) [86]	Mexican Hat (spherical)	Radio	PSD
	Belbachir (2005) [5]	Contourlet + Wavelet	Infrared	FSD
	Bijaoui (2005) [9]	Wavelet + PSF smoothing	Multi-band	SD
	González-Nuevo (2006) [24]	Mexican Hat (family)	Radio	PSD
	Starck (2009) [76]	Multi-scale Variance Stabilisation	$\gamma$ -ray	SD
	Peracaula (2009) [66]	Gaussian + Wavelet	Radio	PSD
	Peracaula (2010) [65]	Gaussian + Wavelet	Radio and infrared	ESD
Broos (2010) [11]	Wavelet	X-ray	SD	

Table 3.2: Summary of the analysed astronomical object detection approach according to the detection methods, the type of the images and the detection aim. The methods are grouped by the way they perform the detection. The acronyms for the detection aim stand for (in alphabetical order): extended source detection (ESD), faint source detection (FSD), point source detection (PSD), and source detection (SD).

	Article	Strategy	Images	Aim
Thresholding	Jarvis (1981) [34]	Local	Optical	FSD
	Irwin (1985) [33]	Global	Optical	SD
	Le fèvre (1986) [23]	Local	Multi-band	SD
	Slezak (1988) [71]	Global	Optical	SD
	Bijaoui (1995) [10]	Global	Optical	SD
	Bertin (1996) [7]	Global	-	SD
	Szalay (1999) [79]	Global	Multi-band	FSD
	Starck (1999) [73]	Global	Mid-infrared	FSD
	Hopkins (2002) [31]	Global	X-ray	SD
	Freeman (2002) [22]	Global	X-ray	SD
	Makovoz (2005) [42]	Global	Multi-band	PSD
	Melin (2006) [43]	Local	Radio and multi-band	PSD
	Yang (2008) [89]	Local	Optical	SD
	Herranz (2009) [28]	Global	Radio	PSD
	Starck (2009) [76]	Global	Gamma-ray	SD
	Peracaula (2009) [66]	Local	Radio	PSD
	Haupt (2009) [27]	Global	Radio	SD
Peracaula (2010) [65]	Local	Radio and infrared	ESD	
Local peak search	Herzog (1977) [29]	Detection threshold	Optical	SD
	Newell (1977) [55]	Detection threshold	Optical	SD
	Kron (1980) [38]	Profile fitting	Multi-band	FSD
	Buonanno (1983) [12]	Detection threshold	Multi-band	SD
	Stetson (1987) [78]	Profile fitting	-	SD
	Vikhlinin (1995) [87]	Detection threshold	X-ray	SD
	Kaiser (1995) [37]	-	Multi-band	SD
	Damiani (1997) [16]	Detection threshold	X-ray	SD
	Mighell (1999) [44]	Profile fitting	-	SD
	Vielva (2003) [86]	-	Radio	PSD
	Hobson (2003) [30]	Profile fitting	-	SD
	López-Caniego (2005) [41]	Profile fitting	-	PSD
	González-Nuevo (2006) [24]	-	Radio	PSD
	Savage (2007) [69]	Profile fitting	Infrared	SD
	Feroz (2008) [21]	Profile fitting	-	SD
	Peracaula (2009) [64]	Contrast radial function	Radio	FSD
	Carvalho (2009) [15]	Profile fitting	Optical	SD
Broos (2010) [11]	-	X-ray	SD	
Other	Andreon (2000) [2]	Neural networks	Multi-band	SD
	Liu (2003) [39]	Neural networks	Multi-band	SD
	Aptoula (2006) [3]	Watershed transform	Multi-band	SD
	Perret (2010) [68]	Connected Component trees	Multi-band	SD
	Torrent (2010) [83]	Boosting	Radio	FSD

### 3.2.1 Pre-processing

Before putting in practice some of the processing steps to the images, some operations may be applied to them in order to suppress undesired distortions or enhance some features to further processing. Pre-processing steps, transform raw images in some way, and as a result, new images with the same information content that the original ones, but with better conditions, are created. Thus, the images are adapted to facilitate the posterior analysis, and to get better results. In astronomical imaging, the objectives of pre-processing are, for instance, to reduce the noise, to estimate the background, or to emphasise the objects. We have classified the literature works in four main groups: basic pre-processes, Bayesian approaches, matched filter-based methods, and multi-scale approaches. Notice that the basic pre-processes group is a mixture of common techniques that are also used in combination with some other methods. For instance, the median filter is used in combination with either morphological operators or matched filter or multi-scale methodologies.

#### Basic pre-processes

We begin the pre-processing review with a range of techniques that, although being simple, offer a good performance, and hence, they are widely used in the whole computer vision domain. These techniques perform small modifications in the image that facilitate the following processes. In astronomical images, they are basically used to reduce noise and to estimate background.

Simple filtering techniques as median or average are used for many authors. They consist of a sliding window centred on a pixel that compute one of the statistics mentioned for all the pixels in the window, and finally replacing the central pixel for the computed value. For instance, the median filter was used for Damiani et al. [16] and Makovoz and Marleau [42] to estimate the background level and to minimise the effect of bright point source light, and also for Yang et al. [89] and Perret et al. [67] to reduce noise. Moreover, with these two purposes, Herzog and Illingworth [29], Mighell [44], and Freeman et al. [22] used the mean filter. Notice that in some cases pixels in the window with high values are removed to avoid biased values.

Background estimation is a common step in astronomical object detection. A good way to carry out this task is just as the way how well-known extraction packages as Daophot (Stetson [78]) and SExtractor (Bertin and Arnouts [7]) compute the background map. Their local background estimation is performed by applying iteratively a thresholding

based on the mean and deviation, that eliminated outliers. Afterwards, a value of the true background is calculated as a function of these statistics (Stetson suggested  $3 \times median - 2 \times mean$ , while Bertin suggested  $2.5 \times median - 1.5 \times mean$ ). Some authors refer to this background estimation as  $\sigma$ -clipping. Other authors as Vikhlinin et al. [87] and Perret et al. [67] also used this method.

Following with the background estimation, some authors [23, 33, 71] mentioned that they have used a method that Bijaoui [8] presented more than twenty years ago. This method was based on a Bayesian estimation of the intensity at each point using the histogram of the densities. Then, a model of this histogram was built, taking into account the granulation and the signal distribution, and obtaining the best threshold to separate the sky from the foreground. Although at the beginning was a common background estimation strategy, it became weaker due to its high computational cost.

Sometimes, when background presents large variations or the level of noise is high, a background subtraction is applied (as [23, 71]). Thus, after the subtraction, the source detection process becomes easier. Usually, the background subtraction is performed from the background estimation, removing those pixels considered as background. Differently, Haupt et al. [27], developed a method so-called “distilled sensing”, which was based on the idea of ruling out the regions where the signal (sources) was not present, and then focusing to the rest of regions. They iteratively perform thresholdings to discard regions where the signal was absent, and then, the source detection was intensified at the not discarded regions.

Another common pre-processing step is to convolve the image with a Gaussian profile. In optical imaging, this process can be understood as an approximation to model the PSF to the image pixels, and thus, obtaining a new map with the probability that each pixel has to be part of an object. Gaussian fitting can be computed subtracting the mean of the sky and dividing by the Gaussian deviation. As Stetson [78] mentioned, Gaussian fitting is equivalent to go through each pixel and ask the question: If there is an object centred on this pixel, how bright is it? A numerical answer of this question is estimated by fitting a Gaussian profile: if a star is truly centred on that pixel, it becomes a positive value proportional to the brightness of the object. Otherwise, the pixel value becomes close to zero or negative. Szalay et al. [79] and Hopkins et al. [31] also applied this strategy to multi-band and radio frequency images. Moreover, Damiani et al. [16] in their multi-scale approach, applied a Gaussian filter to the image in order to smooth the spatial variations of the background. Slezak et al. [71], also applied this convolution to optical images in

order to enhance very faint objects.

Furthermore, Gaussian models may be also used to remove noise, especially in high frequency images (X-ray, Gamma-ray, etc.), where most of the image is quite noisy. Modelling the intensity of the image pixels as a Gaussian, the bell-shaped zone may be considered as noise, while the rest of the distribution may represent background and objects. This noise removal by Gaussian fitting of the histogram was used by Slezak et al. [71], and more recently by Peracaula et al. [66, 65].

Morphological operations are another typical pre-process step used in computer vision. These operations are typically used in binary images and therefore may seem useless in a pre-processing step, since the initial image hardly ever is binary. However, a generalisation to grey-scale images allows to apply the morphological pre-processing step in these type of images. The two main operations in morphology are dilation and erosion. In binary images, white pixels are considered foreground, while black pixels are considered background. As its name suggest, dilation expand white pixels replacing the patch around the pixel for a given structural element (SE - another patch, with a specific shape), while erosion compress the foreground by replacing a patch that match with the SE to a unique white pixel. In other words, dilation add pixels to the foreground edges, while erosion remove pixels from the edges. The combination of dilate and erode (in this order) is called “close” operation, whereas the inverse process is called “open” operation. In grey-scale morphology, structural elements are defined as functions.

Among the works that have used morphological grey-scale pre-processing step we find Aptoula et al [3] and Yang et al [89], who reduced the noise and enhanced the image by computing open and close operations. Another work based on morphology is the one proposed by Perret et al. [67]. They proposed the use of the hit-or-miss transform (HMT) at grey level. The HMT is a morphological operator dedicated to the template matching that uses an erosion and a pair of disjoint structuring elements. In this transform, the image is convolved with two different SE types: while the first one is used to match the object shape (foreground), the second one is used to match the spatial neighbourhood of this shape (background). In the approach of Perret et al., the SE corresponding to foreground and background are patches of objects with variations in orientation and elongation convolved with a Gaussian filter to simulate the PSF. A different grey level according to the background estimation is given to these patches to get, on the one hand, the foreground SE, and, on the other hand, the background SE. After background estimation and noise reduction, the two SE are convolved to the image and the output score image can easily

be thresholded.

### Bayesian approaches

In the current literature we find some authors that propose approaches based on Bayesian methodology. The goal of these approaches applied to the astronomical field, is to prepare the data in order to establish the probability that it has to be either object or background. In other words, their objective is to provide a probability map with higher values in the zones where an astronomical object is more likely to be placed, and lower values in the zones that are more likely to be sky. Bayesian approaches are based on the widely used Bayesian inference, where a set of evidences or observations are used to update the probability that a hypothesis can be true. Bayesian inference tries to estimate the values of a set of parameters  $O$  in some reasonable model (or hypothesis) of the data  $I$ . For any given model, an expression for the probability to obtain the data set given a particular set of values for the parameters (this is so-called likelihood) must be considered. Moreover, a prior probability of the parameters based on some knowledge regarding their values before analysing the data must be imposed. The Bayesian approach consists of constructing the conditional probability density relationship:

$$p(O|I) = \frac{p(I|O)p(O)}{p(I)} \quad (3.1)$$

which gives the posterior distribution  $p(O|I)$  in terms of the likelihood  $p(I|O)$ , the prior  $p(O)$ , and the evidence  $p(I)$ .

Usually, for the purpose of estimating parameters, the evidence is set as a constant value, and for these reason it is usual to talk about unnormalised posterior distribution. It is called maximum-a-posteriori solution (MAP), and we can see it as a maximisation over  $O$  that involves a maximum likelihood and a prior:

$$MAP(O) = \max_O p(I|O)p(O) \quad (3.2)$$

In the likelihood, if we are able to assess it, then (after applying a prior) we will be able to have the posterior probability, which is the result we found. It expresses the probability of the data  $I$  given any particular set of parameters  $O$ . In practice, often the likelihood is based on an exponential function which involves the data (the different pixels), the signal contribution and the noise model (Gaussian, Poisson, etc.).

Referring to the prior knowledge, noise characteristics and the PSF can be used. Any other fit parameters can also be assumed. For example, source position and amplitude may have already been determined in another observing band.

Some of the authors that have employed this Bayesian methodology are Hobson and McLachlan [30], Savage and Oliver [69], and more recently Feroz and Hobson [21], Carvalho et al. [15], and Guglielmetti et al. [26]. Hobson and MacLachlan [30], studied two alternative strategies to perform the detection of discrete objects: the simultaneous detection of all the discrete objects in the image, and the iterative detection of objects one by one. In both cases, the parameter characterisation of the objects of interest was carried out by means of Markov-chain Monte Carlo sampling (MCMC) (see Hobson and MacLachlan, Savage and Oliver, and references therein to know more about MCMC). Using MCMC they could sample numerically from an unnormalised posterior distribution. They used as prior knowledge the mean estimation of the number of objects per image (an empirical value). For instance, in the iterative detection method proposed by Hobson and MacLachlan, this value was set to 1, because it was the number of objects to found at each iteration. In a similar way, Savage and Oliver [69], developed a filter to source detection (and also to simultaneously background estimation) in infrared images. Also using MCMC, they tried to determine the related probability at each pixel to be described by two different models: empty sky and point source in uniform background. Calculating the maximum posterior value for each model (using the PSF as prior knowledge), a map with the probability of where a point source was more likely to be placed was generated.

On the other hand, Feroz and Hobson [21], followed the Hobson and McLachlan approach, but they replaced the MCMC by other Monte Carlo technique so-called nested sampling. They used it to calculate the posterior distribution as a by-product. In a quite similar way, and also following the Hobson and McLachlan approach, Carvalho et al. [15] proposed a method to object detection called PowellSnakes, computationally faster than Bayesian methods based on MCMC. In their approach, sampling was skipped and the detection method was directly applied to the posterior. An estimation of position, amplitude, and spatial shape of sources was estimated to be used as prior knowledge. Guglielmetti et al. [26] applied their Bayesian source detection method to X-ray images. They used two different kinds of prior knowledge: exponential and inverse-Gamma function as probability density functions of sources, and a two-dimensional Thin Plate Splines (TPS - see references in Guglielmetti paper to know more about TPS) to represent the background.

### Matched filter

As we already mentioned, the purpose of applying a filtering step is to emphasise objects and to reduce the background fluctuations. The most commonly used filter to solve these two problems is the matched filter (MF). This filter convolves the image with the profile of objects that are expected to be found (e.g. PSF for detection of point sources or other patterns to extended sources). In addition, the MF may also be used to subtract the background locally, and it is also a filter to consider when the images present quite amount of noise.

Many authors have proposed to filter the raw image with a MF before applying a method to perform the object detection. In the decade of the eighties, Irwin [33], suggested the use of the seeing function<sup>1</sup> as a MF to detect faint sources in a noisy background. The seeing function might be obtained either directly averaging suitable stellar profiles or by an analytic model fit to these profiles. A background estimation (following the Bijaoui method [8]) was also computed previously to correct spurious values and to homogenise the sky. The MF allowed to increase the SNR, so the sources and the background were easily separated by a thresholding.

Vikhlinin et al. [87] proposed a similar strategy focused on X-ray data that, first of all, generated a background map by a sliding box thresholding that detected the brightest sources for then being removed. Afterwards, a MF defined as a piecewise function was applied to the residual image. Depending on two thresholds (obtained with the background estimation), the current pixel was convolved with a different function branch in order to differentiate sources and background. Pixels that were candidates to be sources were convolved with the instrument PSF, whereas pixels that were candidates to be background were convolved so that their values were zero or negative. Thus, a detection method could be applied to the resulting image. This process is repeated iteratively until a stop criterion is reached.

Another approach based on MF was developed by Makovoz and Marleau [42]. It was included in the Mopex package for astronomical image processing. To detect point sources, first and foremost, the background was subtracted from the image by locally calculating the median, and subtracting it from the current pixel. Then, a MF based on point response function<sup>2</sup> (PRF - not to be confused with PSF) was applied to the background-subtracted

---

<sup>1</sup>An astronomical term referring to the blurring and distorting effect caused by the atmosphere in astronomical object images.

<sup>2</sup>A table of values of responses of the detector array pixels to a point source.

image. With the background subtraction step, some bright sources could be extracted, and using patches of these sources, the PRF could be estimated. The detection process was repeated iteratively, and thus, the PRF could be refined with the new sources extracted.

In the literature, some authors have used MF with multi-band images, the so-called matched multi-filters. For example Melin et al. [43], used this extension of the MF to detect clusters. Each band was convolved with the corresponding filter (they used knowledge of the cluster signal, such as its spatial and spectral features at each band), and a unique filtered image was produced by combining all filtered bands. In a similar way, Herranz et al. [28], introduced what they called matrix filters (or matched matrix filters). The main difference was that they convolved each band with its corresponding filter, but a filtered image per band was generated so a final choice of which filtered bands were better to perform the detection step was needed.

### Multi-scale approaches

In Computer Vision, the concept of multi-scale (or multi-resolution) is often used when the image to be segmented shows objects with very different sizes or patterns organised in a hierarchical structure. In astronomical image processing, multi-scale approaches have been extensively used during the last fifteen years, mainly due to the fact that in many cases, they outperform other strategies based on more basic techniques.

Astronomical data generally has complex hierarchical shapes, and for this reason a more suitable way to represent it is in the multi-scale space. Thus, images are decomposed into components at different scales (different spatial frequencies), and objects become emphasised in some scales. Depending on the nature of the objects, they may appear in more or less scales, and closer to low or high frequency scales. Once the decomposition is done, a basic detection algorithm can be applied in the different scales, as if they were single-scale images.

In other words, multi-scale strategies optimise the analysis and detection of astronomical objects, however complex they may be. Among their applications, we find denoising, source deblending<sup>3</sup>, inpainting<sup>4</sup>, among others.

Several multi-scale decompositions are used in the literature, being the wavelet transform the most used by far. This transform and other multi-scale approaches focused on the detection of astronomical objects are commented below.

---

<sup>3</sup>An astronomy technique to isolate overlapped sources.

<sup>4</sup>The process of reconstructing missed or deteriorated parts of images.

### The wavelet transform

If we deal with multi-scale astronomical imaging, we have to unavoidably talk about the wavelet transform (WT). It is the commonly multi-scale technique used in the so-called Multiscale Vision Model (MVM) [10]. The most used transform is the Stationary Wavelet Transform (SWT), more commonly known as “à trous” algorithm (that is the French translation of holey, which means that zeros are inserted in the filters), an extension of the Discrete Wavelet Transform designed to overcome the lack of shift-invariance. Since astronomical sources are mostly isotropic<sup>5</sup> (such as stars) or quasi-isotropic (such as galaxies or clusters), the SWT does not privilege any direction in the image and maintains the sampling at each scale.

The SWT of a signal produces  $J$  scales  $W_j$ , and each scale is composed of a set of zero-mean coefficients. Moreover, a smoothed array is generated using a smoothing filter  $h$  (associated with the wavelet scaling function) in the following way:

$$I(k, l) = F_J(k, l) + \sum_{j=1}^J W_j(k, l) \quad (3.3)$$

where  $F_J(k, l)$  and  $W_j(k, l)$  are calculated through the following iterative process:

$$\begin{aligned} F_0(k, l) &= I(k, l) \\ F_j(k, l) &= \langle H_j, F_{j-1} \rangle(k, l) \\ W_j(k, l) &= F_{j-1}(k, l) - F_j(k, l) \end{aligned} \quad (3.4)$$

with  $j = 1, \dots, J$  and

$$\langle H_j, F_{j-1} \rangle(k, l) \equiv \sum_{n, m} h(n, m) F_{j-1}(k + 2^{j-1}n, l + 2^{j-1}m) \quad (3.5)$$

The set  $W_1, W_2, \dots, W_J$  together with  $F_J$  represent the wavelet transform of the image as can be seen in Figure 3.1.

The discrete filter  $h$  is derived from the scaling function, and as suggested Stark and Murtagh in [77], a good choice for  $h$  is to use a spline of degree 3, and therefore, the mask associated to the filter takes the following form:

---

<sup>5</sup>Uniformity in all orientations. In our case, it means that an astronomical object emits light uniformly in all directions.

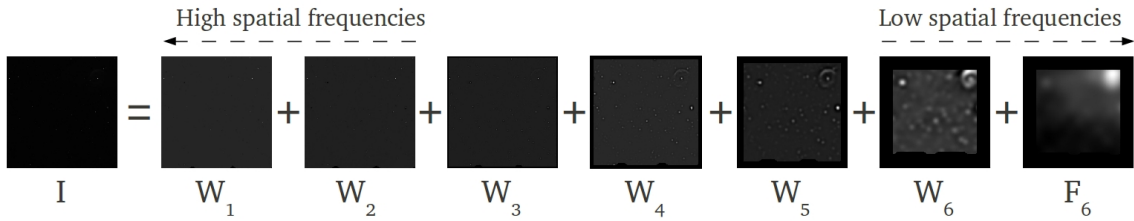


Figure 3.1: A 6-scale wavelet decomposition.

$$h \equiv \frac{1}{256} \begin{pmatrix} 1 & 4 & 6 & 4 & 1 \\ 4 & 16 & 24 & 16 & 4 \\ 6 & 24 & 36 & 24 & 6 \\ 4 & 16 & 24 & 16 & 4 \\ 1 & 4 & 6 & 4 & 1 \end{pmatrix} \quad (3.6)$$

There are a lot of extensions of the WT, that are more suitable depending on the detection goal. For example, Damiani et al. [16] proposed a method based on the Mexican hat wavelet transform (MHWT - a special case of the family of continuous wavelets obtained by applying the Laplacian operator to the 2D Gaussian, that takes its name from its graphical resemblance to a typical Mexican hat as we can see in the Figure 3.2; for more information about it see [37, 16, 22], and references therein) to detect sources in X-ray images. Also other works used this kind of WT, as the Vielva et al. [86] one, that in order to detect point sources in all-sky radio frequency maps, used the spherical Mexican hat wavelet transform (an MHWT extension for spherical functions). More recently, Starck et al. [76] proposed a source detection approach based on the multiscale variance stabilisation transform (MSVST - based on differences of two consecutive WT scales) applied to gamma-ray images. Kaiser et al. [37], pioneered using WT to astronomical object detection. Specifically, they used the MHWT in multi-band images to emphasise faint objects.

As the pre-processing and the detection in multi-scale approaches are quite linked, and sometimes one step overlaps the other, more information about these type of methods is available in Section 3.2.2.

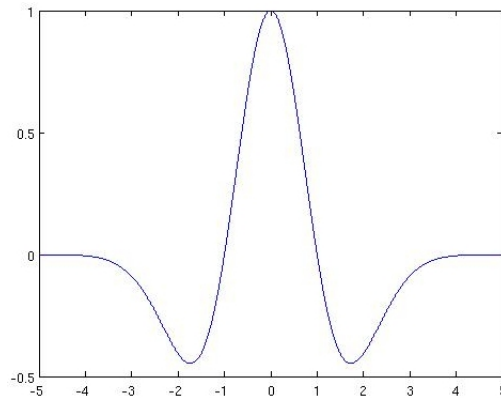


Figure 3.2: The appearance of the MHWT.

### Multi-scale decomposition for anisotropic data

While wavelets have a good performance with isotropic features, they are far from optimal with anisotropic objects. Because of this, the astronomical community has had to find alternatives. Some multi-scale methods have demonstrated that represent well the anisotropic features.

To overcome the weakness of wavelets in anisotropic data, Candès and Donoho [13, 14] proposed two new methods of multi-scale representation so-called curvelet and ridgelet transforms, which are very different from wavelet-like systems. Curvelets and ridgelets take the form of basis elements which exhibit high directional sensitivity and are highly anisotropic. For instance, in two dimensions, curvelets are localised along curves, in three dimensions, along sheets, etc. The ridgelet transform can effectively deal with line-like phenomena in two dimensions, plane-like phenomena in three dimensions, and so on.

In practice, the continuous ridgelet transform (CRT) is used. Its idea is to apply the Radon transform (see [13] and references therein to more information about this transform) and perform a wavelet analysis in the Radon domain. Thus, the image is represented as functions with simple elements that are in some way related to ridge functions. CRT is therefore optimal to detect lines and segments in images.

Curvelets are also an extension of the wavelet concept. The idea of the curvelet transform is to first decompose the image in different scales, and then analyse each scale by means of a local ridgelet transform. They have strong directional character in those elements that are highly anisotropic at fine scales. Hence, for specific astronomical data containing edges (planets surface, for example), curvelets are the best choice because they

provide a mathematical representation that is ideally adapted for representing objects with curved shapes.

As sometimes isotropic and anisotropic data are present in images, combined approaches may be the best solution. Hence, a perfect multi-scale decomposition should benefit from both the wavelet advantages and the ridgelet or curvelet transforms (or maybe others) ones as well. In practice, these combined approaches are the ones that are actually used, instead of using uniquely curvelets or ridgelets. For instance, Starck et al. [72, 75] proposed, on the one hand, combinations of wavelets and ridgelets and, on the other hand, combinations of wavelets and curvelets to detect objects in infrared data. In another work, Belbachir et al. [5] suggested the combined use of WT and contourlet (see the Belbachir paper and references therein to know how contourlets work) for faint source detection also in infrared images. Contourlet is a filter bank transform that can deal with smooth images with smooth contours, so it is similar to the curvelet transform.

### 3.2.2 Detection criteria

As we have seen, pre-processing techniques provide a new image or map ready to be processed. From this point, a detection method is ready to be applied to the images. In most of the reviewed works, thresholding and local peak search are the detection criteria chosen. However, other remarkable works that include other detection strategies are also commented. We analyse how they work and which considerations have took the authors that have used them. We also review a detection model used in multi-scale images so-called Multi-scale vision model.

#### Thresholding

In computer vision, thresholding is a simple method to perform image segmentation. Using this method, a grey-scale image is converted to a binary one where the pixels have only two possible values: 0 or 1. These two values are assigned to pixels which intensities are below (0) or above (1) an specified threshold. In astronomical images (and in many other fields), thresholding is used to decide which regions (connected pixels) are considered as objects and which ones are considered as background.

Defining an appropriate threshold is not an easy task due to several factors like noise, background variations, or diffuse edges of the objects. Any chosen threshold may result in some truly objects overlooked (false negatives) and some spurious objects considered as

real (false positives). Varying the threshold to the extremes minimise one of these types of errors, but the other is maximised. Hence, the difficulty relies on setting the threshold in order to get the two errors as small as possible.

In the reviewed papers, the authors have fixed the threshold with several different strategies. For example, Irwin [33] and Freeman et al. [22] set the threshold depending on the sky estimation computed, while in the Starck et al. [73, 76] approaches, the threshold was set depending on the noise (as a multiple of the noise estimation). In the Szalay et al. [79] work, as they modelled the sky as a  $\chi^2$  distribution, they get the threshold value in the intersection point between the theoretical distribution and the data real distribution. In a different way, Slezak et al. [71] and Herranz et al. [28], determined the threshold by the distribution of the peaks previously found. They set the threshold at 3.8 and 5 times the deviation of the peak distribution, respectively. Hopkins et al. [31], moreover, used a method so-called False Discovery Rate (FDR), a method that select a threshold that controls the fraction of false detections (see the Hopkins paper for more information about FDR). Haupt et al. [27], also used a threshold obtained through FDR after ruling out regions without sources with their “distilled sensing” method.

However not all the methods are fully automated. For instance, source extraction packages as SExtractor (Bertin and Arnouts) and Mopex (Makovoz and Marleau [42]) used user-specified thresholds (for example SExtractor gives the possibility of setting the threshold to an absolute value or as a multiple of the background level). In these tools, when a source is considered too large, which may be assumed that is a cluster of sources, the threshold is raised in order to detect the sources independently.

Mainly due to the background variations, a common practice in astronomical image detection is a local or adaptive thresholding: a different threshold is used for different regions in the image. Typically, it can be computed using a sliding window. For example, Jarvis and Tyson [34], adapted the threshold as the window progress. Starting with an specific threshold, if pixels in the window were lower than the threshold (so they were considered as sky), the threshold value was updated with the sky value of these pixels. Another way to fix locally the threshold was how Le fèvre et al. [23] did. They computed the histogram of pixel intensities at each window, and set the threshold at 1.5 times the deviation distribution. Another possibilities are recently proposed by Peracaula et al. [66, 65], where the local threshold was defined by means of the local noise determined by the pixel intensity histogram, or by Melin et al. [43], where a multiple value of the SNR was used. Yang et al. [89], used a popular method to automated threshold calculation

called Otsu [60], where the intra-class variance is minimised to get a good threshold.

### Local peak search

The main principle of the local peak (or maxima) search method, consists in searching those pixels that are considered peaks, or, in other words, those pixels that are a local maximum in a neighbourhood. In most cases, to avoid the unnecessary analysis of all the pixels, only those peaks that are above a given threshold are considered. When this detection method is used, it is often accompanied with a pre-processing step that enhance the peaks to find, and another step computed after the peak search, that establish or correct the pixels around the peak that belong to the object. Many times, this last step is a fitting process, which is possible because the nature of the objects is well known. So the local peak search as such, provides a list of candidates that can be the central points of an object. For this reason, this method is typically used as the previous step to the photometry calculation. The local peak search is more appropriate to detect stars and other point sources, and is not well suited to detect complex objects (like galaxies and other extended sources).

This method was already used in the late seventies, with the works of Herzog and Illingworth [29], and Newell and O’Neil [55]. They defined a peak as a pixel with its intensity greater than or equal to their eight adjacent pixels (8-connectivity) and over a threshold based on the sky level computed. Therefore, the objects were the connected regions centred on a peak. They computed some tests to deblend objects (connected regions with more than a peak), as Data Over Gradient (DOG) test (see [29, 55] and references therein for more information about this test). Also Buonanno et al. [12] searched peaks over the sky level (in windows of  $N \times N$ ), and all the pixels connected to the peaks above a certain threshold, were added to make the corresponding objects. Vikhlinin et al. [87], in X-ray images, considered a pixel as maximum if it was greater than its 25 neighbours and also above a threshold (based on the background).

In several approaches, once the peaks were found, a known distribution around them was fit. In this sense, Kron [38], opened windows of  $50 \times 50$  around the maximums found, computed the histograms, and selected the distribution (between two different light distributions that model faint and bright sources) that best fit the histograms. In a similar way, Savage and Oliver [69], opened a window for each peak in infrared images, and selected the distribution (among sky, point-shaped source, or extended source) that best fit. López-Caniego et al. [41], searched for local maximums, and distinguished the ones

caused by the presence of sources. This distinction was achieved by a Neyman-Pearson detector (that set out the problem as a constrained optimisation problem), that considered peak densities which leads to an optimal distribution that fit the source in amplitude and curvature (see references in [41] to know more about this method). Other works used for example statistics of sharpness and roundness, and PSF fitting (Stetson [78] in its Daophot software), or analysis of annulus surrounding the peaks to determine what was background and what was source (Mighell [44]).

Some Bayesian approaches as [30, 21, 15] used local peak search. In most cases a local Gaussian was approximated to the peaks in order to define their amplitude. In a slightly different manner, Peracaula et al. [64], recently defined a “contrast radial function” (that relate the central pixel intensity with the mean of its neighbours intensity in a given radius) in different radial distances. First, a low local thresholding was computed to the raw image and a first degree polynomial of the “contrast radial function” was fit to each pixel with intensities over the threshold. The goodness of the fit was given by the slope of the polynomial. The groups of at least four connected pixels with a slope larger than a certain threshold were considered as objects.

### Multi-scale vision model

The multi-scale transform by the “à trous” algorithm, decomposes an image  $I(k, l)$  in  $J$  scales or wavelet planes  $w_j(k, l)$  and segment independently each of these images representing a scale. Each scale has the same number of pixels as the image. As we already mentioned, the original image can be expressed as the sum of all the wavelet scales and the smoothed array  $F_J$ :

$$I(k, l) = F_J(k, l) + \sum_{j=1}^J W_j(k, l) \quad (3.7)$$

A further step is to consider a multi-scale object representation, which associates an object contained in the data with a volume in the multi-scale transform. This representation requires the application of a segmentation method scale by scale. A general idea for object definition lies on the connectivity property. An object is located in a physical region, and the pixels of its region are connected to other significant adjacent pixels. This connectivity is present both in the same scale and in the contiguous scales. Therefore, this is exactly what multi-scale vision model (MVM) [10] does.

These are the steps that the MVM follows:

1. The WT with the "à trous" algorithm is applied to an image.
2. A scale by scale thresholding procedure is performed, obtaining the objects segmentation at each scale.
3. In order to define the objects structure, an inter-scale connectivity graph is established.
4. An object identification procedure extracts each connected sub-graph and considers them as objects.
5. Finally, from each set of pixels an image of the object can be reconstructed using some kind of reconstruction algorithms.

So at each scale, the so-called significant wavelet coefficients (values in a wavelet scale above a given detection limit usually dependent of the noise model) are searched. At each scale we have a boolean image with pixel intensity equals 1 when a significant coefficient has been detected, and 0 otherwise. Afterwards the segmentation is applied by labelling the boolean values (each group of connected significant coefficients gets a different label). An inter-scale relation between two labelled zones in two adjacent scales exists if the maximum significant coefficient of the first one lays into the the region of the second one in the next scale. Therefore, an object is defined as a set of inter-scale relations having a graph structure. A representation of this inter-scale connectivity graph is shown in the Figure 3.3.

This pipeline and similar ones based on WT, have been used as reference work in a lot of posterior multi-scale approaches. For example, in the Damiani et al. [16] approach, after applying a Gaussian fitting and a median filter, they applied the MHWT to the image, and then, local peaks over a significant threshold were considered as sources if they amplitude were significant with respect to the expected fluctuations of the local background. Very similar to this approach we find the Freeman et al. [22] one. They differ in the background estimation, since they carried this step out at each wavelet scale by an average filter and weighting the resulting values with the negative wings of the MHWT. In addition, they proposed a post-processing step that analysed some properties of the detected sources and rejected the ones that were considered as spurious.

Similar to the Bijaoui and Rué work, we find Starck et al. [73], who used the MVM for a decomposition of the signal into its main components. Moreover, Broos et al. [11], recently developed a wavelet-based strategy to find sources in X-ray images from the

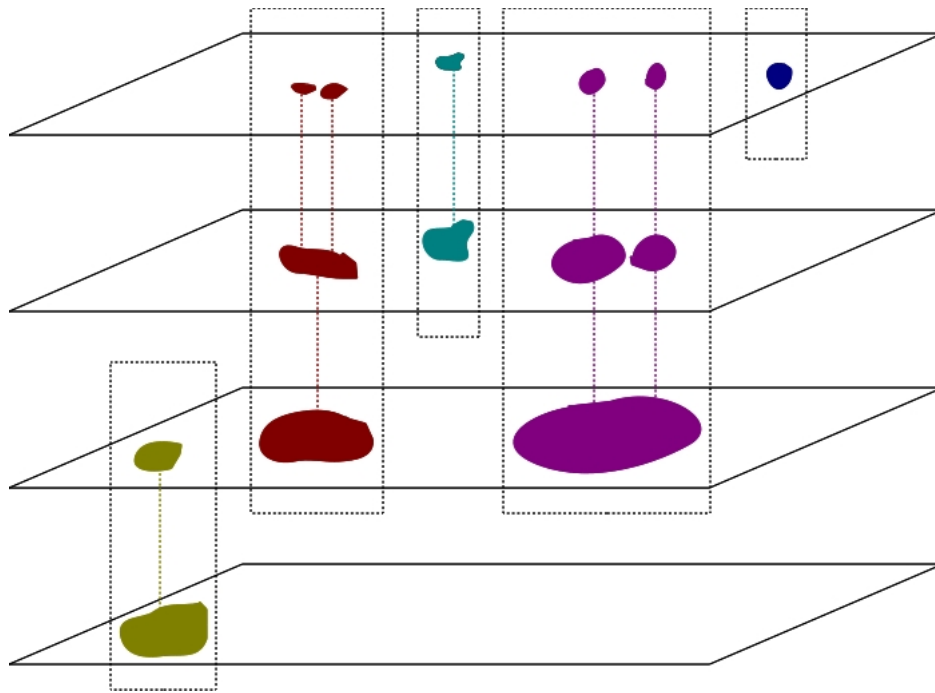


Figure 3.3: An example of the connectivity in the wavelet scales. Adjacent significant coefficients in a scale and between contiguous scales are considered part of the same object.

Chandra telescope. The image was deconvolved using the WT and reconstructed again to smooth the PSF effects (using a reconstruction algorithm called Richardson-Lucy that is explained in [11] references). A candidate list of sources was created by locating peaks in the reconstructed image, and if those peaks fulfilled a number of properties, they were considered as sources, or rejected otherwise.

Nevertheless, the whole MVM process is not required. Executing the detection process in only few scales instead of in all, often may be enough. In the work of Kaiser et al. [37], the source positions and sizes were simply identified by locating peaks at their scales of maximum significance. Vielva et al. [86], deconvolved all-sky surveys with the SMHWT, and proposed to divide the image in different regions, estimating the optimal scale at each region. González-Nuevo et al. [24] also decided to apply some extensions of the MHWT to radio maps. They proposed to use the Mexican hat wavelet family (MHWF - a range of MHWT obtained by applying another Laplacian operator to the MHWT, and repeating this process iteratively) to detect point sources by selecting the optimal scales of different MHWT of the family (they tested the first four members of the family). They finally applied a local peak detection. In a similar way, Starck et al. [76] used the MSVST and a

thresholding was computed in those scales with significant wavelet coefficients, for finally reconstructing the image.

Another way to deal with WT is detecting the objects in specific scales according to the detection purpose. In this sense, during the last few years, Peracaula et al. [66, 65] selected different scales depending on whether the sources to search were extended or point-shaped. As we already mentioned, depending on the type of sources, they appear in lower or higher scales. Peracaula et al. first of all, computed a thresholding to the raw image in order to detect the brighter point sources, and they generated two images: a residual image where bright sources were substituted by local noise, and a binarised image with the bright sources. A WT was then applied to the residual image and different strategies were followed according to the sources to find. On the one hand, in [66], they tried to identify faint point sources, so they decided to use the first three wavelet scales (the higher spatial frequency scales). On the other hand, in [65], they tried to find extended structures, so they decided to focus the detection in the last wavelet scales (the lower spatial frequency scales). In both cases, the selected scales were thresholded, and a binary image was reconstructed from the addition of the binarised scales (in the first case the binary image with the extracted bright sources was also added with the purpose of detecting both bright and faint sources).

### **Other detection methods**

Even though most of the classical approaches are based on thresholding and local peak search, there are other strategies that have been followed to detect astronomical objects. In many cases these approaches have been developed during the last few years, and they are more focused in the techniques from the computer vision field.

For example, Andreon et al. [2], turned the object detection problem into a classification one. They classified the pixels as if they were considered to belong to the class object or to the class background. This task was achieved using a kind of neural networks (so they named this package NExt, from NEural Extractor) so-called Principal Component Analysis Neural Networks (PCA-NN), used to reduce the dimensionality of the input data by eigenanalysis (basically selecting the principal vectors). What they did was to train a PCA-NN with patches of the representative zones of the image, and a vector with less features than the input one was returned. Afterwards, this output became the input of an unsupervised neural network, which was responsible to classify the pixels between object and background. Based on this detection approach, Liu et al. [39], proposed to change

the PCA-NN used by Andreon, to local Principal Component Analysis (a kind of PCA that clusters the input data and find the principal vectors for each cluster). They used the local PCA to automatically extract features of the image. A clustering process was then computed, and from these clusters the pixels were classified.

Aptoula et al. [3], after the application of morphological operations, segmented the image with the “watershed transform”. Notice that in this case, the images contained only one object to segment, mainly galaxies. This unsupervised segmentation acts as a drop of water falling on a topographic relieve corresponding to the image (every grey level may be considered as a height in the relieve). Placing a water source in each regional minimum, the relieve is flood from sources, and barriers are built when different sources are going to merge. To avoid oversegmentations, Aptoula only considered few marked minimums as water sources. Specifically two markers were used: one in the center of the object and another in a minimum external region (these two markers were found by thresholding and morphological techniques). Hence, a good segmentation between object and background was computed.

In a different way, Perret et al. [68] recently used Connected Component trees (CC-trees) to detect sources in multi-band images. CC-Trees have become popular models for the analysis of grey-scale images (the authors used an extension for multi-band images), since they provide a hierarchical representation of images that can be used to segmentation and object detection amongst other. The representation of a grey-scale image is based on the thresholding between its minimum and maximum grey levels (thresholding the image at different levels starting from the minimum value and increasing it until the maximum value is reached). There exists a relationship of the inclusion between components at sequential grey levels in the image. The root is the whole image and at every level of the tree, the different foreground regions are decomposed in some regions obtained with a higher threshold. Perret et al. proposed to equip the nodes with some attributes (multi-spectral information of the thresholded region), and then, they pruned the ones considered as irrelevant, to finally reconstruct the image. Therefore, the remaining nodes at significant levels were considered as sources.

Other machine-learning techniques were used as well, for instance, in the recent work suggested by Torrent et al. [83] to detect faint compact sources in radio frequency images. First of all, a set of local features (patches of faint sources) was extracted from different images convolved with a bank of filters, making the so-called dictionary. Afterwards the images were divided into two sets: the training and the testing sets. The images of

these two sets were characterised by convolutions with the bank of filters and with cross correlations with the dictionary images, obtaining therefore, probability images with high values in the regions similar to the patches. Finally a “boosting” classifier (this algorithm is based on the simple idea that the sum of weak classifiers can produce a strong classifier) was trained with the training set and the detection was performed in the testing set images.

### 3.3 Astronomical detection packages

There are several astronomical packages that provide tools to automatically perform source detection. In what follows, we review the main features of the most relevant astronomical packages. Notice that some of them have already been commented as works in the previous section.

#### **SExtractor**

SExtractor (from Source Extractor) [7] is a program that builds a catalogue of objects from an astronomical image. It is probably the most used package in source extraction due to its good performance. It was developed in 1996 mainly by Emmanuel Bertin, a member of the Institut d’Astrophysique de Paris. Using automated techniques, this package is able to deblend, measure and classify sources. The last SExtractor version released is the V2.8.6 and allows to input parametrisable commands. The whole set of tools that provide, allows to perform:

- Background estimation.
- Convolution with several masks.
- Source detection.
- Source deblending/merging.
- Photometry.
- Star/galaxy classification.

## SAD

SAD [58] is a utility of the Astronomical Image Processing System (AIPS) package to source recognition and fitting. AIPS was originally developed by the National Radio observatory (NRAO) [59], and therefore, is a suitable package to deal with radio images. The current version of AIPS is 31DEC11 and it is available in a command-line interface. The two main functionalities of SAD are:

- Source detection.
- Source fitting (Gaussian fit)

## Mopex

Mopex (MOsaicker and Point source EXtractor) [42] is a package developed in 2005 at the Spitzer Science Center to reduce<sup>6</sup> and analyse imaging data. The current version is 18.4.9, that comes with two different interfaces: GUI and command-line. The main functionalities of Mopex are:

- Point source extraction in a two-step process: point source detection and profile fitting.
- Source deblending.
- Photometry.
- Background and noise estimation.
- Mosaicking.

## Daophot

Daophot [78], is a package for stellar photometry designed by Peter Stetson at the Dominion Astrophysical Observatory [17] to deal with crowded fields. The current version is v1.3-2, and allows the users to interact with it by command-line interface. It allows to perform:

- Source detection.

---

<sup>6</sup>In many fields of computer science, the transformation of raw data into a more useful form.

- Photometry (PSF and profile fitting).
- Background estimation.

### **Wavdetect**

Wavdetect [22] is a wavelet-based source detection algorithm part of the Chandra Interactive Analysis of Observation (CIAO) software package. The current version available of CIAO is the 4.3, being also a command-line package. Wavdetect offers the following functionalities:

- Background mapping and correction.
- Source detection.
- Source extraction.

## **3.4 Reported results**

Since there are many papers that are not exclusively focused on astronomical object detection (as the ones that just make catalogues of new sources found, or the ones that are more focused on compute the photometry of the found sources), in this section we present only the results of those papers that have the source detection as their main objective. We describe the measures computed by these works to evaluate their performance. Finally, we also compare and discuss the results presented, pointing out their most interesting aspects.

### **3.4.1 Evaluation measures**

Each paper evaluates the results in a different way. Nevertheless, most of the results are measured in order to know which of the detected objects are truly objects. This validation is usually done by means of published catalogues or obtained from an astronomical package used as reference (e.g. SExtractor and SAD). In some cases, the validation of the real objects is done with the assistance of an astronomical expert, who considers the detections as either truly or spurious. Moreover, simulated images are widely used, since the simulated sources are placed in known positions, and therefore, it is easy to evaluate the

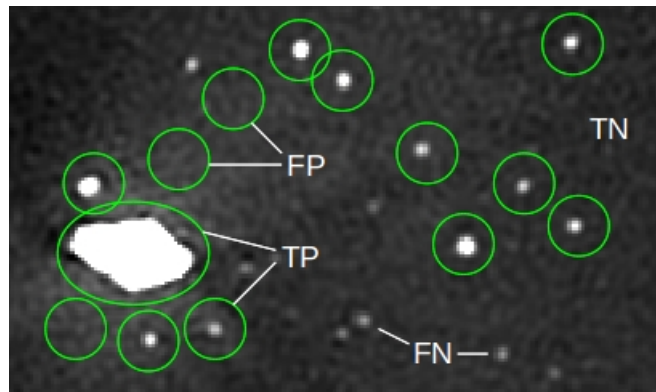


Figure 3.4: A simple example to explain TP, FP, FN, and TN measures. It symbolises the resulting image of an automated detection method. The sources detected by the method are underlined with green circles.

goodness of the results by checking the detected sources that match with the previously simulated.

Whether using a reference catalogue or simulated data as ground truth, an evaluation of the performance of the detection (and segmentation) methods is by computing true positives (TP), false positives (FP), false negatives (FN), and true negatives (TN). TP are detections that are true sources, FP are detections that are not true sources (so they are spurious detections), FN are true sources that have not been detected (they are missed by the method, and therefore, considered as background), and TN are background zones correctly considered as such. Figure 3.4 shows a simple example of these different measures. Obviously the objective is to obtain the maximum number of TP and TN, and at the same time the minimum number of FP and FN. However, in practice, increasing the number of TP usually increases the number of FP, while reducing the number of FN also reduces the number of TN. Therefore, an effort must be taken to set the parameters of the detection method in order to maximise TP and TN and to minimise FP and FN.

Reference catalogues may also be used to directly compare the performance of the methods. As the catalogues used as reference tend to be published in remarkable journals, they have a reliable list of sources, and therefore, they can be used to extract some measures between the reference sources and the detected ones. The two catalogues can be compared for example by the sources that coincide in both catalogues or by the sources that only appear in one. If in addition, more reference catalogues are available, cross comparisons may be performed, and for example, the goodness of the method can be estimated by com-

putting the number of missed sources (sources not being part of a catalogue but appearing in the rest of catalogues).

### 3.4.2 Analysis of the results

We provide a qualitative comparison of the results obtained from the approaches analysed. Table 3.3 summarises the evaluation measures and the catalogues or tools used as reference. A qualitative evaluation of these approaches is difficult to carry out because of the work has been done in different types of images and with different purposes.

Table 3.3: Summary of the results presented in the analysed articles. We show the source catalogues or the source detection packages used as reference (second column), the number of images used and if they have real or simulated (sim) origin (third column), the number of detected objects (forth column), the measures used to evaluate the results (fifth column), and the performance (last column). Notice that forth and sixth columns may have more than one value. Slashes separate (“/”) different experiments (as different parameter setting or different test images), while values in parentheses refer to the reference catalogues (in the same order that in second column). Value “n/a” means “not available”.

Article	Reference	Images	Detections	Measures	Performance
Slezak (1988) [71]	Manually	1 (real)	363	TP	353
				FP	10
Damiani (1997) [16]	MPE and WGA catalogues	7 (real)	453	Missed	10 (75,47)
Starck (1999) [73]	-	1 (sim)	46	TP	45
				FP	1
Andreon (2000) [2]	SExtractor	1 (real)	2742/3776	TP	2059/2310 (2388)
				FP	683/1466 (1866)
Freeman (2002) [22]	MPE and WGA catalogues	1 (real)	148	Coincidences	81 (12,27)
Perret (2008) [67]	Manually	18 (real)	17	Recall (%)	82%/87%
Peracaula (2009) [64]	Reference catalogue (SAD)	1 (real)	83	TP	70 (68)
				FP	13 (33)
Peracaula (2009) [66]	Reference catalogue (SAD)	1 (real)	86	TP	71 (68)
				FP	15 (33)
Guglielmetti (2009) [26]	Wavdetect	3 (sim)	100	TP	64/41/25 (56/37/23)
				FP	8/9/0 (4/1/1)
Carvalho (2009) [15]	-	3 (sim)	n/a	TP (%)	67.41%/56.41%/82.95%
				FP (%)	9.6%/8.62%/8.19%
Torrent (2010) [83]	Reference catalogue (SAD and SExtractor)	1 (real)	601	TP	505 (455,473)
				FP	96 (474,n/a)
Broos (2010) [11]	Reference catalogue	1 (real)	100	TP	89
				FP	11

Several works used TP and FP rates to evaluate the performance of their approaches. For instance, Slezak et al. [71], in the late eighties, first of all estimated by eye the different sources present in a wide field from Schmidt plates, and afterwards applied they detection method with different detection thresholds. As the threshold was raised, the number of detected sources increased, but also the percentage of well-detected sources.

The best results were obtained with a low threshold: from the 363 sources detected, 353 were TP and 10 FP. Starck et al. [73], created a simulated image of the ISO (Infrared Space Observatory) Hubble Deep Field, and after applying their approach, they detected 45 sources from the 46 generated (which means  $TP = 45$  and  $TN = 1$ ). Andreon et al. [2], tested several types of neural networks to a field from the Canadian Astronomy Data Center. This field has been widely studied, so they take an specific published catalogue as reference that consists of 4819 objects (with  $\sim 2400$  objects too faint to be visible). The best tests found 2742 and 3776 sources in the field, among which 2059 and 2310 were TP and 683 and 1466 were FP, respectively. Moreover, they applied the detection tool of the SExtractor package to the same field, obtaining a catalogue with 4254 sources, with 2388 TP and 1866 FP. Although SExtractor detected more sources (a quite similar number of sources that the one found by the reference catalogue), the absolute number of TP computed by Andreon et al. was slightly lower than SExtractor TP, and in the FP case, they were substantially lower.

More recently, Peracaula et al. [64, 66], tested their approaches on a deep radio map obtained by the Giant Metrewave Radio Telescope (GMRT). They compared their results with a reference catalogue that detected 101 sources (68 TP and 33 FP). Peracaula et al. approaches presented similar results, both outperforming the reference values (especially in terms of FP). In [64] they found 70 TP and 13 FP, whereas in [66] they found 71 TP and 15 FP. Torrent et al. [83] also used a radio map of the GMRT but covering a different region of the sky. They applied their method and the detection tool of SAD and SExtractor to the image, and compared the sources detected to a reference catalogue. Their approach achieved better results than SAD and SExtractor. While SAD obtained 455 TP and 474 FP, and SExtractor 473 TP (the number of FP was not available), they found 505 TP and 96 FP.

Guglielmetti et al. [26], used simulated images with 100 simulated sources and added to them three different levels of noise. They applied their method and obtained 64, 41, and 25 TP, and 8, 9, and 0 FP, respectively. They compared these results to the ones obtained with Wavdetect. With this package they found 56, 37, and 23 TP, and 4, 1, and 1 FP, respectively. Therefore, in terms of TP, Guglielmetti et al. obtained better results than Wavdetect, but not with FP. Carvalho et al. [15], also used three simulated images (the first two with 16 objects and the last one with 8). Their method was able to detect (in percentages) 67.41%, 56.41%, and 82.95% of the simulated sources (TP), and obtained 9.6%, 8.62%, and 8.19% of spurious detections (FP). They also estimated the performance of their method by an error computed by adding the number of FP and FN

(42.19%, 52.2%, and 25.15%, respectively).

There are other works that have used different ways to estimate their results. For instance, Damiani et al. [16], in order to compare the performance of their method on 7 images of the ROSAT satellite, used two published catalogues called MPE (286 sources in total) and WGA (389 sources in total) as reference, and counted the number of sources detected by two catalogues and missed by the other one. Their method detected 453 sources (244 coincidences with MPE, 272 coincidences with WGA, and 197 sources present in all catalogues). They found that their method missed 10 sources, less than MPE and WGA, which missed 75 and 47 sources, respectively. Freeman et al. [22], also used crossed comparisons between the sources found with their method in a ROSAT image and the ones found by MPE (100 sources found) and WGA (127 sources found). They found 148 sources, of which 81 appear in all three catalogues. The coincidences between their work and MPE were 97, while the coincidences with WGA were 108 (the coincidences between MPE and WGA were 84). Broos et al. [11], tested their local peak method in combination with Wavdetect to find 100 sources (50 with Wavdetect and 50 with their source detection method) in a map from the Chandra X-ray Observatory. They compared these sources with a reference catalogue and found 89 coincidences. Perret et al. [67], had a reference catalogue with 9 galaxies detected. To validate the good performance of their method finding galaxies, first of all, they tested their method on two images, and found 17 objects: 6 galaxies of the reference catalogue and 8 new sources that an expert considered also as galaxies. It means a recall (percentage of true detected galaxies) of 82%. Testing the method on 16 images they found a recall of 87%.

In some works, the performance depends on the selected parameter setting. For instance, in the approaches of Vielva et al. [86] and González-Nuevo et. al [24], they repeated several experiments with different thresholds until they got a rate of spurious sources lower than the 5% of the total number of sources detected. Moreover, these two approaches worked with images with several frequency channels, and therefore, a different threshold was needed at each channel. Vielva et al. used all-sky maps with 10 channels, and for example, in the three lower channels they obtained 27257, 5201, and 4195 sources, respectively. González-Nuevo et al. also performed this strategy in an image with 3 frequency channels, and for each channel they applied the first four transforms of the Mexican Hat Wavelet family. For example for the channel with lower frequency the sources detected were 543, 639, 583, and 418, respectively.

### 3.5 Discussion

As we have seen in this chapter, several strategies are used to face up the astronomical source detection. Most of them coincide in focus the detection on the intensity of the image pixels, whether in the pre-processing steps in order to enhance the sources with respect to the background, or in the detection process, choosing those pixels with an intensity value which suggests that they are likely to be part of an object. We have realised that all the different pre-processing and detection steps are used indistinctly in all types (all frequency bands) of astronomical images. An overview of the different techniques reviewed with their strengths and weaknesses are shown in the Table 3.4.

Regarding the astronomical images, two main drawbacks caused by the acquisition process hinder the detection purpose: the variable background and the noise. Hence, pre-processing steps have take a fundamental role in astronomical image processing. Therefore, some pre-processing steps must be applied depending on if images have background variations, noise, or both. Concerning to the background, its inhomogeneity can be corrected by applying a smoothing with filters or by removing the background. Perhaps the background subtraction is preferable to the filtering, because implicitly is already performing the source detection by discarding those regions that with high probability are not sources. Furthermore, although filtering decreases the impact of background variations (and also noise), it may blur the sources. In the case of noise reduction, filtering seems to be the most widely used technique [44, 42, 89, 67].

Multi-scale approaches are also gaining popularity because they are techniques that allow to remove background and to reduce noise at the same time (more advantages are shown in Table 3.4). Since they extract the signal at different scales, they are suitable when the images have sources with different sizes and complex shapes. Furthermore, being able to work with multiple scales (so multiple images), this technique offers the possibility to extract the best of each one, or select the better suited scales to perform the detection aim. Most multi-scale analyses are based on the wavelet transform or variants of it [16, 73, 22, 86, 24, 66].

Regarding the detection criteria, the vast majority of works reviewed used thresholding and local peak search, and both methods seems to have similar performance. We have realised that after any kind of pre-process, both methods are used interchangeably. However the choice may depend of some characteristics as can be seen in Table 3.4. Local peak search is not suitable to detect extended sources, and it is preferable when images are noisy and have point sources, since it is a neighbourhood-based algorithm and easily

discard noise pixels (avoiding to be confused with source pixels). When image has an inhomogeneity background, the best choice is to tackle the detection with a local thresholding, whereas global thresholding is preferable when image has a significant contrast among objects and background or a high SNR. The rest of approaches that do not use neither thresholding nor local peak search have in common that are relatively recent (most of them developed in the last years), and besides they are all innovative works, they perform object detections on a par with the two typical methods.

Analysing the results, we noticed that the best performances in terms of TP were obtained by Slezak et al. [71], Starck et al. [73], Peracaula et al. [64, 66], and Torrent et al. [83]. Moreover, Damiani et al. [16] and Freeman et al. [22] also obtained satisfactory results in terms of coincidences with published catalogues. Some other works obtained good results, but we consider that the selected ones are more significant because they dealt with considerable amounts of sources (in most cases hundreds of them) and did not use additional resources as astronomical packages. We want to stress on the one hand, that of those approaches that apply any kind of pre-processing, most of them used multi-scale strategies, specifically the wavelet transform [16, 22, 73, 66]. On the other hand, the detection step that they use, is mostly a thresholding [71, 73, 22, 66] (the rest of detection criteria used were two innovative methods as “contrast radial function” and “boosting” in the approaches of Peracaula [64] and Torrent [83], and a local peak search in the Damiani [16] approach).

Table 3.4: Overview of the different techniques reviewed with their advantages and drawbacks.

		Description	Strengths	Weaknesses
Pre-processing	Basic	Basic pre-processing steps as filtering, profile fitting or morphological operators	Intuitive, fast and easy Slightly emphasise sources Correct background variations Reduce noise	Limited May blur and twinkle the image Often need more pre-processing steps
	Bayesian	Methodologies based on Bayesian inference	Emphasise sources Good results with source variability Reduce background variability and noise	Quite slow Need prior knowledge
	Matched filter	Methods based on filters with the profile of the objects to find	Rather emphasise sources Reduce background variability and noise	Need prior knowledge Different filters required for different sources
	Multi-scale	Approaches that decompose the image in several scales	Reduce noise and delete background at the same time Good results with source variability Allow working with different scales Implicitly performs source detection Can deblend sources	Quite slow Often need combinations of transforms
Detection criteria	Thresholding	Pixels above a certain threshold are considered as part of the object	Good results with all sources Good results with inhomogeneous background Good results with significant contrast and high SNR	Difficult to select the optimal threshold Not suitable for faint sources
	Local peak search	Search pixels that are maximums in a neighbourhood	Good results with point sources Good results with noisy images	Need an additional detection process Not suitable for extended sources
	Other	Other innovative detection methods	Similar results than the other two methods	Still not have enough acceptance

## Chapter 4

# Experimental work

*Astronomical detection methods are usually evaluated by comparing the detected sources to a reference source catalogue and also through a visual evaluation by an expert. The goodness of the different methods is determined by the rate of sources in the catalogue which have been correctly detected by the method. In other words, the best methods are mainly those with a greater number of true positives (TP). In this chapter, after presenting the dataset used to test different detection strategies, we present and discuss the results obtained with the experiments performed, highlighting the most interesting aspects. Finally, we propose a new detection method that combines some of the most salient steps of the state-of-the-art methods, and we compare the obtained results with the ones obtained with the other approaches.*

### 4.1 Data used

In order to properly compare the performance of different methods, we have to test them in the same dataset of images. To perform this comparative analysis, we have used a set of 19 deep radio (fields) obtained by Paredes et al. [62] at the frequency of 610 MHz (49 cm of wavelength) through the Giant Metrewave Radio Telescope (GMRT) [80] located in Pune (India). The region surveyed in these images is centred on a unidentified extended source of very high energy gamma-rays called MGRO J2019+37. The 19 images, that show regions of the sky with an area of  $2.5^\circ \times 2.5^\circ$ , form a mosaic that covers 6 square degrees with a resolution of 5 arc seconds. In terms of size, each of the 19 images is of  $3385 \times 3397$  pixels, with the observed region having a circular shape (of radius  $28'$ ). The resulting overlapped image has a hexagonal shape of size  $14000 \times 14000$  pixels as can be

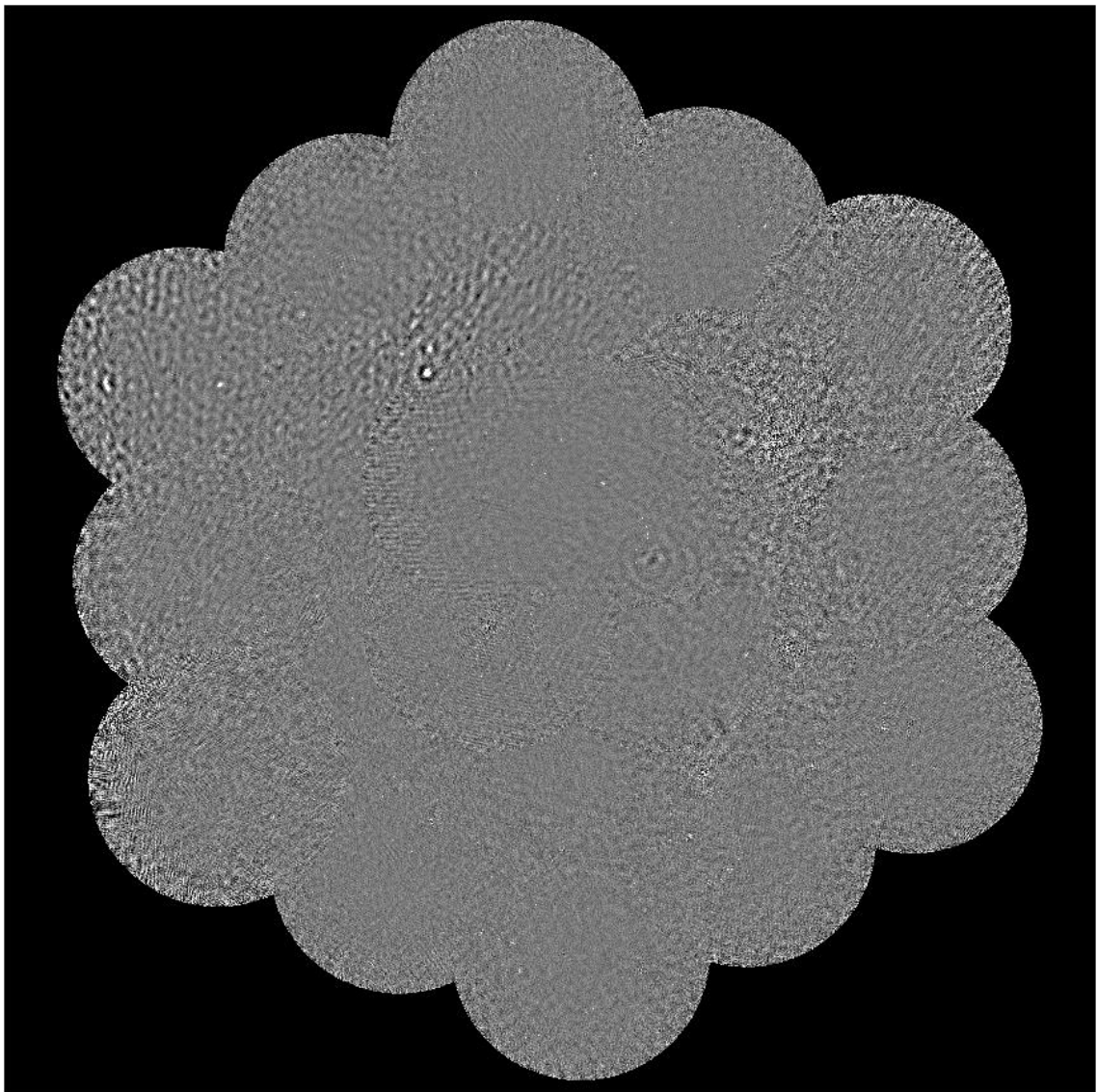


Figure 4.1: The 19 circular images forming the resulting mosaic. In order to appreciate better the content of the image, a 0.5% of outliers has been removed, and the intensity of pixels has been rescaled.

seen in Figure 4.1. Each observation (image) has a circular shape stored in a rectangular image, those pixels that do not belong to the observation have the value NaN (Not a Number) and appear in black. The same happens in the outer pixels of the resulting mosaic.

Regarding this image, despite it has a high noise level and interferences, some sources

can be detected with a naked eye. However, some regions as the edges of the external fields of the mosaic may cause unreliable detections by the methods because they are very noisy. For this reason we have limited the region where to find sources by removing these problematic regions. Moreover, some other internal regions have also been excluded because they have a lot of interferences and noise (sometimes caused by the presence a bright source in the region). Figure 4.2 shows the image after removing the problematic regions.

In order to be able to perform comparisons between methods, we need a reference catalogue indicating where the sources are really located. To deal with this issue, an expert of our research group has manually annotated the sources in the GMRT images, providing us the ground truth (gold standard). Obviously, the manual detection of sources is a subjective practice, which depends on the criterion of the expert, and therefore it may be variability in the manual detection between different experts (what one expert considers as a source, may be rejected by another expert). However, this manual procedure is still the best way to perform reliable catalogues. The final set of true sources of the reference catalogue consists of 632 sources as it is shown in Figure 4.3.

## 4.2 State-of-the-art implemented approaches

Through the analysis of the state-of-the-art carried out in Section 3.5, we have seen different strategies to tackle the detection of astronomical sources in images. Some of them have been of our interest basically due to their performance (the results reported), but also due to the way used to solve the detection problem. As we have seen, these works use different images with different characteristics, and for this reason, a comparison of their results is not reliable. Due to this fact, we have implemented approximations of these reference works in order to test them with the same data (the image presented in the previous section) and be able to perform a proper evaluation and comparison. As we have just mentioned, the methods have been implemented and reproduced as close as possible to the idea presented in the original articles. Moreover, we have also obtained published catalogues with SExtractor and SAD because they are usually used by the astronomical community to detect sources.

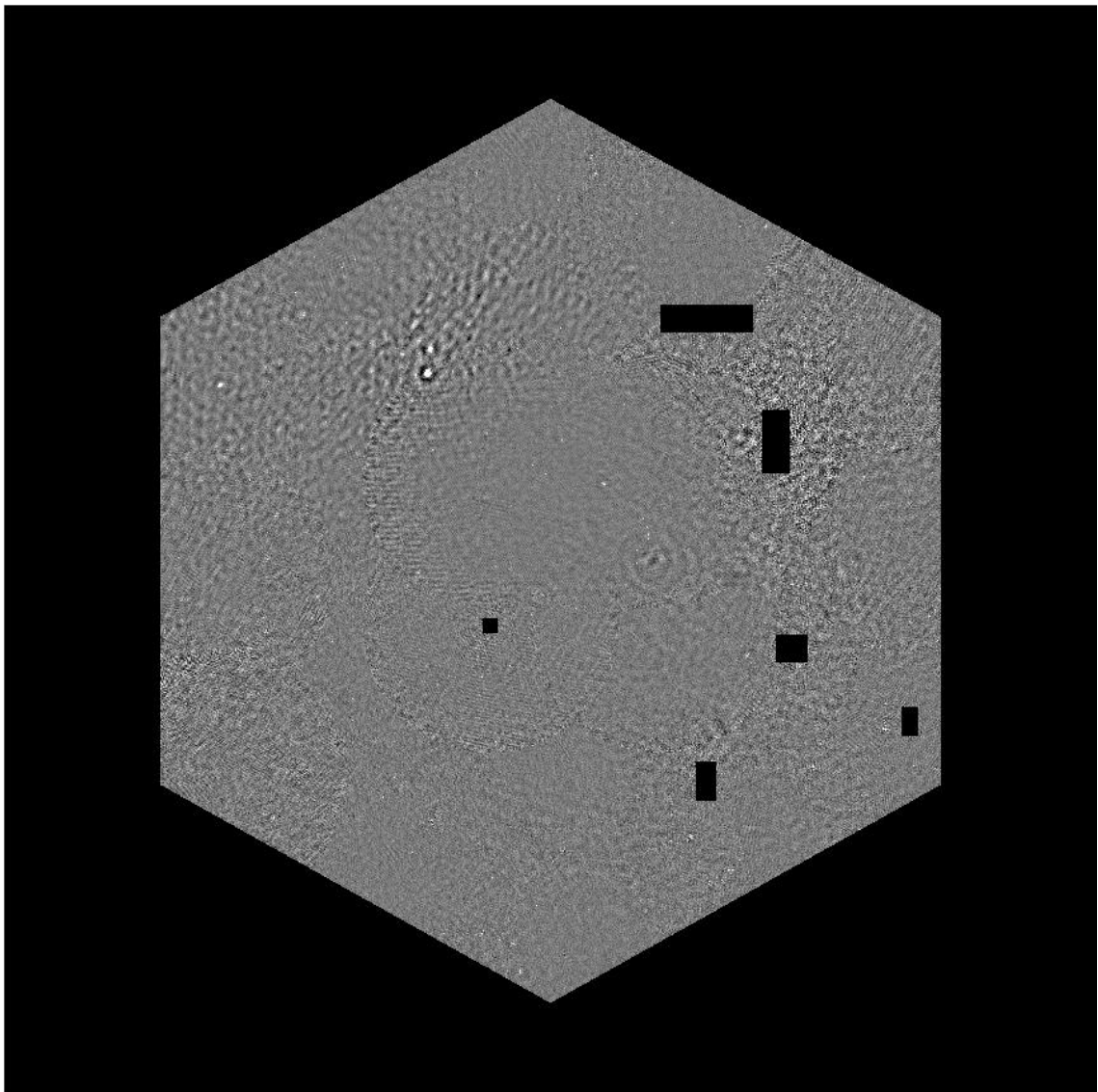


Figure 4.2: The resulting mosaic after excluding regions with high level of noise and interferences that may cause unreliable detections. Black pixels indicate the regions not taken into account when a detection method is applied to the image.

#### 4.2.1 Methods implemented

According to the analysis of the reported results done from the state-of-the-art (see section 3.5), the strategies that have implemented are the ones of: Slezak et al. [71], Starck et al. [73], Peracaula et al. [64, 66], and Torrent et al. [83]. Hereafter, we are going to refer to these approaches also as Slezak, Starck, Peracaula<sub>alg1</sub>, Peracaula<sub>alg2</sub>, and Torrent,

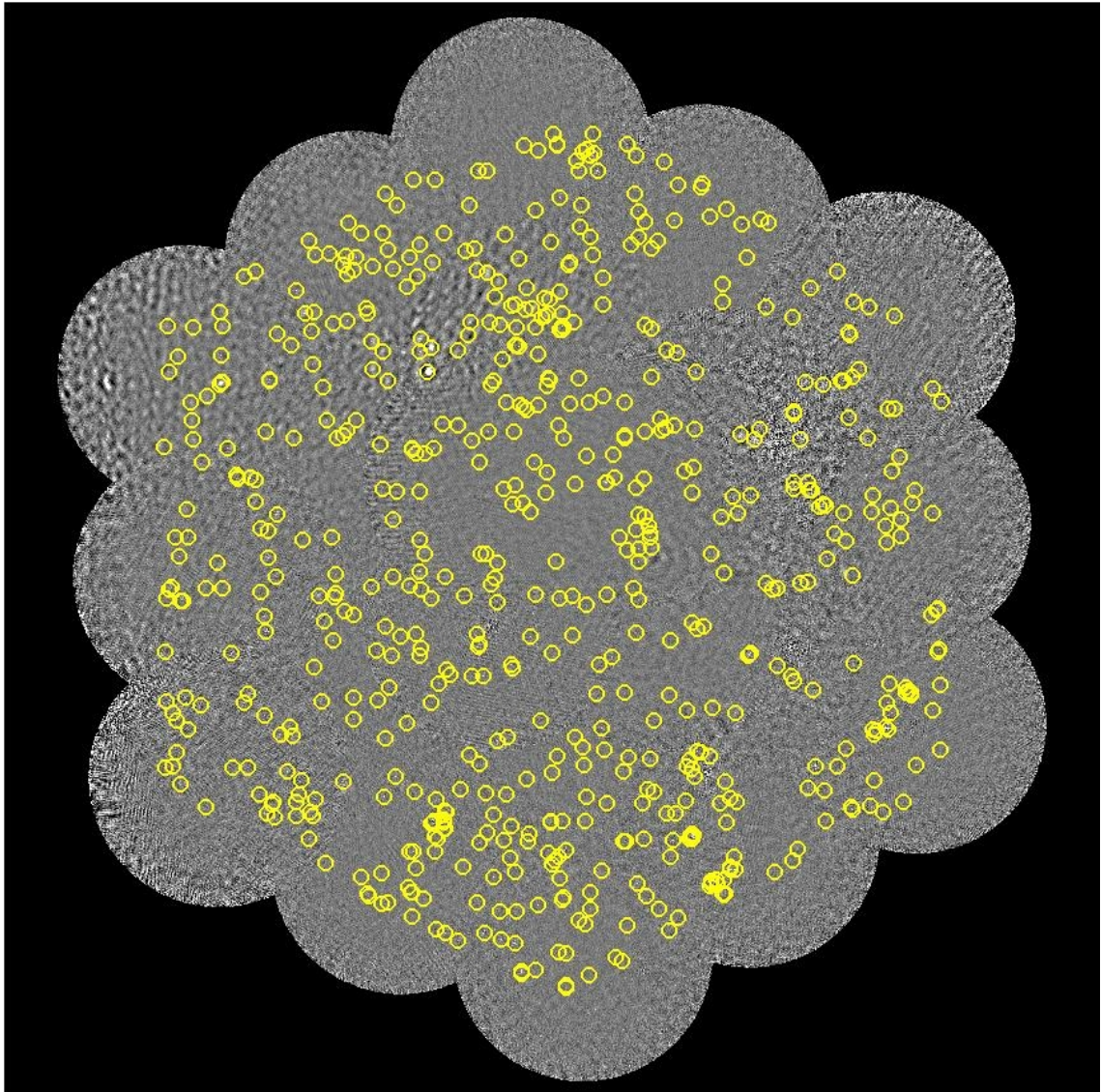


Figure 4.3: The 632 true sources manually detected in the GMRT image.

respectively). As we have done in the state-of-the-art, we describe the methods used to implement the different strategies dividing them in pre-processing steps and detection criteria. All the methods and strategies have been implemented using Matlab 7.10.0 (R2010a).

### Pre-processing

As we noticed in the discussion of the previous chapter, the wavelet transform (WT) is the most common pre-processing method in the works with best reported results. For this reason we have implemented the WT, and more specifically the “à trous” algorithm with a spline of degree 3 (following the way specified in Section 3.2.1). The first scale is obtained by subtracting the raw image and the raw image filtered with the spline, and the process continues iteratively generating new scales by mainly subtracting the last scale obtained and the filtered last scale. The number of scales computed may be defined as a parameter by the users. Figure 4.4 shows an example of wavelet decomposition. It shows the application of the WT to one of the 19 fields of the GMRT.

We use this WT method in the implementation of the works of Starck and Peracaula<sub>alg2</sub>. As we mentioned in the presentation of the test images, the vast majority of objects that we try to detect are point sources. In this respect, Peracaula et al. [66] argued that the three first scales are the most suitable to detect this kind of sources. Therefore, we decided to implement these two approaches so that they use these three scales.

As we are going to see in the next section, Starck and Peracaula<sub>alg2</sub> methodologies detected the sources applying respectively a global and a local thresholding based on the global and the local level of noise. Moreover, the Slezak strategy also needed to compute an estimation of the noise to remove the background. For this reason we have implemented a method to calculate an estimation of the noise level in a whole image or in a sub-image as the way proposed by Slezak et al. [71] and Peracaula et al. [66]. They used a Gaussian fitting of the histogram of pixel intensities of the region where define the noise level. As Bijaoui [8] stated, the histograms of astronomical images usually show an asymmetry around the principal maximum, having a less steep slope at the right part of the peak (see Figure 4.5). The bell-shaped region of the histogram represents the noise, whereas the right long region that starts where the bell-shaped region finishes, may be considered as sources. For this reason, once a Gaussian function is fitted to the histogram, it is easier to delimit the intensity from which we can consider that we are dealing with noise. Thus, a threshold can be defined for example, as a multiple of the noise level estimation.

The last type of pre-processing that the reference approaches use is a smoothing with a Gaussian filter. It was the first step computed in Slezak approach in order to facilitate the detection of faint sources. We have used a  $5 \times 5$  filter as suggested by Slezak et al. [71]:

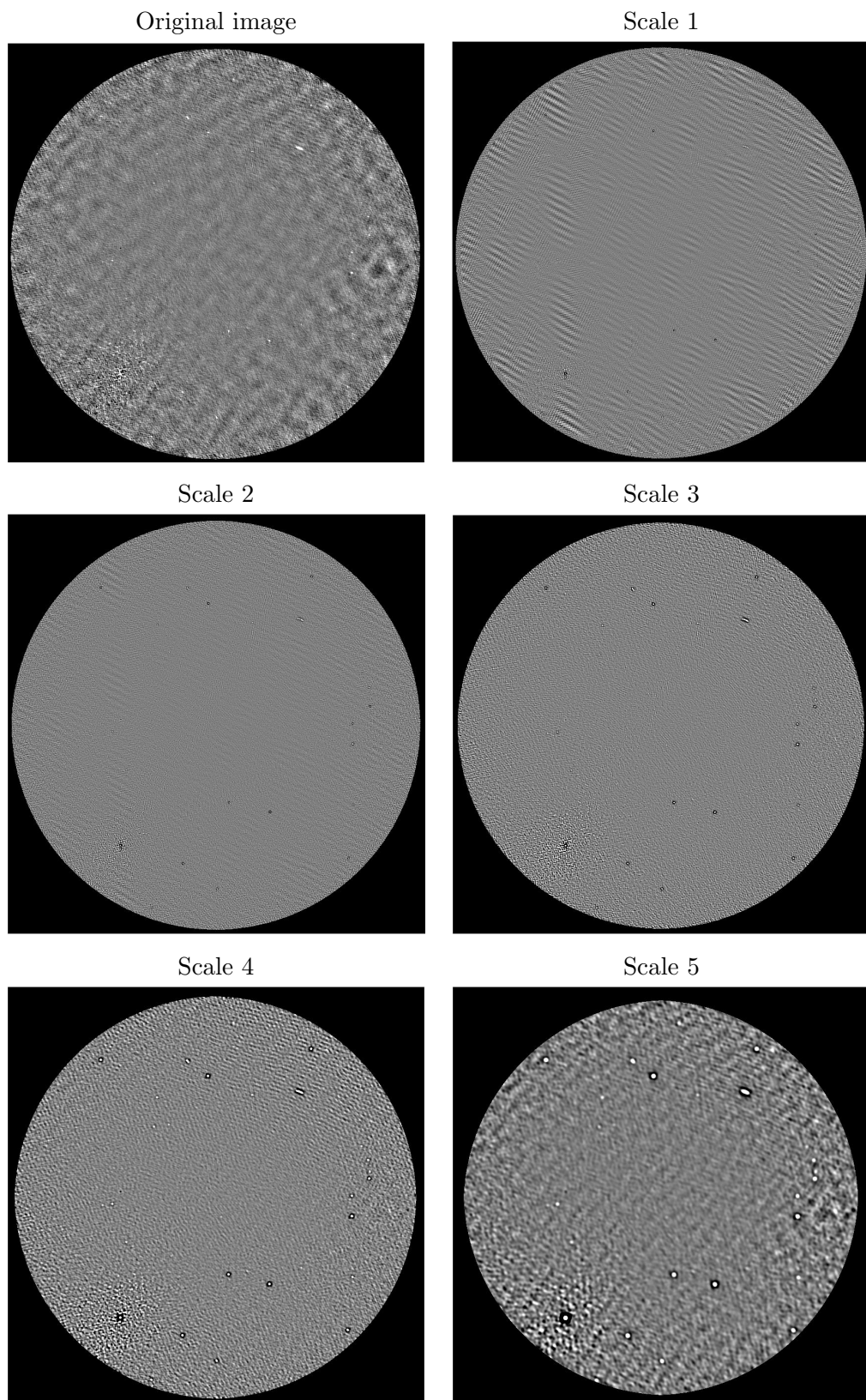


Figure 4.4: Application of a 5-scale WT to the central field of the GMRT mosaic.

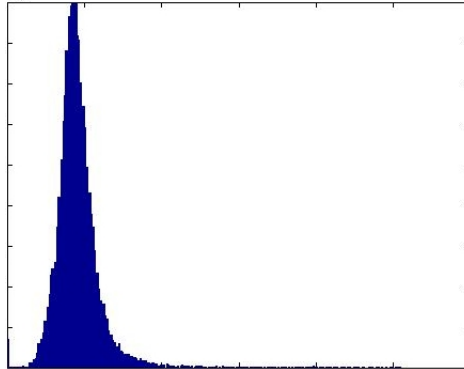


Figure 4.5: Typical histogram of an astronomical image.

$$\begin{pmatrix} 0.0030 & 0.0133 & 0.0219 & 0.0133 & 0.0030 \\ 0.0133 & 0.0596 & 0.0983 & 0.0596 & 0.0133 \\ 0.0219 & 0.0983 & 0.1621 & 0.0983 & 0.0219 \\ 0.0133 & 0.0596 & 0.0983 & 0.0596 & 0.0133 \\ 0.0030 & 0.0133 & 0.0219 & 0.0133 & 0.0030 \end{pmatrix} \quad (4.1)$$

### Detection

If WT is the most used pre-processing step in the state-of-the-art, in the detection criteria, thresholding is the majority preference. The key-point of this kind of methods lies in finding a threshold capable to distinguish source pixels from background pixels. For instance, in the Slezak strategy, a global threshold was defined by searching the most bright sources using a local peak search, computing the histogram of the intensity of the peaks, and selecting 3.8 times the standard deviation of this histogram. Starck and Peracaula<sub>alg2</sub> used similar strategies that apply a global and a local threshold at each of the different WT scales. Both methods defined the thresholds through a multiple of the level of noise estimated (Starck multiplied by 5 and 7 the global level of noise, while Peracaula<sub>alg2</sub> multiplied each local noise level by 4). Notice that in local thresholding the size of the sliding window can be an input parameter or otherwise, may be calculated based on the size of the image.

In a different way, in Peracaula<sub>alg1</sub> strategy, a novel detection algorithm based on the neighbourhood around each pixel was presented. This analysis was performed defining an intensity “contrast radial function” and studying the behaviour of its slope. First of all,

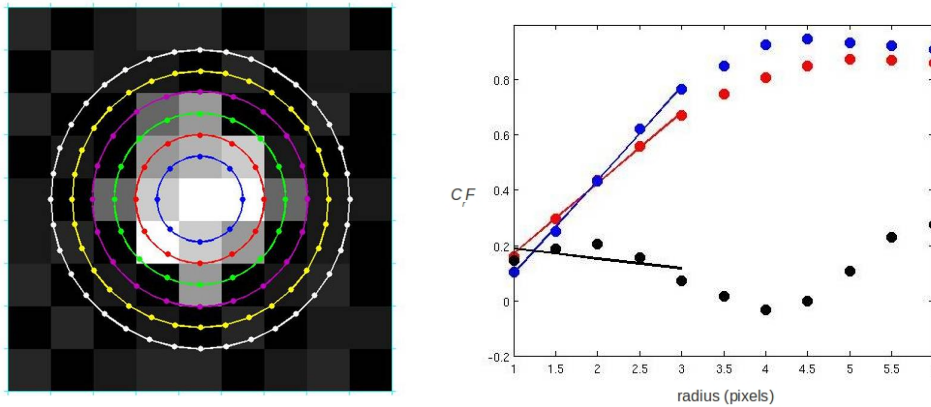


Figure 4.6: An scheme that shows how the  $C_r F$  and its associated fitted polynomial are computed. On the left, the different radii to which the function is computed. On the right, different examples of first degree polynomial fitting. These images have been extracted from [64].

a local thresholding based on the local noise was applied to the original image in order to select candidate areas with at least eight connected pixels. Afterwards, a “contrast radial function”  $C_r F$  was calculated for all the candidate pixels up to a defined value  $N_r$  of radius ( $N_r = 1, 2, \dots, N_r$ ). They defined the  $C_r F$  as follows:

$$C_r F(R) = \left( I_{ij} - \frac{\sum I_{neigh}(R)}{N_{neigh}(R)} \right) / I_{ij} \quad (4.2)$$

where  $R$  is the radial distance in pixels,  $I_{ij}$  is the intensity of the central pixel,  $I_{neigh}$  is the intensity value of every neighbour of the central pixel, and  $N_{neigh}$  is the number of neighbours at distance  $R$ . At this point, each pixel had a set of values corresponding to the calculation of the  $C_r F$  with different radii. For each pixel, a first degree polynomial was fit to these values and its slope was calculated in order to know the goodness of the fit. This process is illustrated in Figure 4.6. Finally, connected groups of at least four pixels with a significant goodness were considered as sources.

The last detection method that we have selected as a remarkable work is the strategy presented in Torrent et al. [83]. This approach is a supervised strategy quite different to the typical ones proposed in the field of astronomical detection. It tries to detect sources using local features and a classification technique as can be seen in the scheme in the Figure 4.7. Notice that in this case, different images (or sub-images) are needed in order to create different image sets devoted to create the reference dictionary, the training (we know the position of the sources present in these two datasets), and the testing of the

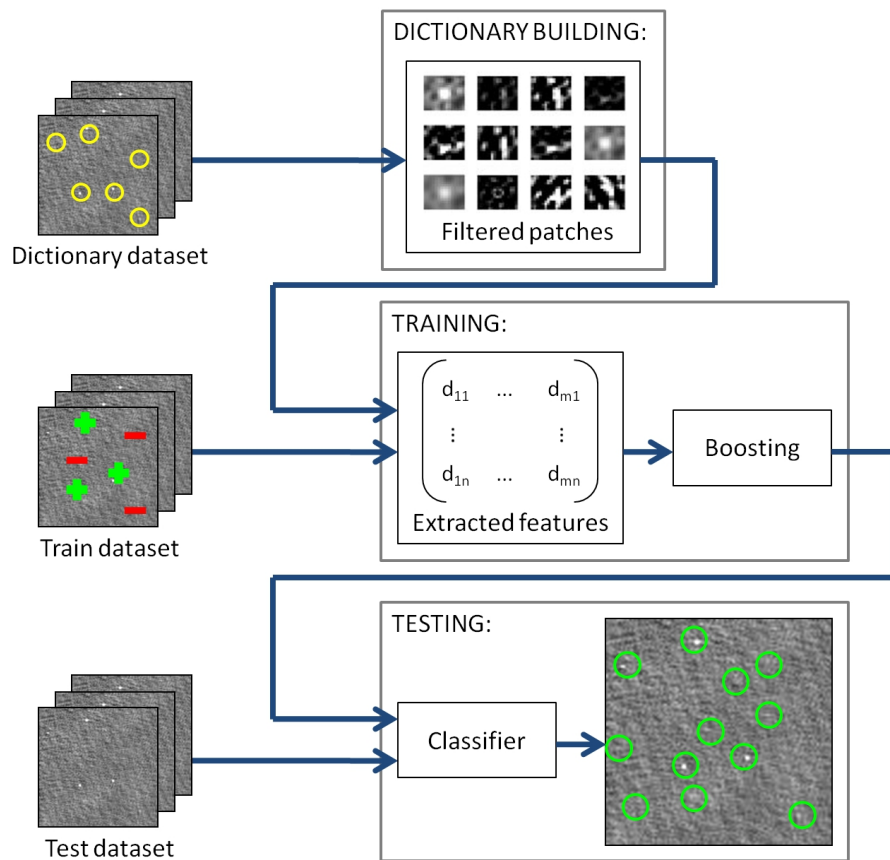


Figure 4.7: Graphical scheme of Torrent approach.

classifier. These three datasets are different, and do not have overlapped (same) sources. First of all, a feature dictionary was built from a set of images devoted to this purpose. These images were convolved with a bank of filters, and then, the filtered images were used to extract different patches centred on known sources (the same patches were extracted in all filtered images). These patches became the visual words of the dictionary.

Afterwards a training step was carried out. Its goal was to train a classifier with positive and negative examples. Specifically, Torrent et al. [83] used a “boosting” classifier, based on the sum of weak classifiers that produces a strong classifier. In Torrent strategy, the weak classifiers were simple regression stumps with one of the features of the dictionary, so several rounds were executed, and at each round the feature with less error was selected. The examples from which the classifier was built, were cross correlations between the words of the dictionary and the different patches extracted from the training image set: positive examples were extracted where a known source was located, while negative examples were

extracted from random locations.

Once the classifier was built, it was applied to the images of the test dataset in order to perform the detection of sources. At each round, the best feature selected on the training step was correlated to the features extracted at each pixel of the test images. Finally, a probability image was obtained, and therefore pixels with high values represented more confidence of being part of sources.

### 4.2.2 Experiments

From the different methods described in the previous section, we have built the approaches of the state-of-the-art. Below, we summarise the steps that follow the strategies implemented and comment the experiments performed with them.

Our implementation of **Slezak** strategy follows the steps:

1. The raw image is convolved with a Gaussian filter.
2. Local peaks are searched, and a detection threshold is set at 3.8 times the standard deviation of the histogram of their intensities.
3. The background of the image is locally subtracted by estimating the local level of noise (values below 4 times the local noise level are considered background).
4. A global thresholding is applied (with the threshold obtained in Step 2)

**Starck** approach has been implemented following these steps:

1. A 3-scale WT is applied to the image.
2. For each scale, a threshold is defined by means of the level of noise (5 or 7 times the noise level).
3. A global thresholding is applied to each scale.
4. Detections at each scale are added, obtaining the resulting detection.

**Peracaula<sub>alg1</sub>** approach uses the following steps to implement an approach based on a “contrast radial function”:

1. A low local thresholding based on the local level of noise is applied to select candidate areas (the low local threshold is set at 2.5 times the local noise level).
2. For every pixel, a  $C_r F$  is calculated at different radii.
3. For each candidate pixel, a first degree polynomial is fit with the values obtained in Step 2, and its slope is calculated in order to define the goodness of the fit.
4. Groups of at least four pixels with a significant goodness are considered as part of sources.

The implementation of the **Peracaula**<sub>alg2</sub> strategy follows these steps:

1. Bright sources are extracted using a local thresholding based on a Gaussian fitting of the histogram of local intensities (4 times the local noise level).
2. Two images are created: a residual image where bright sources have been replaced by local noise, and a binarised image with bright sources detected.
3. A 3-scale WT is applied to the residual image.
4. Local thresholding is applied to each scale (the thresholds are defined at 4 times the local noise level at each scale).
5. The binary image and the detections at each scale are added, obtaining the resulting detection.

As this approach is the combination of different simple detection methods based on thresholding, we think that we also could test the steps separately to test the improvement of the general approach. Therefore, with this approach, we test three experiments: the whole strategy, the strategy without extracting bright sources (without Step 1), and only the application of the local thresholding (only step 4).

**Torrent** approach has the following steps:

1. A dictionary of visual words is built from a set of images devoted to this purpose. These images are convolved with several filters and patches of different sizes are extracted from each filtered image at locations where a know source is placed. Each extracted patch is a word in the dictionary.
2. From a set of training images, a boosting classifier is trained. These images are also convolved with the same bank of filters, features are extracted from some representative points (positive and negative examples) in the images, and the classifier is trained with the correlation of the features extracted with the dictionary words.
3. The classifier is applied to the test images obtaining probability images. Pixels above a given threshold (usually set to 0) are considered part of sources.

Each of these implemented strategies provide a catalogue as output. The catalogues consist in sets of coordinates ( $x$  and  $y$ ) which indicate the centroids of the detected sources. Therefore, we can compare the obtained catalogues with the reference catalogue (ground truth) in order to see their performance. In addition, we have also analysed published catalogues that used SExtractor [62] and SAD (private communication), and their results are also compared with the reference catalogue. With SExtractor we only have TP (the sources published in the catalogue), while with SAD we have TP and FP. The results obtained with these two astronomical packages must be taken into account, since they are widely used by astronomers due to their reliability.

To automatically know if a detected source is a true positive (TP), a false positive (FP) or a false negative (FN), we have implemented a method that given two catalogues of the same region of the sky, considers that two sources in the two catalogues are the same source if the distance between their centroids do not exceed a maximum distance specified (for example 15 or 20 pixels).

### 4.2.3 Analysis of the results

Results obtained with the different experiments performed in terms of number of detections, TP, TN, the percentage of detections that are true sources, percentage of true sources detected, and FN are summarised in table 4.1. Regarding this table, the first thing that we notice is the different number of detections reached by the methods, both above and below the number of true sources annotated in the reference catalogue. To have

Table 4.1: Results obtained with the experiments performed. Each column represents the number of detected sources, TP, TP/detections (that means from the detected sources which percentage is a true source), TP/annotations (that means the percentage of true sources detected), FP, and FN found with the different experiments.

Experiments	Detections	TP	TP/detections (%)	TP/annotations (%)	FP	FN
Slezak	177	165	93.22	26.11	12	468
Starck (5 times the noise level)	840	347	41.31	54.91	493	312
Starck (7 times the noise level)	349	266	76.22	42.09	83	376
<b>Peracula<sub>alg1</sub></b>	<b>820</b>	<b>487</b>	<b>59.39</b>	<b>77.06</b>	<b>333</b>	<b>189</b>
Peracula <sub>alg2</sub> (whole strategy)	405	370	91.36	58.58	35	272
Peracula <sub>alg2</sub> (without removing bright sources)	379	353	93.14	55.85	26	290
Peracula <sub>alg2</sub> (local thresholding only)	373	355	95.17	56.17	18	281
Torrent	430	312	72.56	49.37	118	343
SExtractor	n/a	298	n/a	46.68	n/a	366
SAD	445	279	62.70	44.15	166	355

a more representative measure of the goodness of the detections, we can analyse the TP (column three) and especially, the values derived from the TP (columns four and five). High percentages in column four indicate that the detections performed are very reliable, since most of the sources detected are true sources. On the other hand, high percentages in column five indicate that most of the true sources in the image have been detected. So, referring to reliability, the best results were obtained by the approaches of Slezak and Peracula<sub>alg2</sub> (especially using only the local thresholding), both over 90%.

Referring to the number of true sources detected by the approaches, we want to stress especially the Peracula<sub>alg1</sub> approach, which allowed to detect more than two-thirds of the true sources. Peracula<sub>alg2</sub>, Starck, and even Torrent strategies have also an acceptable number of true detections, with approximately the half of the true sources detected. Notice that in most of the cases, the strategies only present high values in one of the two percentage measures, and a compromise between which of the two measures boost must be taken: if we want to have reliable detections, we have to be aware of the fact that we will probably obtain a low number of detections, whereas if we want to detect the maximum number of true sources, we have to be aware of the fact that many spurious sources will be detected. However, we want to emphasise Peracula<sub>alg1</sub> as the method that globally provided better results: 95.17 and 56.17, respectively. Notice that with this method, 355 sources of the total of 632 sources have been correctly detected, with only 18 FP found. Some visual results obtained from the application of the different methods to the central field of the GMRT mosaic are shown in Figures 4.8, 4.9, 4.10, and 4.11.

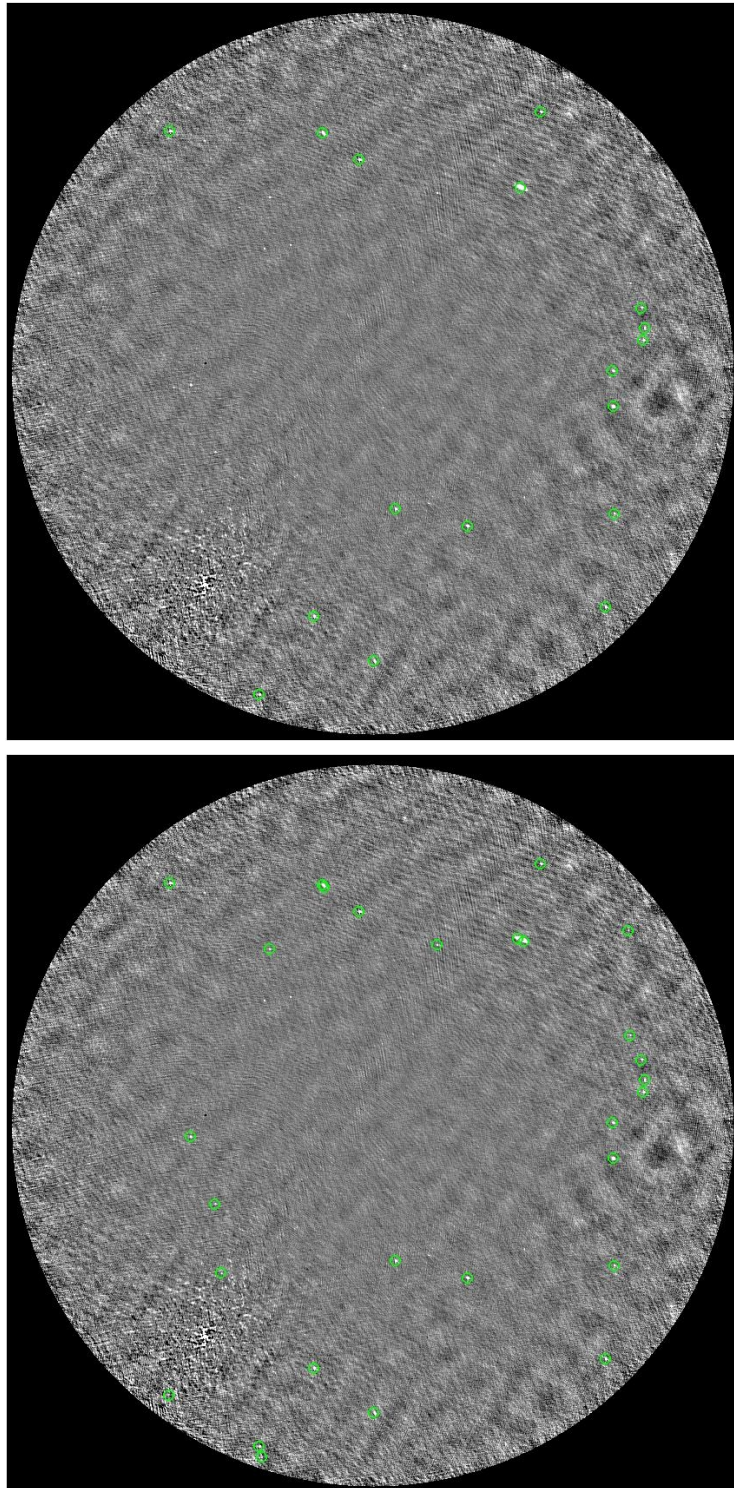


Figure 4.8: Sources detected in the central field of the GMRT mosaic by Slezak and Starck (7 times the noise level) approaches. Green circles mean TP (no FP have been obtained in this field).

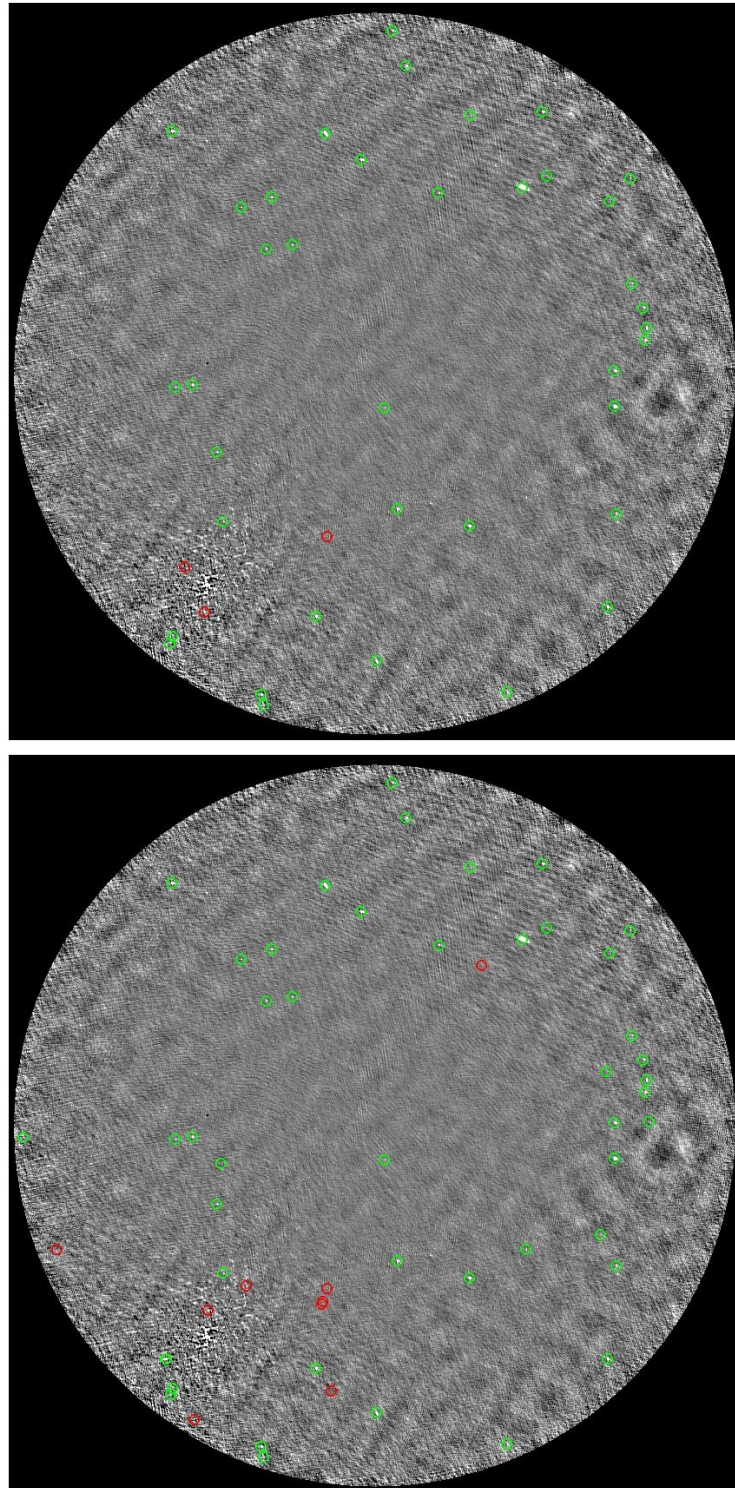


Figure 4.9: Sources detected in the central field of the GMRT mosaic by  $\text{Peracaula}_{alg1}$  and  $\text{Peracaula}_{alg2}$  approaches. Green circles mean TP while red circles mean FP.

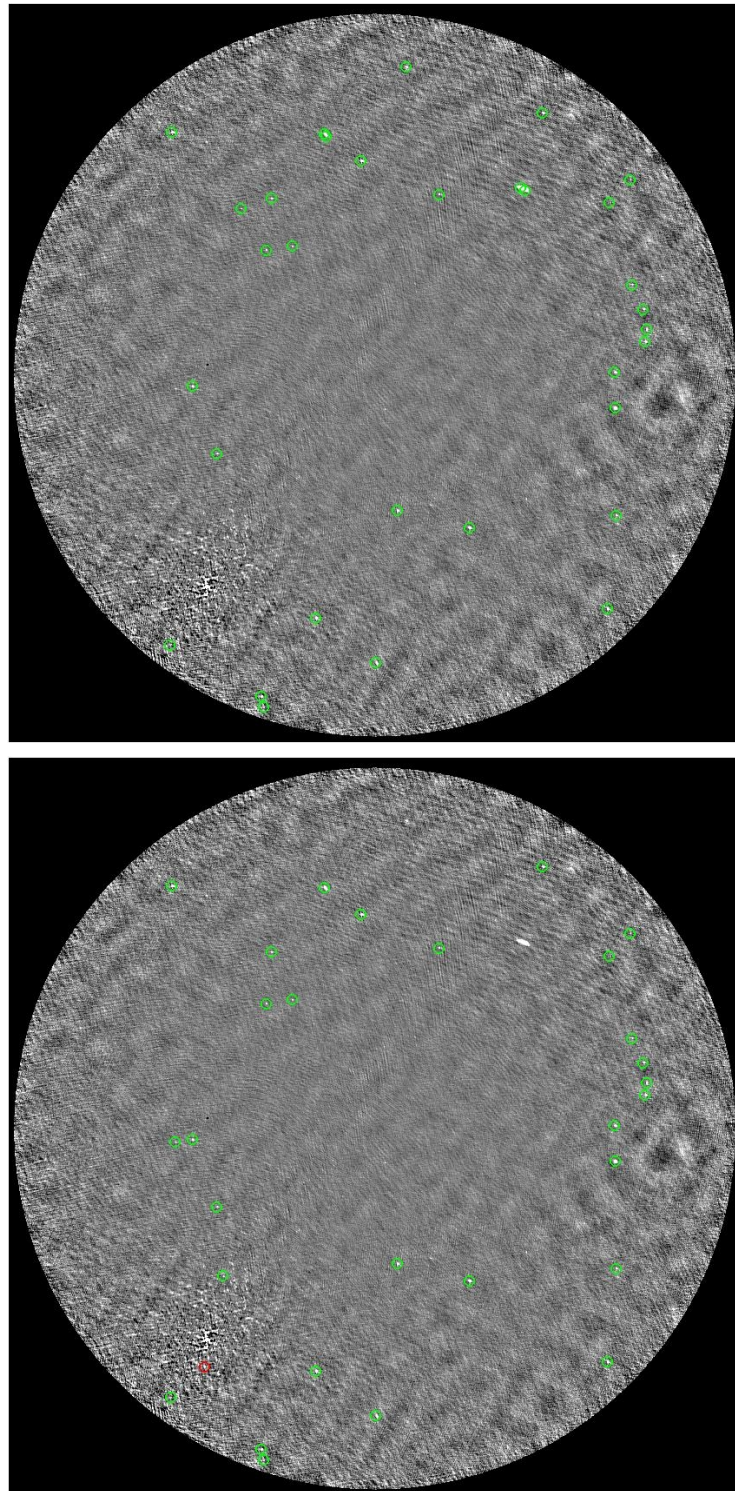


Figure 4.10: Sources detected in the central field of the GMRT mosaic by SExtractor and SAD packages. Green circles mean TP while red circles mean FP.

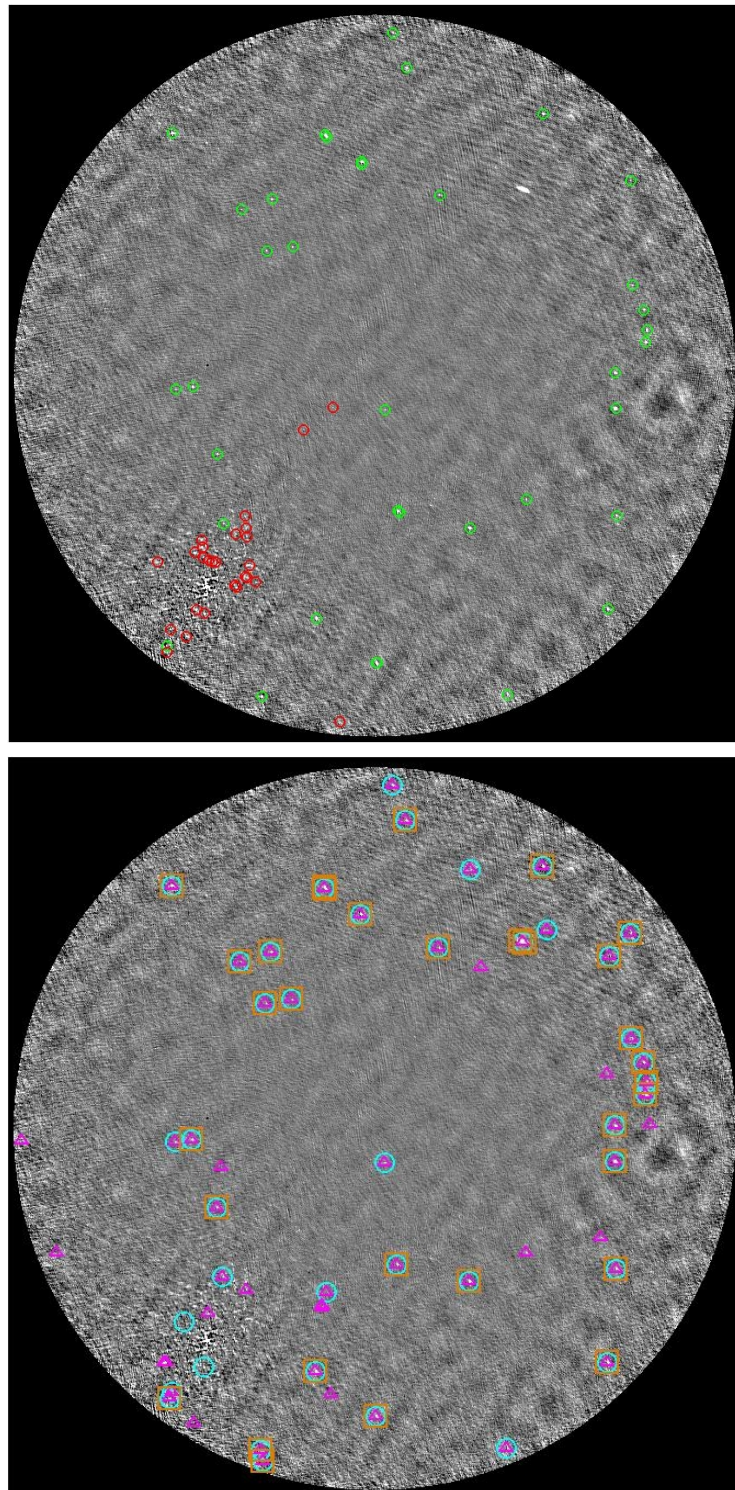


Figure 4.11: Sources detected in the central field of the GMRT mosaic by Torrent and some overlapped approaches. On the top, green circles mean TP while red circles mean FP. On the bottom, overlapped detections of Peracaula<sub>alg1</sub> (cyan circles), Peracaula<sub>alg2</sub> (pink triangles), and SExtractor (orange squares) strategies.

### 4.3 Proposal of source detection

At this point we have already seen a comparative analysis of the different approaches selected, and it is the moment to think possible new strategies which may improve the state-of-the-art results. As we are involved in a computer vision research group, and this master thesis is the first step toward the development of a PhD thesis, we consider that may be more interesting to pay attention at innovative techniques as the proposed by Andreon et al. [2], Liu et al. [39], Aptoula et al. [3], Perret et al. [68], and especially Torrent et al. [83]. We like the idea to develop a supervised method based on characterisation and classification through local features to detect astronomical sources, due to the fact that, in other fields of computer vision, this kind of strategies provide good performance in object detection, and we think that it could work as well in the astronomical field.

From the Torrent approach, we have though in some ideas to develop:

- a) To implement a strategy that merge the Torrent approach with the best techniques found in the state-of-the-art, in order to see their performance together.
- b) To test several classifiers (different from the classifier used in Torrent approach), in order to improve the results.
- c) Instead of select the best features at each round, to generate a descriptor consisting in a vector of elements of all patches extracted.

We have decided to focus the proposal of source detection of this master thesis in tackle the first idea (a). Thus, we have developed a mixture of strategies as initial work, by replacing some stages of the Torrent approach, leaving the other ideas to future work. In this sense, as we have seen in the state-of-the-art, multi-scale strategies are been increasingly used for its good performance. Therefore, we propose to develop a supervised pixel classification method that can take advantage of the benefits of the multi-scale approaches as the WT.

Therefore, our proposal is directed toward an image classification approach that use features extracted from several wavelet scales. Actually, we propose a strategy similar to the Torrent et al. [83] one but which uses features from the wavelet decomposition (specifically, a 3-scale WT) of an image instead of filtered images. Figure 4.12 shows the differences between Torrent approach and our proposal: while Torrent extract features (patches) from images convolved with some filters (mostly edge detection filters), we propose to extract the patches from wavelet scales. Our goal is to test this approach with

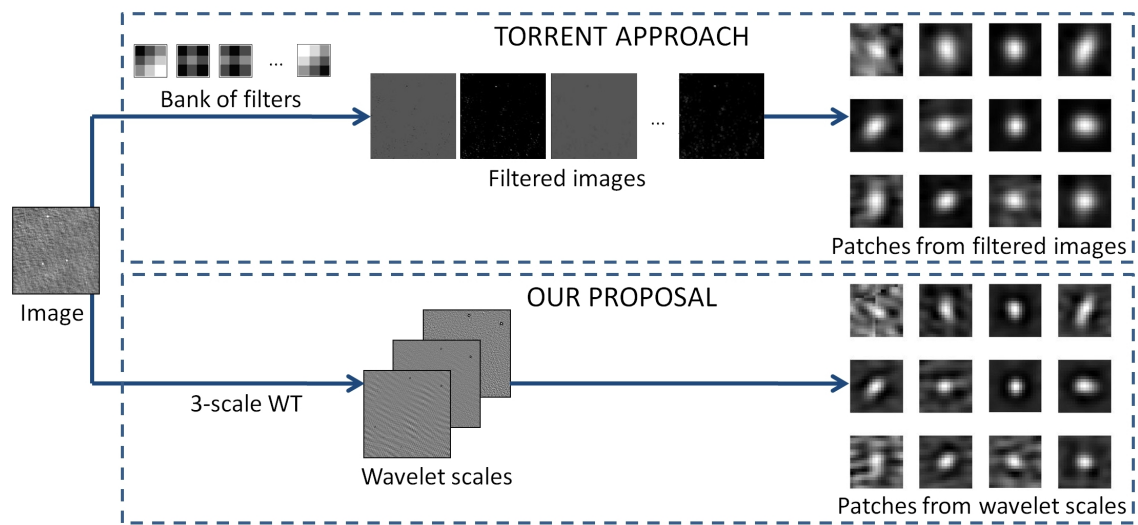


Figure 4.12: Feature extraction through filtered images (Torrent approach) and wavelet scales (our proposal).

different types of classifiers, although to correctly verify the performance of our proposal, we use the same “boosting” algorithm used in the implementation of the Torrent strategy.

Referring to future works (ideas b and c), after completing this master thesis we will focus our efforts on test other different classifiers and extract features from the wavelet scales by generating a descriptor consisting in a vector of elements of the different patches extracted (all values one after another in a one column vector). Thus, a descriptor can be extracted from each pixel in test images, and the pixel can be classified by comparing the similarity. As we are dealing with vectors, this similarity can be easily achieved using a cross product between the descriptor of the pixel and the descriptors of the dictionary words.

Our first experiment was performed in the central field of the GMRT mosaic that had 59 true sources. All results are shown in Table 4.2. On the one hand, using features extracted from filtered images, we found 64 sources from which 38 were TP, 26 were FP, and also 26 FN were found; on the other hand, using wavelet scales instead of filtered images, we found 77 sources, from which 49 were TP, 28 were FP, and 22 FN were found. As the number of FP and FN was similar, we can say that the performance of the approach using the WT was satisfactory, since it detected a relatively acceptable number of true sources (49 from 59, what means a 83.05%), and this number of detections is even greater than the one obtained with the Torrent approach using a bank of filters. Regarding the detections

Table 4.2: Comparison our proposal and Torrent approach applied in the central field of the GMRT image.

Experiments	Detections	TP	TP/detections (%)	TP/annotations (%)	FP	FN
Torrent	64	38	59.38	64.41	26	26
Our proposal	77	49	63.64	83.05	28	22

Table 4.3: Results obtained with the experiments performed in comparison with our proposal.

Experiments	Detections	TP	TP/detections (%)	TP/annotations (%)	FP	FN
Starck	349	266	76.22	42.09	83	376
Peracaula <sub>alg1</sub>	820	487	59.39	77.06	333	189
Peracaula <sub>alg2</sub>	405	370	91.36	58.58	35	272
Torrent	430	312	72.56	49.37	118	343
SExtractor	n/a	298	n/a	46.68	n/a	366
SAD	445	279	62.70	44.15	166	355
Our proposal	474	342	72.15	54.11	132	341

of each approach in Figure 4.13, we realise, for example, that the cluster of sources on the top right zone (it seems a unique big source) was not detected by the Torrent work, while using our strategy, some of these sources were correctly detected.

Once we saw that our proposal was valid, we wanted to be able to compare its performance with the rest of strategies implemented, so we applied our approach to the whole GMRT mosaic. We obtained 474 detections (see Figure 4.14), from which 342 were TP, 132 FP, and 341 FN were found. These values indicate that the 72.15% of the sources detected were true sources, and in general, we detected correctly the 54.11% of the sources of the image. These results indicate that, in relation to Torrent approach, we detected more true sources (TP) at the expense of have more spurious detections (FP). In terms of TP, our approach presented similar values than Starck, Peracaula<sub>alg2</sub>, SExtractor, and SAD strategies, it had a reliability on a similar level as Starck approach (almost two-thirds of the detected sources were true), and it was able to detect similar number of true sources than Starck and Peracaula<sub>alg2</sub> approaches, outperforming commonly used tools as SExtractor and SAD. From the other hand, its main drawback was the number of FP found (132). This fact reduced the reliability of the approach. Note that it was not the method with the worst number of FP, but in this aspect, it was still far from approaches like Starck and Peracaula<sub>alg2</sub>. Nevertheless, we consider that the new strategy is capable to compete with the best works in the state-of-the-art (see Table 4.3).

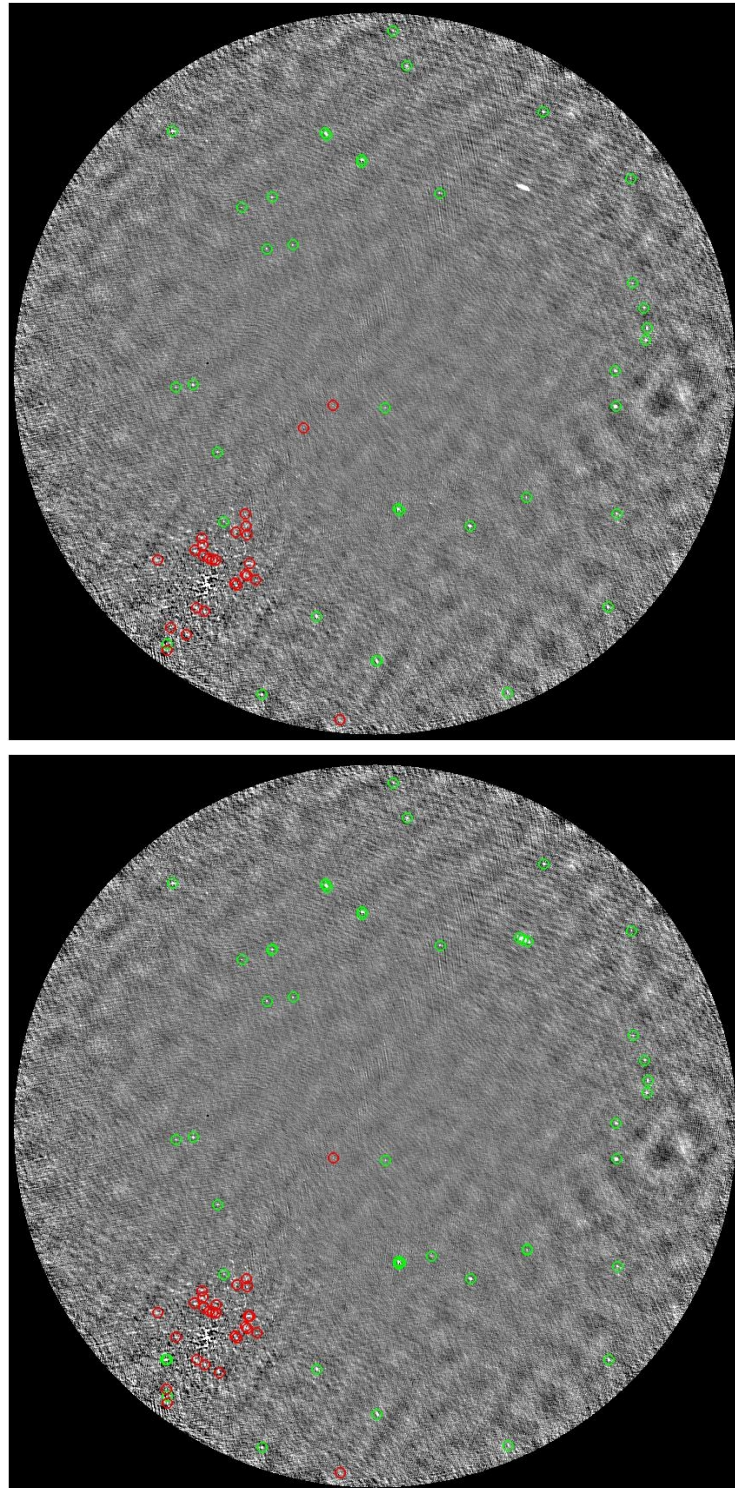


Figure 4.13: Sources detected in the central field of the GMRT mosaic. On the top, sources detected using features extracted from filtered images. On the bottom, sources detected using features extracted from wavelet scales.

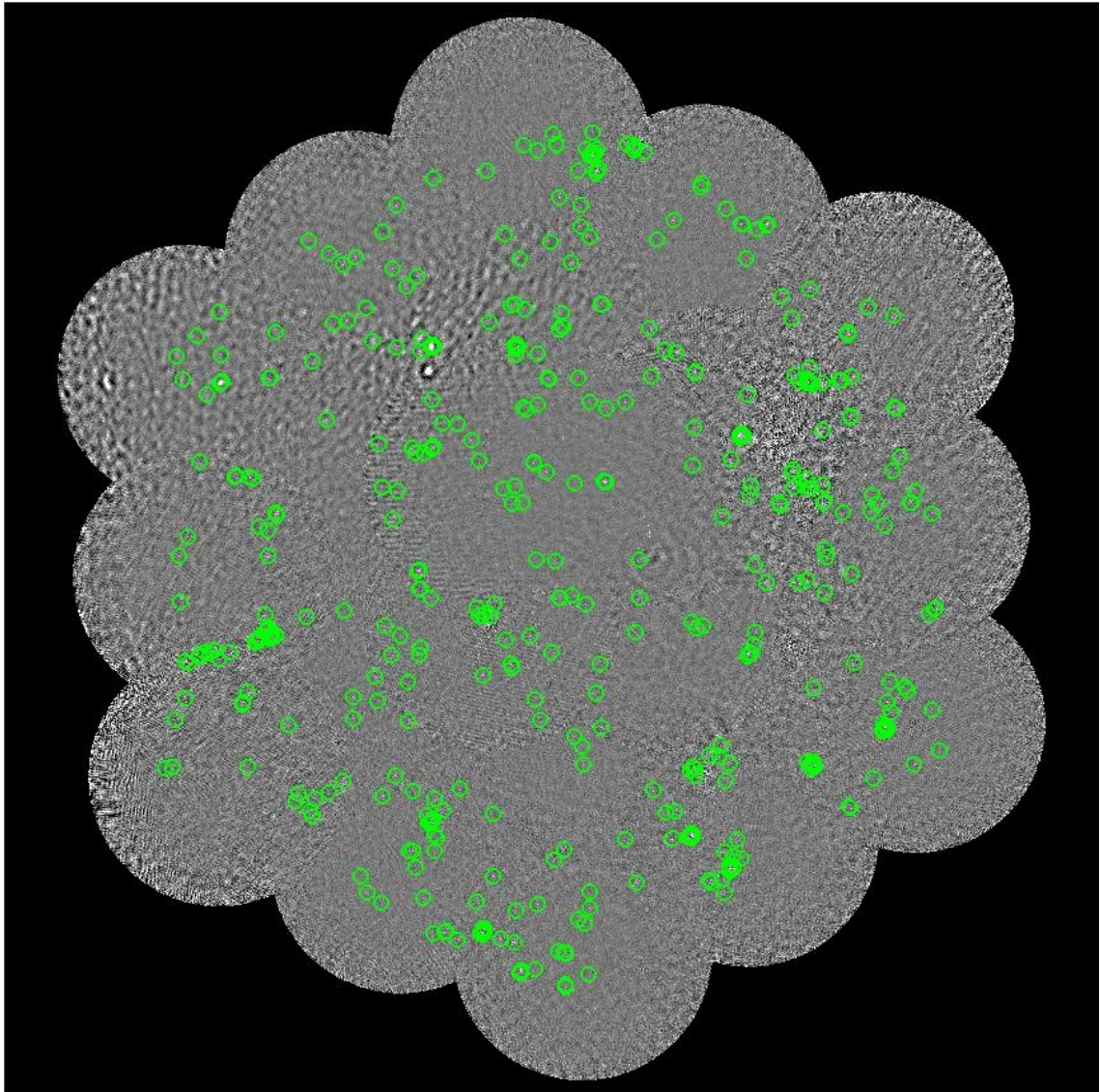


Figure 4.14: The 474 sources detected in the GMRT image.

## Chapter 5

# Conclusions and future work

*After the analysis of the representative astronomical detection techniques, the implementation of the best strategies, and the description of a new proposal based on them, we extract conclusions. Moreover, we present future works that will be involved in my PhD thesis.*

### 5.1 Conclusions

Firstly, **we have exhaustively analysed the state-of-the-art on astronomical object detection.** We have proposed to classify the different strategies according to the pre-processing step that they use and the way how sources are detected. Pre-processing steps have been divided in basic pre-processes, matched filtering, Bayesian methodologies, and multi-scale approaches; on the other hand, detection criteria has been subdivided in thresholding, local peak search, multi-scale vision model, and other strategies. Moreover, we have described the main features of the most commonly used astronomical packages that provide a detection tool. Part of this work will be submitted to the XXI Astronomical Data Analysis Software & Systems (ADASS) conference, and furthermore, will be attempted to be published in an international astronomical or computer vision journal.

Secondly, **we have selected and implemented the works that reported better results.** We have noticed that several remarkable works used multi-scale approaches (especially the wavelet transform) as pre-processing and some kind of thresholding to detect sources. As these results were obtained from different images, we have decided to implement them as close as possible to the explanation provided in the papers, and we have applied them to the same dataset of images (a mosaic of radio images from the Giant Metrewave Radio Telescope). Thus, we have obtained a comparison between the

selected different approaches, and we have highlighted the strengths and weaknesses that they have.

Finally, after analysing the obtained results of the selected works, **we have proposed a new strategy based on mixing ideas of some of the reference approaches in the literature.** We have taken our inspiration from the work of Torrent et al [83] which used a supervised methodology that trained a classifier with features extracted from filtered images, and used it to say whether a pixel belong to a source or not. Instead of filtered images we have used the wavelet transform (used for example by Starck [73] and Peracaula [64, 66]) and the results have improved, having similar values, and even better, than some of the state-of-the art strategies.

## 5.2 Future work

We have performed a depth analysis of the state-of-the-art of the astronomical source detection techniques, and as we already mentioned, there are no updated surveys in this research topic. Therefore, one of our first future works will be writing a survey of techniques that may be submitted to an international conference (as ADASS) and to an international journal.

We have presented a new proposal based on the classification of the pixels of an image by means of features extracted from different WT scales. As we have obtained satisfactory results, we will continue investigating in this strategy, starting with the already commented idea of, instead of select the best feature at each round, the features will be descriptors with the values of the different patches extracted at each scale. Thereby, we will be able to test other types of classifiers. If this strategy or another one implemented for the short term provides good results, we are going to try to publish it. Moreover, some improvements can be applied to our proposal, for example some post-processing step with the aim of remove false positives.

The approaches implemented have been tested on radio images, but as we have seen, there are other types of astronomical image according to the frequency of the photons captured. Therefore, it would be interesting to test the methods with other datasets with more images and at other frequency bands. Moreover, in order to have more reliable reference catalogues, we want to obtain more annotations of the GMRT image, performed by more than an expert (inter-expert variability) and by the same expert (intra-expert variability). Thus, reliable true sources will be those annotations matching in several

annotated catalogues.

Following the objectives specified in the second research project within which this master thesis is located (reference AYA2010-21782-C03-02), we will focus on characterise the point spread function of the Fabra-ROA Baker-Nunn Camera located in the Observatori Astronòmic del Montsec (OAdM) [61, 82]. The optical images that we will obtain from this device will be registered with radio images from the LOw Frequency ARray (LOFAR) interferometer [40], and we will obtain correspondences between the sources of the two types of images (the main goal of this observations is to detect stars with variable intensity so-called transient stars).

Obviously, the work developed in this master thesis will be used in the development of my PhD thesis. The next section shows the thesis planning.

### 5.2.1 Thesis planning

After completing this master thesis we will further investigating in astronomical detection and segmentation as research line of the PhD thesis under a FI grant (reference 2011FI\_B 00081) awarded by the Generalitat de Catalunya. Our main goal is the design and implementation of an automatic system to detect sources in astronomical images, having as starting point the work developed in this master thesis. We can see a scheme of the planning of the first year of the thesis in Figure 5.1.

Just after the submission of this project, we will focus our efforts on publishing the survey of source detection techniques that we have performed in the next ADASS conference and in an international journal. Moreover, we will further study techniques to detect astronomical objects, and for this purpose we are going to study different pre-processing and detection steps to apply, for example, techniques applied to other research lines, like medical imaging. We want to test these techniques in different types of astronomical images. We think that could be interesting to develop this task during a research stay. With the analysis of different pre-processes and detection criteria, we will be able to develop a new proposal of source detection.

The PhD thesis will be focused on detection (obtaining the centroid coordinates of the sources in images), but in order to perform a more complete astronomical image processing pipeline, we will additionally study and implement techniques to segment the sources (specifying which pixels belong to each source), to classify sources (identifying if they are stars, clusters, galaxies, etc.), and to cross different catalogues of detections of the

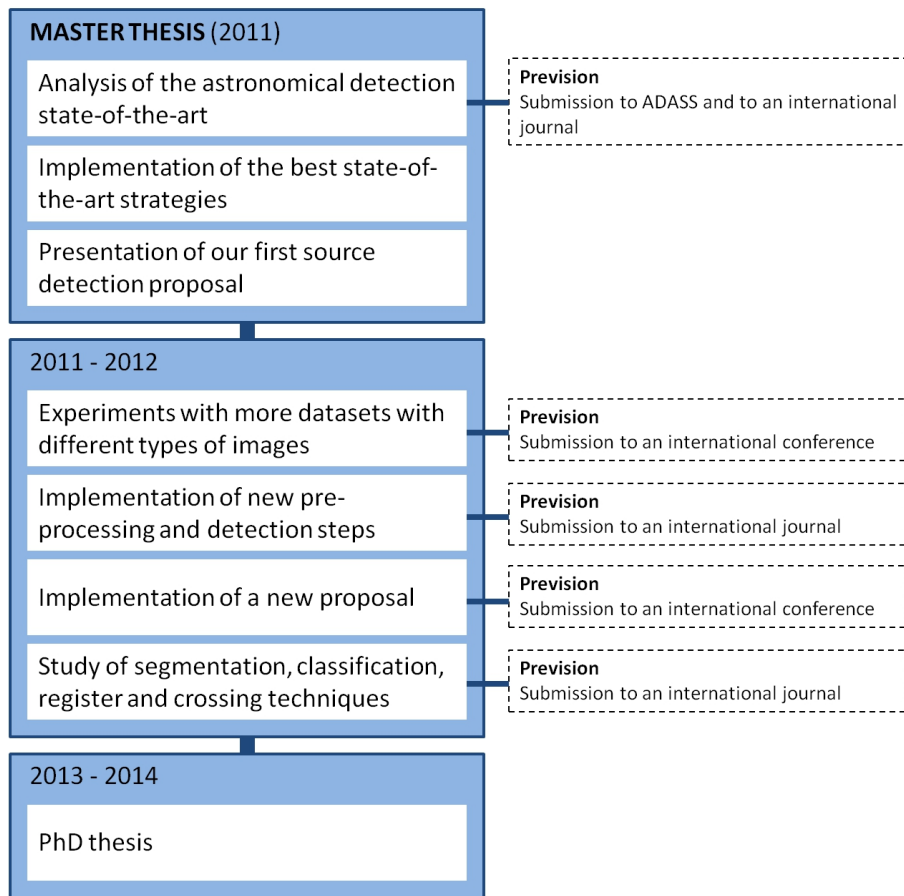


Figure 5.1: PhD planning scheme.

same region of the sky (identifying the same sources in the different catalogues). These techniques will allow us to face up the objectives of the research project where we are involved in (reference AYA2010-21782-C03-02), as the registration and correspondence of optical and radio images to detect transient stars, and the implementation of an integrated interface that allow users to run different astronomical image processing techniques in an easy and intuitive way.

# Bibliography

- [1] ALMA. Atacama Large Millimeter/submillimeter Array. <http://www.almaobservatory.org/>, 2011. [Online; accessed May-2011].
- [2] S. Andreon, G. Gargiulo, G. Longo, R. Tagliaferri, and N. Capuano. Wide field imaging - I. Applications of neural networks to object detection and star/galaxy classification. *Monthly Notices of the RAS*, 319:700–716, 2000.
- [3] E. Aptoula, S. Lefèvre, and C. Collet. Mathematical morphology applied to the segmentation and classification of galaxies in multispectral images. In *EUSIPCO 2006 Proceedings*. EURASIP, 2006.
- [4] R. B. Barreiro, J. L. Sanz, D. Herranz, and E. Martínez-González. Comparing filters for the detection of point sources. *Monthly Notices of the RAS*, 342:119–133, 2003.
- [5] A. N. Belbachir and P. M. Goebel. A combined multiresolution approach for faint source extraction from infrared astronomical raw images sequence. In *Workshop on Statistical Signal Processing Proceedings*, pages 459–464. IEEE, 2005.
- [6] E. Bertin. Mining pixels: The extraction and classification of astronomical sources. In A. J. Banday, S. Zaroubi, & M. Bartelmann, editor, *Mining the Sky*, pages 353–+, 2001.
- [7] E. Bertin and S. Arnouts. SExtractor: software for source extraction. *Astronomy and Astrophysics, Supplement*, 117:393–404, 1996.
- [8] A. Bijaoui. Sky Background Estimation and Applications. *Astronomy and Astrophysics*, 84:81–84, 1980.
- [9] A. Bijaoui, A. Guennec, C. Benoist, and E. Slezak. Analysis of multiband astronomical images using multiscale tools. In *Proceedings of SPIE - The International Society for Optical Engineering*, volume 6001, pages 1–12, 2005.

- [10] A. Bijaoui and F. Rué. A multiscale vision model adapted to the astronomical images. *Signal Processing*, 46:345–362, 1995.
- [11] P. S. Broos, L. K. Townsley, E. D. Feigelson, K. V. Getman, F. E. Bauer, and G. P. Garmire. Innovations in the Analysis of Chandra-ACIS Observations. *Astrophysical Journal*, 714:1582–1605, 2010.
- [12] R. Buonanno, G. Buscema, C. E. Corsi, I. Ferraro, and G. Iannicola. Automated photographic photometry of stars in globular clusters. *Astronomy and Astrophysics*, 126:278–282, 1983.
- [13] E. J. Candès and D. L. Donoho. Ridgelets: The key to high dimensional intermittency? *Phil. Trans. Royal Soc. Lond. A*, 357:2495–2509, 1999.
- [14] E. J. Candès and D. L. Donoho. Curvelets, multiresolution representation, and scaling laws. In *Proceedings of SPIE - The International Society for Optical Engineering*, volume 4119, pages 1–12, 2000.
- [15] P. Carvalho, G. Rocha, and M. P. Hobson. A fast Bayesian approach to discrete object detection in astronomical data sets - PowellSnakes I. *Monthly Notices of the RAS*, 393:681–702, 2009.
- [16] F. Damiani, A. Maggio, G. Micela, and S. Sciortino. A method based on wavelet transforms for source detection in photon-counting detector images. I. Theory and general properties. *Monthly Notices of the RAS*, 483:350–369, 1997.
- [17] DAO. The Dominion Astrophysical Observatory. <https://www.astrosci.ca/DAO/>, 2011. [Online; accessed May-2011].
- [18] ESA. Herschel Space Observatory. <http://www.herschel.caltech.edu/>, 2011. [Online; accessed May-2011].
- [19] ESA. INTEGRAL. <http://sci.esa.int/science-e/www/area/index.cfm?fareaid=21>, 2011. [Online; accessed May-2011].
- [20] ESA. XMM-NEWTON. <http://xmm.sonoma.edu/>, 2011. [Online; accessed May-2011].
- [21] F. Feroz and M. P. Hobson. Multimodal nested sampling: an efficient and robust alternative to Markov Chain Monte Carlo methods for astronomical data analyses. *Monthly Notices of the RAS*, 384:449–463, 2008.

- [22] P. E. Freeman, V. Kashyap, R. Rosner, and D. Q. Lamb. A wavelet-based algorithm for the spatial analysis of poisson data. *Astrophysical Journal, Supplement*, 138:185–218, 2002.
- [23] O. Le fèvre, A. Bijaoui, G. Mathez, J. P. Picat, and G. Lelièvre. Electronographic BV photometry of three distant clusters of galaxies. *Astronomy and Astrophysics*, 154:92–99, 1996.
- [24] J. González-Nuevo, F. Argüeso, M. López-Caniego, L. Toffolatti, J. L. Sanz, P. Vielva, and D. Herranz. The Mexican hat wavelet family: application to point-source detection in cosmic microwave background maps. *Monthly Notices of the RAS*, 369:1603–1610, 2006.
- [25] Gran Telescopio CANARIAS. GTC digital. <http://www.gtcdigital.net/>, 2011. [Online; accessed May-2011].
- [26] F. Guglielmetti, R. Fischer, and V. Dose. Background-source separation in astronomical images with Bayesian probability theory - I. The method. *Monthly Notices of the RAS*, 396:165–190, 2009.
- [27] J. Haupt, R. Castro, , and R. Nowak. Distilled sensing: selective sampling for sparse signal recovery. In *Proceedings of The 12th International Conference on Artificial Intelligence and Statistics (AISTATS)*, pages 216–223, 2009.
- [28] D. Herranz, M. López-Caniego, J. L. Sanz, and J. González-Nuevo. A novel multifrequency technique for the detection of point sources in cosmic microwave background maps. *Monthly Notices of the RAS*, 394:510–520, 2009.
- [29] A. D. Herzog and G. Illingworth. The structure of globular clusters. I. Direct plate automated reduction techniques. *Astrophysical Journal, Supplement*, 33:55–67, 1977.
- [30] M. P. Hobson and C. McLachlan. A Bayesian approach to discrete object detection in astronomical data sets. *Monthly Notices of the RAS*, 338:765–784, 2003.
- [31] A. M. Hopkins, C. J. Miller, A. J. Connolly, C. Genovese, R. C. Nichol, and L. Wasserman. A new source detection algorithm using false-discovery rate. *Astronomical Journal*, 123:1086–1094, 2002.
- [32] Institute for Space Imaging Science, University of Calgary. The Canadian Galactic Plane Survey. <http://www.ras.ucalgary.ca/CGPS/>, 2011. [Online; accessed May-2011].

- [33] M. J. Irwin. Automatic analysis of crowded fields. *Monthly Notices of the RAS*, 214:575–604, 1985.
- [34] J. F. Jarvis and J. A. Tyson. FOCAS: Faint Object Classification and Analysis System. *Astronomical Journal*, 86:476–495, 1981.
- [35] John Hopkins University. FUSE. <http://fuse.pha.jhu.edu/>, 2009. [Online; accessed May-2011].
- [36] Joint Astronomy Centre. James Clerk Maxwell Telescope. <http://www.jach.hawaii.edu/JCMT/>, 2011. [Online; accessed May-2011].
- [37] N. Kaiser, G. Squires, and T. Broadhurst. A method for weak lensing observations. *Astrophysical Journal*, 449:460–475, 1995.
- [38] R. G. Kron. Photometry of a complete sample of faint galaxies. *Astrophysical Journal, Supplement*, 43:305–325, 1980.
- [39] Z. Liu, K. Chiu, and L. Xu. Improved system for object detection and star/galaxy classification via local subspace analysis. *Neural Networks*, 16:437–451, 2003.
- [40] LOFAR. LOFAR. <http://www.lofar.org/>, 2011. [Online; accessed July-2011].
- [41] M. López-Caniego, D. Herranz, J. L. Sanz, , and R. B. Barreiro. Detection of Point Sources on Two-Dimensional Images Based on Peaks. *EURASIP Journal on Applied Signal Processing*, 15:2426–2436, 2005.
- [42] D. Makovoz and F. R. Marleau. Point-Source Extraction with MOPEX. *Publications of the ASP*, 459:341–352, 2006.
- [43] J. B. Melin, J. G. Bartlett, and J. Delabrouille. Catalog extraction in SZ cluster surveys: a matched filter approach. *Astronomy and Astrophysics*, 117:1113–1128, 2006.
- [44] K. J. Mighell. Algorithms for CCD stellar photometry. *Astronomical Data Analysis Software and Systems VIII, ASP Conference Series*, 172:317–328, 1999.
- [45] NASA. RXTE. <http://www.nasa.gov/centers/goddard/missions/rxte.html>, 2010. [Online; accessed May-2011].
- [46] NASA. About the Kuiper Airborne Observatory (KAO). <http://quest.nasa.gov/lfs/about-kaos.html>, 2011. [Online; accessed May-2011].

- [47] NASA. Chandra X-ray Observatory. <http://www.nasa.gov/centers/goddard/missions/rxte.html>, 2011. [Online; accessed May-2011].
- [48] NASA. Fermi Gamma-ray Space Telescope. <http://fermi.gsfc.nasa.gov/>, 2011. [Online; accessed May-2011].
- [49] NASA. GALEX Galaxy Evolution Explorer. <http://www.galex.caltech.edu/>, 2011. [Online; accessed May-2011].
- [50] NASA. Spitzer Space Telescope. <http://www.spitzer.caltech.edu/>, 2011. [Online; accessed May-2011].
- [51] NASA. WISE. <http://wise.ssl.berkeley.edu/>, 2011. [Online; accessed May-2011].
- [52] NASA/DLR. SOFIA Science Center. <http://www.sofia.usra.edu/>, 2011. [Online; accessed May-2011].
- [53] NASA/ESA/STScI. HUBBLESITE. <http://hubblesite.org/>, 2011. [Online; accessed May-2011].
- [54] NASA/GSFC. The FITS Support Office. [http://fits.gsfc.nasa.gov/fits\\_home.html](http://fits.gsfc.nasa.gov/fits_home.html), 2011. [Online; accessed February-2011].
- [55] B. Newell and E. J. O’Neil Jr. The reduction of panoramic photometry. I. Two search algorithms. *Publications of the ASP*, 89:925–928, 1977.
- [56] NRAO. Welcome to the Very Large Array! <http://www.vla.nrao.edu/>, 2009. [Online; accessed May-2011].
- [57] NRAO. Welcome to the Very Long Baseline Array! <http://www.vlba.nrao.edu/>, 2009. [Online; accessed May-2011].
- [58] NRAO. Astronomical Image Processing System. <http://www.aips.nrao.edu/>, 2011. [Online; accessed May-2011].
- [59] NRAO. National Radio Astronomy Observatory. <http://www.nrao.edu/>, 2011. [Online; accessed May-2011].
- [60] N. Otsu. A Threshold Selection Method from Gray-Level Histograms. In *International Conference on Systems, Man and Cybernetics Conference Proceedings*, volume 9, pages 62–66. IEEE, 1979.

- [61] Parc Astronòmic Montsec. Observatori Astronòmic del Montsec. <http://www.parcasironomic.cat/observatori-astronomic-montsec.php>, 2008. [Online; accessed July-2011].
- [62] J. M. Paredes, J. Martí, C. H. Ishwara-Chandra, J. R. Sánchez-Sutil, A. J. Muñoz-Arjonilla, J. Moldón, M. Peracaula, P. L. Luque-Escamilla, V. Zabalza, V. Bosch-Ramon, P. Bordas, G. E. Romero, and M. Ribó. Radio continuum and near-infrared study of the MGRO J2019+37 region. *Astronomy and Astrophysics*, 507:241–250, 2009.
- [63] W. D. Pence, L. Chiappetti, C. G. Page, R. A. Shaw, and E. Stobie. Definition of the Flexible Image Transport System (FITS), version 3.0. *Astronomy and Astrophysics*, 524, 2010.
- [64] M. Peracaula, J. Freixenet, and X. Lladó. Detection of Faint Compact Radio Sources in Wide Field Interferometric Images using the Slope Stability of a Contrast Radial Function. *ASP Conference Series*, 411, 2009.
- [65] M. Peracaula, X. Lladó, J. Freixenet, and A. Oliver. Segmentation and detection of extended structures in low frequency astronomical surveys using hybrid wavelet decomposition. *ASP Conference Series*, 442, 2010.
- [66] M. Peracaula, J. Martí, J. Freixenet, J. Martí, and J. M. Paredes. Multi-scale image analysis applied to radioastronomical interferometric data. *Lecture Notes in Computer Science*, 5524:192–199, 2009.
- [67] B. Perret, S. Lefèvre, and C. Collet. A robust hit-or-miss transform for template matching applied to very noisy astronomical images. *Pattern Recognition*, 42:470–2480, 2008.
- [68] B. Perret, S. Lefèvre, and C. Collet. Connected Component Trees for Multivariate Image Processing and Applications in Astronomy. In *Proceedings - International Conference on Pattern Recognition*, pages 4089–4092, 2010.
- [69] R. S. Savage and S. Oliver. Bayesian methods of astronomical source extraction. *Astrophysical Journal*, 661:339–1346, 2007.
- [70] SKA. Square Kilometre Array. <http://www.skatelescope.org/>, 2011. [Online; accessed May-2011].

- [71] E. Slezak, A. Bijaoui, and G. Mars. Galaxy counts in the Coma supercluster field. *Astronomy and Astrophysics*, 201:9–20, 1988.
- [72] J.-L. Starck. Multiscale Methods in Astronomy: Beyond Wavelets. *ASP Conference Series*, 281:391–400, 2002.
- [73] J.-L. Starck, H. Aussel, D. Elbaz, D. Fadda, and C. Cesarsky. Faint source detection in ISOCAM images. *Astronomy and Astrophysics, Supplement*, 138:365–379, 1999.
- [74] J.-L. Starck and J. Bobin. Astronomical data analysis and sparsity: From wavelets to compressed sensing. In *Proceedings of the IEEE*, volume 98 (6), pages 1021–1030, 2010.
- [75] J.-L. Starck, D. L. Donoho, and E. J. Candès. Astronomical image representation by the curvelet transform. *Astronomy and Astrophysics*, 398:785–800, 2003.
- [76] J.-L. Starck, J. M. Fadili, S. Digel, B. Zhang, , and J. Chiang. Source detection using a 3D sparse representation: application to the Fermi gamma-ray space telescope. *Astronomy and Astrophysics*, 504:641–652, 2009.
- [77] J.-L. Starck and F. Murtagh. *Astronomical Image and Data Analysis (Astronomy and Astrophysics Library)*. Springer-Verlag New York, Inc., Secaucus, NJ, USA, 2006.
- [78] P. B. Stetson. Daophot. a computer program for crowded-field stellar photometry. *Publications of the ASP*, 99:191–222, 1987.
- [79] A. S. Szalay, A. J. Connolly, and G. P. Szokoly. Simultaneous multicolor detection of faint galaxies in the Hubble Deep Field. *Astronomical Journal*, 117:68–74, 1999.
- [80] Tata Institute of Fundamental Research. Giant Metrewave Radio Telescope. <http://gmrt.ncra.tifr.res.in/>, 2010. [Online; accessed June-2011].
- [81] A. R. Taylor, S. J. Gibson, M. Peracaula, P.G. Martin, T.L. Landecker, C.M. Brunt, P.E.Dewdney, (...), and D. Durand. The Canadian Galactic Plane Survey. *Astronomical Journal*, 125:3145–3164, 2003.
- [82] Telescope Fabra ROA Montsec. Fabra-ROA telescope at Montsec. <http://www.am.ub.es/bnc/index.php>, 2011. [Online; accessed July-2011].
- [83] A. Torrent, M. Peracaula, X. Lladó, J. Freixenet, J. R. Sánchez-Sutil, J. Martí, and J. M. Paredes. Detecting faint compact sources using local features and a boosting

- approach. In *Proceedings - International Conference on Pattern Recognition*, pages 4613–4616, 2010.
- [84] Universidad de Jaén. Fuentes de alta energía en la galaxia. <http://aljayani.ujaen.es/faeg/index.php>, 2011. [Online; accessed June-2011].
- [85] Universitat de Barcelona. Group on Galactic Compact Sources at High Energies. <http://www.am.ub.es/~josep/group/index.html>, 2007. [Online; accessed June-2011].
- [86] P. Vielva, E. Martínez-González, J. E. Gallegos, L. Toffolatti, and J. L. Sanz. Point source detection using the Spherical Mexican Hat Wavelet on simulated all-sky Planck maps. *Monthly Notices of the RAS*, 344:89–104, 2003.
- [87] A. Vikhlinin, W. Forman, C. Jones, and S. Murray. Matched filter source detection applied to the ROSAT PSPC and the determination of the number-flux relation. *Astrophysical Journal*, 451:542–552, 1995.
- [88] W. M. Keck Observatory. W. M. Keck Observatory. <http://www.keckobservatory.org/>, 2010. [Online; accessed May-2011].
- [89] Y. Yang, N. Li, and Y. Zhang. The structure of globular clusters. I. Direct plate automated reduction techniques. In *International Conference on Systems, Man and Cybernetics Conference Proceedings*, pages 650–655. IEEE, 2008.